Université catholique de Louvain

École polytechnique de Louvain (EPL)

Modelling and Low-level control of a new generation of transfemoral prosthesis.

Dissertation presented by
Charles Boussemaere, Virgil Hinque

for obtaining the Master's degree in
Electro-mechanical Engineering
Option: Mechatronics

Supervisor
Renaud Ronsse

Readers
Paul Fisette, Joost Geeroms, Sophie Heins

Academic year 2015-2016

ABSTRACT

Limb amputation is a growing problem nowadays. It originates mainly from vascular diseases like diabetes. Even if most amputees are transtibial (below the knee), transfemoral amputees (above the knee) still represent a fair part of amputations cases among the world.

They are treated with transfemoral prostheses. These are used to replace the missing knee and ankle joints. The CYBERLEGs project, which includes a UCL research team, aims to develop an energy-efficient actuated transfemoral prosthesis. The current version of this prosthesis, the CYBERLEGs-Beta prosthesis, is the focus of this thesis.

A quasi-static and analytical model of this device has been developed. However, these models do not include the dynamic effects in the joints of the prosthesis, such as inertial, gyroscopic and centrifugal forces.

This master thesis has two goals. First, develop a dynamic model of the CYBERLEGs-Beta prosthesis to investigate on these dynamic effects. Secondly, augment it with the electromechanical model of the actuators to finally design a low-level controller for these actuators.

ACKNOWLEDGEMENT

We would like to take this opportunity to thank all the people who have contributed in some way to this thesis.

Particularly Renaud Ronsse, our advisor, who initiated the project. We would like to thank him for his continuous and regular support and guidance throughout the year.

Then, we would like to thank Sophie Heins for her help and patience. Her knowledge of the prosthesis was crucial for this project.

We also would like to thank Joost Geeroms and Louis Flynn of the Vrije Universiteit Brussel for their help when we needed information about the prosthesis and for their warm welcome in the VUB locals.

We would like to thank Paul Fisette as well, for accepting to read our thesis.

A warm thanks to the *Robotran* support team as well. They helped us a lot during this year.

Finally, we would like to thank our friends and family who encouraged and supported us during this long project.

CONTENTS

INTRODUCTION

Limb amputations affect annually more than one million people in the world [1]. They are mostly due to complications of the vascular system, the most common being diabetes. In fact, up to 82% of the limb losses are dysvascular-related while only 16% of them result from an accident [1]. The last 2% are either congenital or due to cancer. Most of these amputations (∼86%) are transtibial, i.e. below the knee [2]. The rest of them are called transfemoral amputations and need a specific treatment, as not one but two joints must be replaced.

To replace these two joints, prostheses are used to allow amputees to regain their lost ability. There are three kind of prostheses: passive, semi-active and active. Active prostheses are powered by actuators and are important for amputees because they allow more activities like stair climbing or certain sports by generating mechanical power. The control of these actuators, their power consumption as well as their prices are current challenges for researchers [3]. Indeed, despite their mediocre performances, passive prostheses might be preferred over the active devices because of bad autonomy or expensive prices. The CYBERLEGs project tries to develop an artificial cognitive system for transfemoral amputees [56]. This system is meant to replace the missing lower-limb and give assistance in activities of daily living. To do so, several projects are realised in parallel. One of these projects is the development of a transfemoral prosthesis with an energy transfer system between the knee and the ankle. Two prostheses have been built and one is the subject of this thesis: the CYBERLEGs-Beta.

This prosthesis has already been presented [4] and studied [5]. Its performances are improved over time. In this process, a quasi-static model of the CYBERLEGs-Beta prosthesis has been developed [5]. It can predict the torques and forces in the mechanism depending on the position of its joints. However, it does not yet take into account the dynamic effects due to the velocities and accelerations of the joints. The first goal of this project was thus to quantify these effects and their contribution to the overall mechanic of the prosthesis using a multibody model of the device. From there, the second goal was to augment this model with the prosthesis actuators in order to develop a low-level control method. This controller should compute the actuators commands required to get a desired torque in the knee and ankle joints.

This thesis is divided in six chapters. The first chapter focuses on what already exists, i.e. the state-of-the art regarding ankle, knee and transfemoral prostheses. The second chapter explains the CYBERLEGs-Beta prosthesis and its mechanisms. The chapter 3 and 4 respectively describe the multibody modelling of the prosthesis and its dynamic analysis. Chapter 5 is dedicated to an actuator dimensioning resulting from this analysis. Chapter 6 will finally explain the principle of the low-level controller.

CHAPTER 1

STATE-OF-THE-ART OF LOWER-LIMB PROSTHESES

Most of the transfemoral amputees actually use independent knee and ankle modules as prostheses. Consequently, the existing solutions for ankle and knee prostheses are also reviewed. Terms related to the biomechanics of the human gait will be used in this thesis. A deeper description of this topic can be found in Appendix D.

1.1 Ankle prostheses

In this section, the distinction is made between prostheses and implants. Prostheses are devices designed to replace the entire foot, i.e. devices for people who have completely lost their foot for reasons such as trauma or disease. These people are called transtibial amputees. The ankle implants are used when the foot is not entirely lost. They require a surgery to be placed inside the foot, around the ankle joint. Implants will thus not be covered here because their development is rather based on surgery and biomechanics than mechatronics and control.

Ankle prostheses can be classified according to their energetic behaviour: passive, semi-active and active. Passive prostheses do not embed any actuator and are only composed of passive elements such as springs or dampers. Active prostheses can provide mechanical energy in order to assist the ankle movement. Finally, semi-active prostheses embed actuators that can only tune one of their elements parameter (such as a spring stiffness).

The whole classification of ankle prostheses is shown in Figure 1.1.

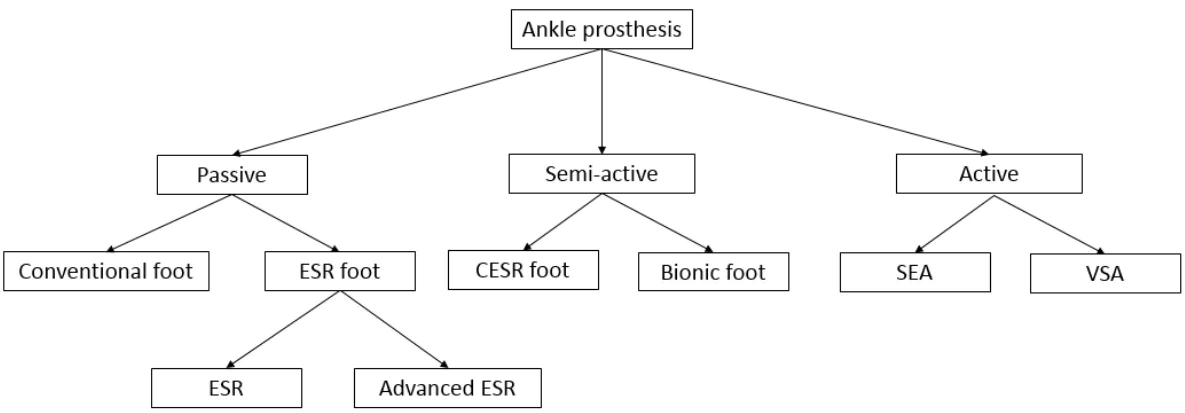

Figure 1.1: Classification of ankle prostheses

1.1.1 Passive ankle prostheses

As said previously, these prostheses cannot create mechanical energy to support the gait. They are divided into two kinds: the conventional feet and the passive energy storage and return feet(ESR), embedding springs.

1.1.1.1 Conventional feet

For transtibial amputees with an expected low activity level (hypomobile), the conventional foot is considered to be the most appropriate device. Indeed, it is inexpensive, easy-to-use, stable and safe. However, it also has many disadvantages. For example, the time between heel strike and mid-stance phase is twice as long as in a normal gait because the rigid ankle prevents any rotation around the ankle axis [6].

Figure 1.2: A conventional foot: the SACH [7]

An example of a conventional foot is given in Figure 1.2, i.e the SACH (Solid Ankle Cushioned Heel) developed in 1950 [8]. It is the most popular prosthetic device. It looks like a simple rigid foot and is in fact based on it. However, a compressive keel (made of rubber) is added to the device. Its compliance provides mid-stance stability and shock absorption by cushioning at heel strike (cushion heel). It also has no ankle joint mechanism, which means there is no need for maintenance [8].

One of the SACH limitations is that it only has a single degree of freedom. Therefore, a better version of this design is the multi-axial foot like the 1M10 Adjust by Otto Bock [7]. It allows more anatomical motions of the foot, such as the inversion/eversion and the dorsiflexion/plantarflexion. It results in a better emulation of a natural foot-ankle system and allows the wearer to walk on uneven terrains.

1.1.1.2 Passive Energy Storage and Return (ESR) feet

Thanks to the progress of others technologies, the ankle prostheses evolved to improve the amputee gait. It resulted in the ESR foot, first introduced in 1981. The ESR is able to store energy in the early stance and then release it to the amputee during the late stance to propel the body forward. As no external energy is provided, it is indeed a passive device. This kind of prostheses can not be used by hypomobile users due to the instability of energy return [7].

Basic ESR

The first design of the ESR is shown in Figure 1.3 [9]. It looks quite like the SACH foot, the difference being the flexible keel and the shell made of rubber or foam. The flexible keel acts like an elastic spring, storing energy during heel strike and early flat foot and then releasing it during push off [10].

Compared to the SACH foot, this design offers a better stability during the mid-stance phase and a reduced energy cost as well. The improved stability is due to the flexible keel [7] [11].

Advanced ESR

Nowadays, new versions of the ESR are available. New materials, such as carbon composites, are used to design these new prostheses. They typically contain a flexible carbon fibre shank and a

Figure 1.3: First design of ESR [9]

heel spring. Instead of devices with a single flexible part, it results in prostheses that are entirely elastic. More energy is absorbed thanks to the new materials and this energy is released more slowly in the mid-stance phase, without impulses. As the heel stiffness increases, the duration of shock absorption decreases and therefore less energy is wasted. One of those designs is shown in Figure 1.4.

The Vary-Flex prosthesis [12] was developed for active users. It allows them to practice physical activities like sport and achieve everyday tasks with the same prosthesis. For this purpose, the Vary-Flex possess a carbon sole that absorbs vertical and rotational shocks. But at the same time, this sole is very comfortable, which is perfect to perform common tasks with ease. There are other devices on the market with dampers or additional springs to allow multi-axes motion. From the point of view of the users, these new passive ESR designs seem to be more comfortable and to respond better [11].

Figure 1.4: Vari-flex from Ossür [12]

1.1.2 Semi-active ankle prostheses

With the progresses of fields like electronics and control, a lot of prostheses added actuators in their design. In semi-active devices, these actuators do not provide any energy for the gait but are rather used to tune, activate or disengage a part of the system.

1.1.2.1 Controlled Energy Storing and Returning (CESR) feet

This new type of "Energy Storage and Return" devices uses an actuator to engage and disengage a locking mechanism, which creates a delay between the energy storage and release. It is stored during the heel strike and returned during the push-off phase. All designs are based on this principle: storing the most energy and returning it at the proper time by controlling the actuator. An example is given in Figure 1.5.

The AMP-Foot 1.1 [13] is the new version of the AMP-Foot 1.0 and includes a motor for the locking mechanism. This motor is coupled to a planetary gearbox and then combined with springs and paw-ratchet mechanisms that performs the gait motion. The purpose of the motor is only to lock and unlock the pawls as a function of the gait progress.

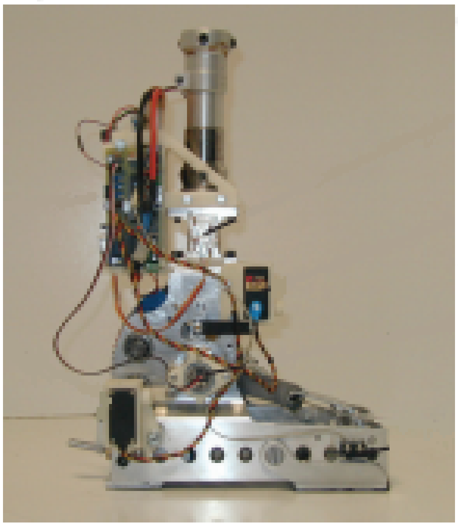

Figure 1.5: AMP-Foot 1.1 [13]

In an newer version of this device, the AMP-Foot 2.0 [14] [15], the locking and unlocking of the mechanism is done by a lever arm rather than a planetary gearbox. The principal advantage of this improvement is the reduced weight of the overall mechanism. Indeed, with the lever arm, only a low power motor is required, and these motors are lighter.

1.1.2.2 Bionic feet

Since the 1990 decade, ankle prostheses have used hydraulic or pneumatic systems in their design to improve the damping effect and the energy storage and release [16]. The actuation of these systems is done with electrical actuators. Those systems also provide a better stability of the ankle because they can be controlled. These devices have recently converged towards a specific design, which is a double plate upon which is placed the block containing the hydraulic system and the electrical actuator. This kind of ankle prostheses is called "Bionic feet" [17]. Bionic feet can be classified either as semi-active or as active prostheses.

Figure 1.6: Proprio Foot from Össur [18]

An example of this type of bionic feet is the Proprio Foot from Össur [18]. It is classified as a semi-active prosthesis because the actuator does not provide any energy for the gait but only serves to lock or unlock the hydraulic system. It is composed of an advanced ESR combined with an hydraulic system as explained above. The hydraulic system damps the ankle during the foot-flat phase.

1.1.3 Active ankle prostheses

The active prostheses inject external power into mechanisms to assist or even control the gait. A healthy ankle produces more energy than it dissipates (see Appendix D.3). Therefore, it makes sense to provide this energy with actuators. Powered ankle prostheses are thus better at emulating a healthy ankle behaviour than the passive or semi-active devices. They can be classified according to their actuation principle: variable stiffness actuation or series elastic actuation.

1.1.3.1 Series elastic actuation

In robotics, a traditional premise of good design is *"The stiffer the better"* [19]. Indeed, a stiff manipulator allows precise position control. The problem with stiffness is that it makes force control difficult. Such an actuator can provide high forces from small displacements but these displacements have a order of magnitude similar to the resolution of joint sensors. This is why the control becomes a tedious task. It also results in instabilities in the system, especially when in contact with hard surfaces (e.g. the ground). Because of the stiff actuators, the generated forces and torques are quite large. Moreover, gearboxes are generally added, in order to improve the actuator efficiency (typical electrical motors have a better efficiency if running at a speed being much higher than the typical speed of the task). It results in noise, friction, backslash and large reflected inertia of the motor.

Stiffness and bandwidth can thus be sacrificed to get more stability. This is the principle of the Series Elastic Actuators (SEA), displayed in Figure 1.7.

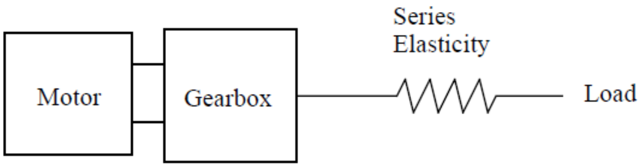

Figure 1.7: Schematic of series elastic actuation [20]

As seen in this Figure, a SEA is implemented by placing an elastic element into the actuator, between the gearbox and the load. Unfortunately, gears introduce friction, blackslash and noise if the control of the motor is made with just force control [19]. To reduce this effect, the force control can be transformed into position control thanks to the elastic element. Indeed, the force transmitted to the load is proportional to the spring displacement.

However, the spring also filters the output of the actuator, thus limiting the bandwidth that can be achieved. But overall, a SEA better approaches the human behaviour because the spring in series can store and release energy unlike traditional stiff actuators. And moreover, the amount of energy provided by the actuator can be controlled.

Finally, the spring storing and releasing energy during task completion reduces the global power consumption of the actuator. Indeed, energy is stored during periods of negative power. And during periods of positive power, this energy is released to assist the actuator. To further diminish this power requirement, a parallel spring can be introduced. It helps reducing the power peaks of the motor. The device is then called SPEA [21].

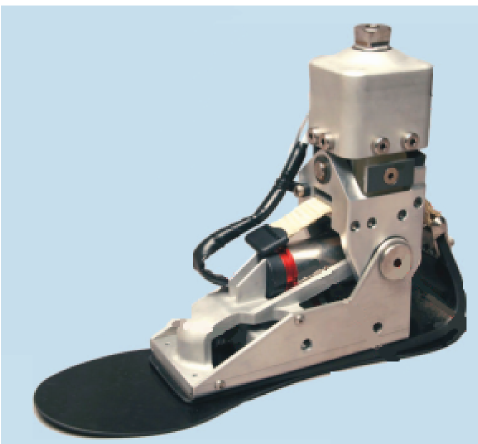

Figure 1.8: Power ankle-foot prosthesis with SPEA [21]

Here is an example of an ankle prosthesis that uses the SPEA system, in Figure 1.8. It was produced by two researchers of the MIT [21]. The system contains two springs, one in series and one in parallel with the actuator. The parallel spring is used to improve the open-loop force bandwidth because the forces provided by the sole SEA are not enough. To save weight, the springs are made of a carbon composite material. The total prosthesis weights 2 Kg.

1.1.3.2 Variable stiffness actuation

The principle of Variable Stiffness Actuation (VSA), as its name stands for, is to modify the stiffness of the actuator during the gait [22]. The previous concept, SEA, uses a mechanical stiffness being fixed for a precise task. A VSA allows to modify the actuator stiffness not only to fit the user anatomy, but also to work with different gaits, different walking speeds, different step lengths and with terrain adaptation. A device using this actuation improves the global safety, the energy efficiency and the dynamic range. To realize this stiffness variation, two actuators are used as well as a passive elastic element. Together, they can control the compliance and the equilibrium position of the actuated joint. The disadvantages of a VSA device are the increased weight and the complexity of control [23].

An example of VSA system is the MACCEPA architecture [24]. A MACCEPA (Mechanically Adjustable Compliance and Controllable Equilibrium Position Actuator) system is an electrical actuator whose compliance and equilibrium position are fully independently controllable. By controlling both the equilibrium position and compliance, a variety of natural motions is possible, consuming less energy.

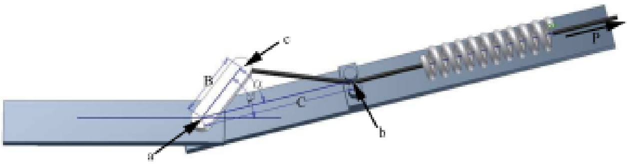

Figure 1.9: Drawing of MACCEPA system [25]

The MACCEPA system is composed of three bodies rotating around a common axis. In Figure 1.9, the first is the reference body (on the left). It holds an actuator in order to control the torque around the rotation axis. Then, there is the body on the right, called the lower leg and a smaller body used as a lever arm. This lever arm extremity is fixed on the rotation axis.

On this lever arm is attached a cable. It goes from point c (on its other extremity) to point b on the lower leg (see Figure 1.9). This cable is attached to a pretension mechanism, depending on angle φ which is controlled by another actuator. Finally, a spring with stiffness k is placed on the cable [24].

The spring in this system is put into pretension. To do so, the pretension actuator defines the position of point c, by controlling the value of φ with $\alpha = 0$. This sets the equilibrium position. The actuator on the reference body can then control the angle α to generate a force in the spring. This force creates a torque that tends to line up the right body with the lever arm [26].

There are different MACCEPA architectures. For example, a MACCEPA with two degrees of freedom can be created. It is displayed in Figure 1.10. Another example is a MACCEPA architecture using rigid bodies instead of the cable. It is detailed in section 2.2.

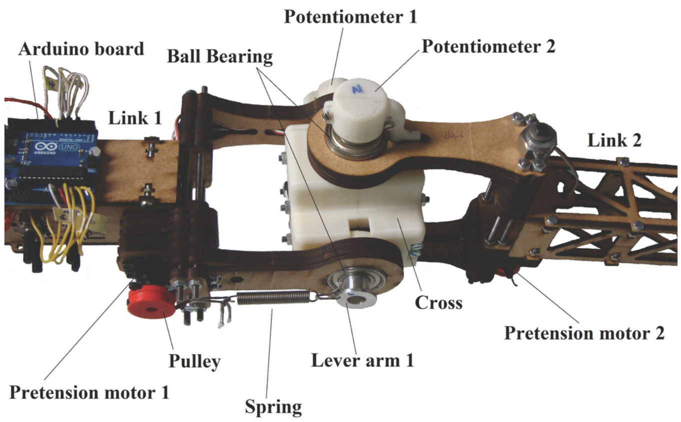

Figure 1.10: The two-degree of freedom MACCEPA [27]

1.2 Knee prostheses

Regarding the knee prostheses, the distinction between prostheses and implants is made as well. The former are used for transfemoral amputees, i.e. patients who have been amputated above the knee[28]. The latter are placed during a surgery to replace just a part of the knee. Only prostheses are covered in this chapter for the same reason than for the ankle devices.

Like ankle prostheses, knee prostheses can be classified into three categories according to their energetic behaviour: passive, semi-active and active devices. During a healthy human stride, the knee joint only dissipates energy (see Appendix D). Consequently, passive devices only using springs and dampers make sense, since they can reproduce this passive behaviour. However, for other activities like sit-to-stand, more energy might be needed. This is why semi-active and active prostheses are present in the market. The classification is shown in Figure 1.11.

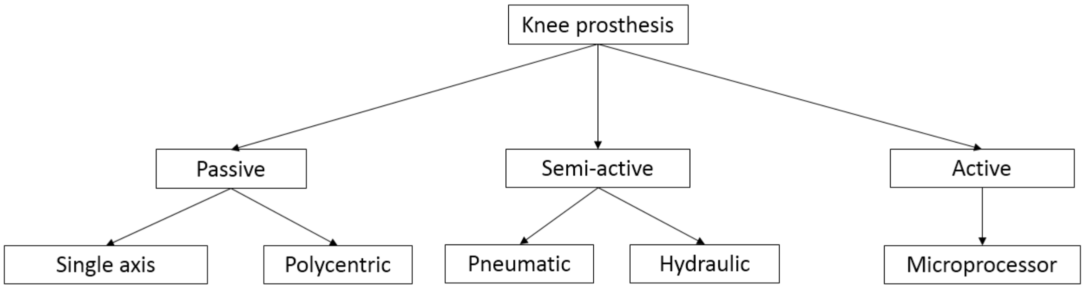

Figure 1.11: Classification of knee prostheses

In passive devices, friction is used to modify the speed of the knee joint motion during walking. Friction warrant how far and how fast the knee bends and straightens during the gait. Most knee prostheses use mechanical friction while others use hydraulic damping.

If the user wants to do other tasks such as stair climbing or sit-to-stand motion, the knee needs to produce energy. Therefore, these passive devices are not sufficient anymore. Active knee prostheses can provide this energy. They can also control the knee joint position and speed to match a healthy gait, through their embedded electronics.

1.2.1 Passive knee prostheses

Passive knee prostheses are the basis of all knee prostheses, using mechanical components. The simplest way to achieve the motion of a knee is to use the mechanical friction of a bolt that connects the socket to the shank. This bolt is placed adequately so that it will not buckle when the patient is standing straight. This friction may also be designed with a simple braking system in order to keep the shank from moving too fast during the different gait phases.

As Figure 1.11 shows, passive prostheses are divided into two types: single-axis and polycentric. The first type works like a hinge. The second is more complex, allowing more degrees of freedom to the motion [29].

1.2.1.1 Single-axis knee

Single-axis knees are basic knees that bend freely. An example is shown in Figure 1.12, it is the Locking knee from Össur [30].

Figure 1.12: Locking knee from Össur [30]

This knee prosthesis can be used for rehabilitation and for permanent use as well. The stability is ensured by the patient himself, using hip motions. The mechanical friction is constant: this is in fact the main limitation of this design. Consequently, this knee prosthesis is only recommended to patients having an excellent musculature control, who only walk at a single speed and have a low activity level. The advantages of such a prosthesis are the durability, the low-weight and the low price [30].

1.2.1.2 Polycentric knee

Figure 1.13: GeoFlex knee from Willow Wood [31]

Polycentric knees allow to have a variable center of rotation which increases the stability during all phases of the gait. When the knee flexion angle is increasing or decreasing, the position of the instantaneous center or rotation changes. If a four bar system is added to the mechanism, it also allows the knee to better collapse during the swing phase of the gait. An example is shown in Figure 1.13, i.e the GeoFlex knee from WillowWood [31]. This system provides a better control of the stability with its friction controller. One of the limitations of this design is that the range of motion of the knee joint might be restricted to some extent, although it is generally enough for most people.

1.2.1.3 Stability

After having chosen which of the previous designs is most appropriate for the patient, doctors and prosthetists have to decide how the stability in the stance phase will be handled. There are two possible choices:

- Manual locking knee: It is the most stable knee of all the ones used in prosthetics. The knee is locked during the gait and the patient releases the lock mechanism when he wants to sit down. This can be used by amputees who have a low activity level or are unstable. This is why those prostheses are quite popular in rehabilitations. An example is the 3R17 from OttoBock [32], see Figure 1.14(a).

- Weight-activated stance-control knee: This is the most used system in knee prosthetics. This knee is like a single axis constant friction knee with a braking mechanism. When weight is applied on the knee during the gait, the mechanism of braking is activated which prevents the knee from buckling. That way, the patient just has to play with his own weight to bend the knee, he does not have to touch the prosthesis to lock or unlock the mechanism. The "Balance knee Control" from Össur [33] in Figure 1.14(b) uses this option.

(a) 3R17 from Otto bock [32] (b) Balance Knee Control from Össur [33]

Figure 1.14: Examples of knees prosthesis to insure more stability

Between these two possibilities, the weight-activated stance-control knee is preferred by older or less active users because the system is independent [34]. They do not have to stop themselves to activate the locking mechanism.

1.2.2 Semi-active knee prostheses

In the semi-active knee prostheses, there are actuators that can tune damping parameters in order to improve the motion quality. This kind of prostheses is called "variable-damping". With these actuators, the prostheses can mimic a biological knee in a better way and the control is more sensible.

The variable-damping systems allow variable walking speeds. During the gait, if the user wants to increase his speed, the prosthesis can follow him. An example of users walking faster and faster is shown in [35]. As the patient cadence increases or decreases, the hydraulic/pneumatic damping system is adjusted during swing phase to control the speed at which the tibia of the prosthesis swings forward and bends backwards [36].

This type of prosthesis is often used for more active patients whose walking speed varies and who do not need assisting walking devices. An example of a single-axis hydraulic knee is given in Figure 1.15(a) and a polycentric pneumatic knee in Figure 1.15(b). With these devices, users can walk with a better gait pattern and in a more comfortable manner than with passive devices. The disadvantages are mainly cost and maintenance.

1.2.3 Active knee prostheses

The last category of knee prostheses is the active or powered knee devices [37]. They are relatively new in the global prosthetic technology. They use microprocessors in order to provide a more sophisticated method of control.

Current approaches of powered prostheses are mainly focused on the use of single-motor transmission systems directly coupled to the knee joint. These direct-drive designs require a high electrical power consumption to fully imitate the mechanical behaviour of a healthy knee but they can help the patients to walk with a much more stable and efficient gait. These prostheses need sensors, software and batteries [38]. They can also contain hydraulic or pneumatic systems to damp the knee joint.

(a) Mauch knee from Össur [39]

(b) 3R106 from Otto bock [40]

Figure 1.15: Examples of semi-active prostheses

(a) The C-Leg knee from Otto Bock [39]

(b) Rheo Knee from Össur [41]

Figure 1.16: Examples of active prostheses

The C-Leg knee from Ottobock, in 1.16(a) [42], is an example of this kind of prostheses. It is the first microprocessor-controlled swing and stance hydraulic knee and was first introduced in 1999. Currently, a new C-leg prosthesis is designed. It uses hydraulic cylinders to control the flexion of the knee. Sensors send signals to the microprocessor. This one analyses them and compute what resistance the hydraulic system should apply. These sensors send feedback 50 times per second, allowing real-time control. A wireless remote control allow to switch modes. These different modes can allow the users to either ride a bike or to stand with any knee flexion getting stabilized. With this prosthesis, users can also climb stairs [43] and realize sit-to-stand motion [44].

Rheo Knee from Össur, in 1.16(b) [41], is a microprocessor-controlled knee that uses resistance control magnetorheologic technology in order to get an almost instantaneous response time. Similar to the C-leg, the microprocessor receive the magnitude of the knee torque with sensors. It can then act on the system by using magnetorheological brakes. The principle of these brakes is to change the viscous properties of the fluid in function of an externally applied magnetic field. Changing these properties makes the device extremely energy efficient. More details on this technology can be found in [45].

1.3 Transfemoral prostheses

As said previously, most designs of transfemoral prostheses are combinations of a knee module and an ankle module, each module being chosen according to the level of activity of the amputee, his/her strength, weight and ability to control the prosthesis. All knee modules can be combined with any ankle module but it is better to optimize the combination with the level activity of the amputee. For example, if the amputee plays sports, he probably desires to use a prosthesis that allows this activity level and then a conventional foot is not recommended.

Transfemoral prostheses can be classified in two parts: prostheses with and without energy transfer between both modules.

1.3.1 Transfemoral prostheses without energy transfer

These transfemoral prostheses are simply a knee prosthesis connected to a ankle prosthesis. The 3R60 transfemoral prosthesis form Ottobock is a good example of this configuration, in Figure 1.17.

The knee is the 3R60 knee prosthesis [46]. It is a polycentric knee joint with a hydraulic system that controls the pendulum movement of the lower prosthetic limb during the swing phase. The polycentric part has five axes to improve the protection against unwanted buckling and to diminish the risks of falling. The knee can be flexed up to 175°.

The ankle prosthesis is the Trias prosthetic foot made of carbon fibre [47]. It is used by patients with moderate activity levels. It is a passive ankle because it does not use any actuator to improve the gait quality. However, two springs are further added to approach a healthy motion of the ankle joint. They can absorb, damp and return energy at the same time. The global design of this transfemoral prosthesis allow the user to walk at different speeds and on different surfaces. The connexion between the two parts of the prosthesis is a simple rod. No transfer of mechanical energy between the knee and the ankle is possible.

Figure 1.17: 3R60 transfemoral prosthesis from Ottobock [46]

1.3.2 Transfemoral prostheses with energy transfer

Nowadays, new transfemoral prostheses attempt to include an energy transfer in their mechanisms. They try to make the prosthesis a complete device instead of a combination of modules. During the gait, a healthy knee dissipates energy while a healthy ankle generates it. Instead of wasting this energy, the knee can send it to the ankle through an appropriate mechanism. This energy transfer can reduce the global energy consumption by lightening the actuators load if it is made in the phase where the ankle needs this energy. This transfer must therefore be timed. Reducing the power consumption is a big deal because the autonomy of the prosthesis is one of the most important quality criteria of active systems [48].

An example of such a prosthesis with energy transfer is the CYBERLEGs-Alpha prosthesis [49]. It is the first transfemoral prosthesis created in the framework of the CYBERLEGs project (see in Appendix C). It uses an active ankle prosthesis and a passive knee prosthesis coupled through an innovative energy transfer system between both.

Figure 1.18: CYBERLEGs-Alpha [49]

The ankle is a variation of the MACCEPA-design (explained in section 1.1.3.2), i.e a variable stiffness actuation system [26]. The knee consists of two springs in series (a baseline spring and a weight-acceptance spring) and two locking mechanisms. All springs and locking mechanisms can be activated and used at different phases of the gait.

The energy transfer system is made of a cable between the two parts and can be locked or unlocked at specific times during the gait cycle. Two pulleys guide the cable from a ratchet in the knee to the lever arm in the ankle. The resulting torque in the ankle is then the product between the moment arm length and the tension force in the cable. The motor power consumption in the ankle system is thus reduced thanks to this energy transfer system, as seen in Figure 1.19. The limitations of this design is that the user can neither climb stairs nor realize the sit-to-stand motion. This is due to the lack of actuator in the knee mechanism.

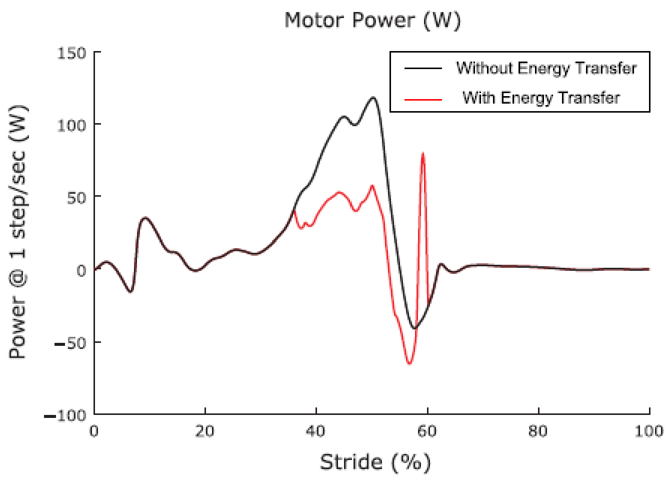

Figure 1.19: Results of the energy transfer [50]

CHAPTER 2
CYBERLEGS-BETA PROSTHESIS

The CYBERLEGs-Beta prosthesis is the transfemoral prosthesis that was more thoroughly analysed in this thesis. In this chapter, its principle will be explained in details so that the dynamical analysis performed in chapter 4 makes sense to the reader. This chapter is mostly adapted from [4] and [50], i.e. the papers describing this design with a lot of details.

The CYBERLEGs-Beta prosthesis, represented in Figure 2.1, is a new active transfemoral prosthesis built with an active knee mechanism and an active ankle mechanism. Its predecessor, the CYBERLEGs-Alpha prosthesis, described in section 1.3.2, was built with a passive knee and an active ankle prosthesis. It uses the same energy transfer system as the Alpha version. A description of the CYBERLEGs project is done in Appendix C.

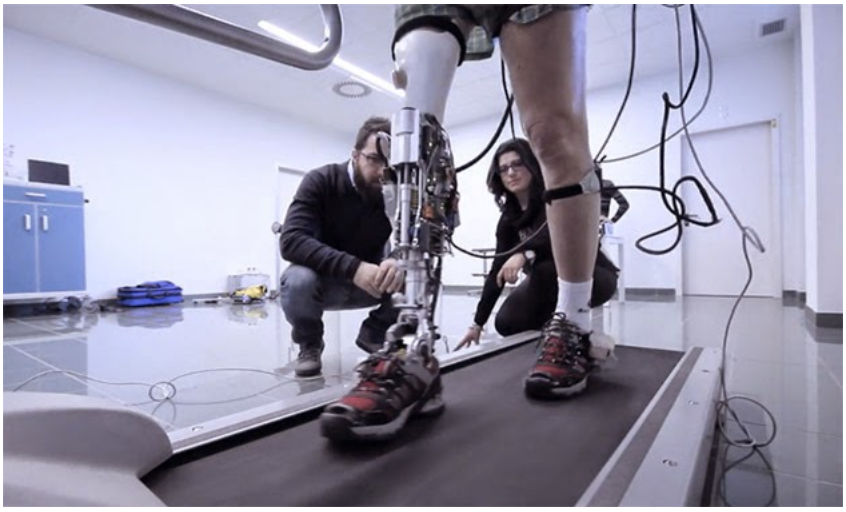

Figure 2.1: The CYBERLEGs-Beta prosthesis [4]

The point of adding an active module to the knee mechanism is to allow the user to climb stairs and to perform sit-to-stand motions, as displayed in Figure 2.2.

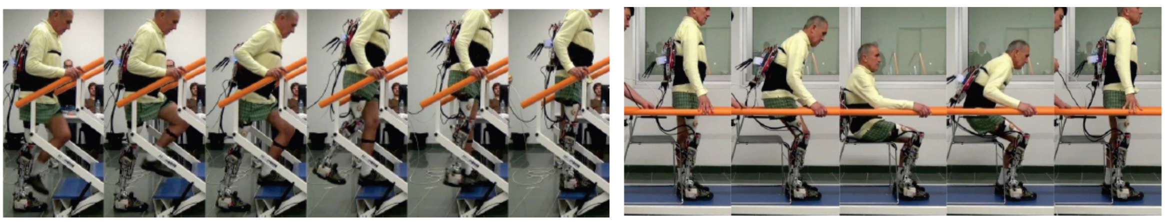

Figure 2.2: Subjects performing two different motions with the prosthesis [4]

2.1 Knee mechanism

The knee mechanism is by itself a new design of knee prostheses. A schematic of this system is provided in Figure 2.3. Unlike its predecessor, it is an active prosthesis which can potentially track as much as possible the kinematic and dynamic behaviour of a healthy knee. The actuator allows to perform energy-consuming tasks if necessary.

It couples two different systems in order to produce the torques required for the gait:

- A weight acceptance mechanism
- A knee drive system

Both mechanisms produce forces thanks to springs and these are linked to the knee joint through a moment arm that converts them into torques. The combination of these two systems allows to approach a healthy knee dynamic.

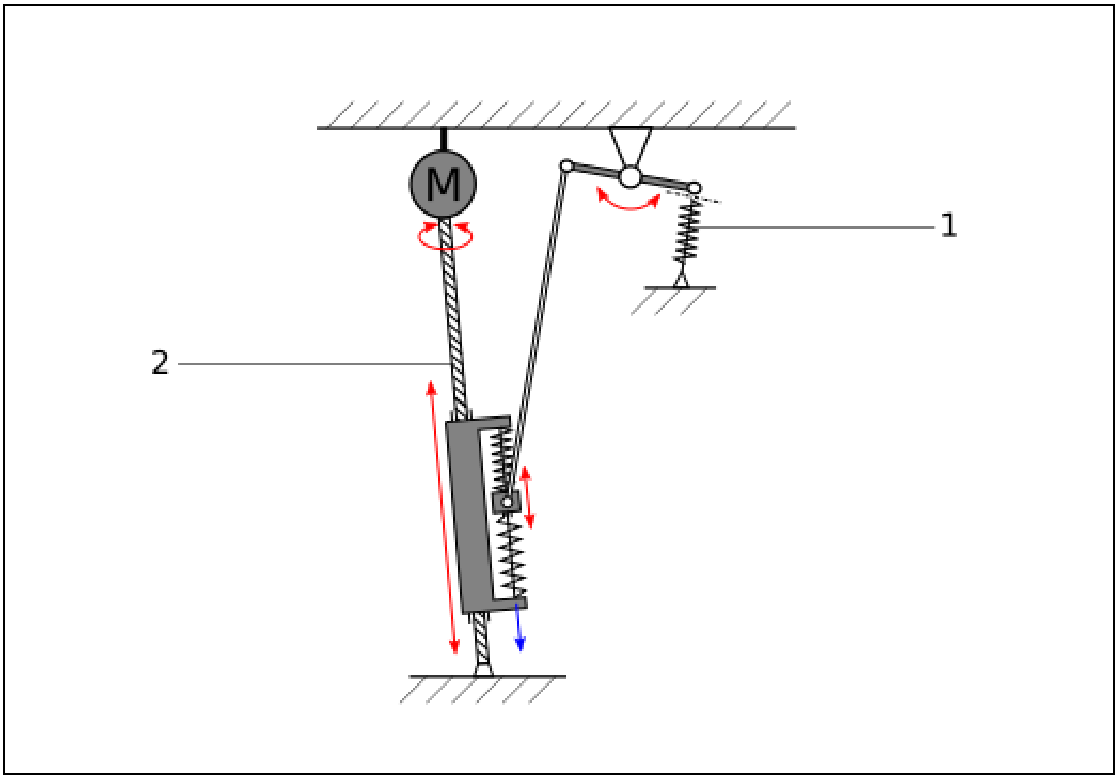

Figure 2.3: Schematic of the knee prosthesis, inspired from [4]. The part 1 is the weight acceptance system and the part 2 is the knee drive system. The base is the housing of the prosthesis. The red arrows show the motion of the joints. The blue arrow shows the energy transfer direction.

2.1.1 Weight acceptance mechanism

The first phase of a normal gait cycle is the stance flexion phase. The whole weight of the body is applied to the limb. During that period, the knee must not bend and carry all that weight in an efficient manner.

This is where the weight acceptance mechanism does its job. This system is mainly composed of a high stiffness spring. The purpose of this spring is to generate a large force whenever the knee tries to bend. This force is converted into a torque preventing the knee flexion.

However, during the swing phase, the knee should flex with no restriction. The weight acceptance system must therefore be disengaged. To do so, the spring is attached on a support that can move along a non-backdrivable screw. A DC motor controls this non-backdrivable screw to engage or disengage the weight acceptance spring. The screw is non-backdrivable so that the spring does not get disengaged when it is under load.

The weight acceptance system is shown in Figure 2.4. The flexion motion of the knee joint and the force opposed to it are explicit in the Figure. The red arrow represents the (dis-)engaging motion of the spring. Note that the spring can obviously only work in compression. Also, when the mechanism is active, a flexion angle up to 10° is possible before starting to push on the spring.

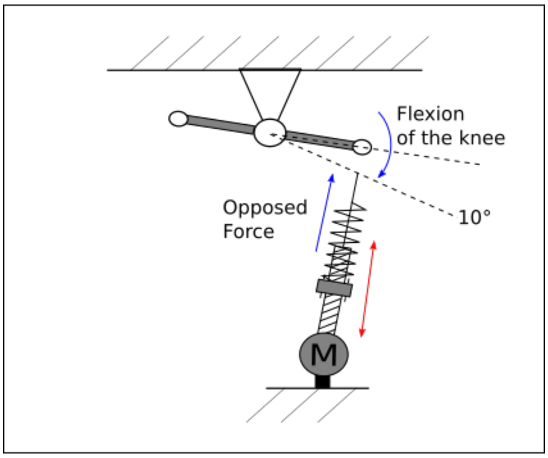

Figure 2.4: Schematic of the weight acceptance mechanism, inspired from [4]

2.1.2 Knee drive system

The knee drive system is based on a Series Elastic Actuation mechanism, described in section 1.1.3.1. Four springs are placed in series with a DC motor. They go by pairs that are symmetrical in the direction normal to the sagittal plane. The first pair of springs is the baseline springs and the second is the extension springs. They are placed on a carriage driven by the motor through a spindle. Between both pair of springs is placed a slider. The force created by the springs is converted into a torque around the knee joint through a connecting rod. It is important to add that these springs are independent and only work in compression: when the extension springs are engaged, the baseline springs stay at their free length and are not tensed.

Each pair of springs has a distinct role. The baseline springs combined with the motor make a series elastic actuation system. The energy used to damp the swing motion of the leg is stored into the baseline springs. This energy can then be transferred to the ankle, if the energy transfer mechanism is engaged. The motor is there to dissipate an eventual excess of energy or to provide more if needed or commanded by the controller.

The extension springs are the opposite of the baseline springs. Their function is to provide more energy when the device needs it, e.g. for stair climbing. The combination of these two sets of springs allow the device to generate torques with a magnitude up to ~75 Nm, depending on the knee angle.

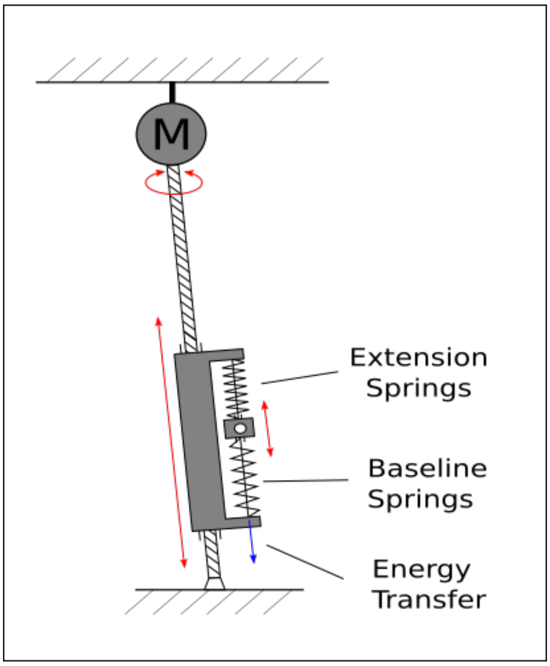

Figure 2.5: Schematic of the knee drive system, inspired from [4]

The schematic of the system is shown in Figure 2.5. The extension pair of springs and the baseline pair of springs are highlighted in the Figure. The direction of the energy transfer is also shown by the blue arrow. The rotation of the motor, the translation of the carriage along the spindle and the movement of the slider between the springs are displayed with double red arrows.

2.2 Ankle mechanism

The ankle mechanism was redesigned for the Beta prosthesis. It now consists of a combination of the MACCEPA architecture [26] and a parallel spring system. It is a Variable Stiffness Actuation (discussed in section 1.1.3.2) that offers a very simple mechanical design, which is designated by the number 1 in Figure 2.6.

The MACCEPA consists of two rigid linkages, the connecting rod and the moment arm (or crank), a slider and a linear spring. A DC motor is present at the top and drives the angle between the spring shaft (fixed on the foot) and the moment arm. The transmission between the motor and this MACCEPA angle is done through a bevel gears system. When this angle is modified, the moment arm and the connecting rod move as well. This motion compresses or decompresses the spring causing a reaction force. This force results in a torque in the ankle joint. This mechanism is used to produce the energy needed by the ankle during the gait.

The parallel spring system is fully passive. The slider moving along the spring shaft is connected to the housing with a rod. Therefore, the spring stores energy during the early phases of the stride and releases this energy later on. Being connected to the foot and the housing, the reaction force of the parallel spring is directly transformed into a torque in the ankle joint. This fully-passive torque causes the motor torque profile to reach smaller peaks.

The last part of the system is a lever arm attached to the ankle joint, which is connected to the energy transfer system. When the energy transfer cable is tensed, it pulls on this lever arm, creating a torque in the ankle joint.

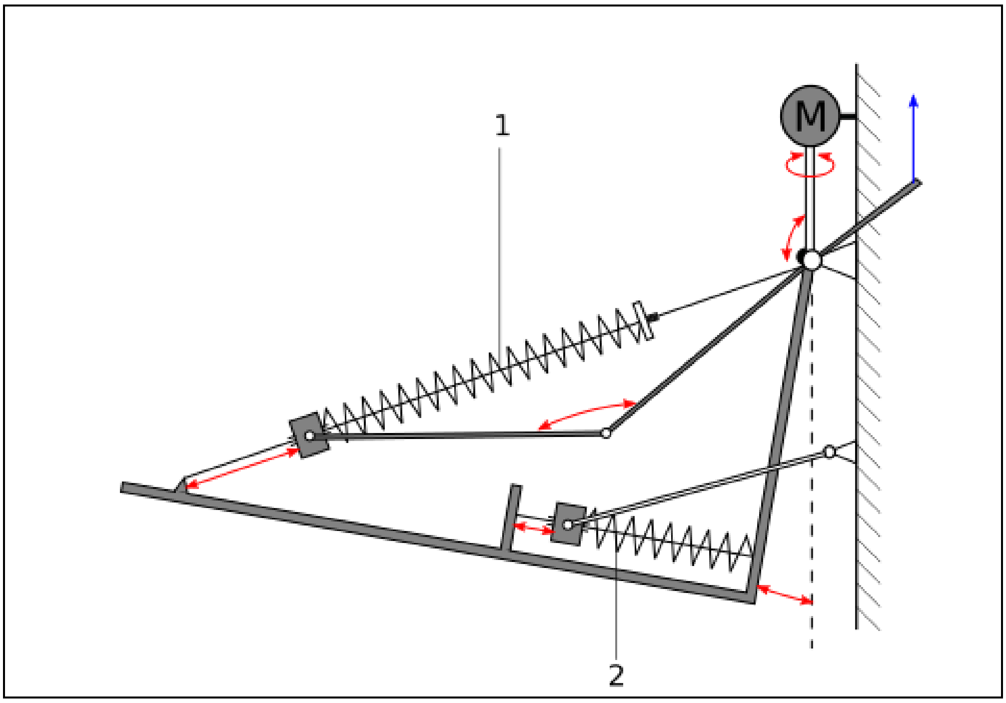

Figure 2.6: Schematic of the ankle mechanism, inspired from [50]. The part 1 is the MACCEPA system. The part 2 is the parallel spring system. The red arrows show the motions of the joints. The blue arrow is the energy transfer.

2.3 Energy transfer mechanism

As written in section 2.1, the knee dissipates energy and for a more efficient walk, this energy can be transferred to the ankle. This is the purpose of the energy transfer mechanism. It consists of a cable linking the knee carriage to the ankle joint. The cable is tensed by two pulleys, as seen in Figure 2.7. That way, when the baseline springs release the energy, they pull on the cable, which pulls on the lever arm, creating a torque in the ankle joint. This system can be engaged or disengaged, depending on the gait phases. To do so, the second pulley is moved downwards by a motor controlling a non-backdrivable screw. When disengaged, the cable is no longer tensed, and therefore the force cannot be transferred.

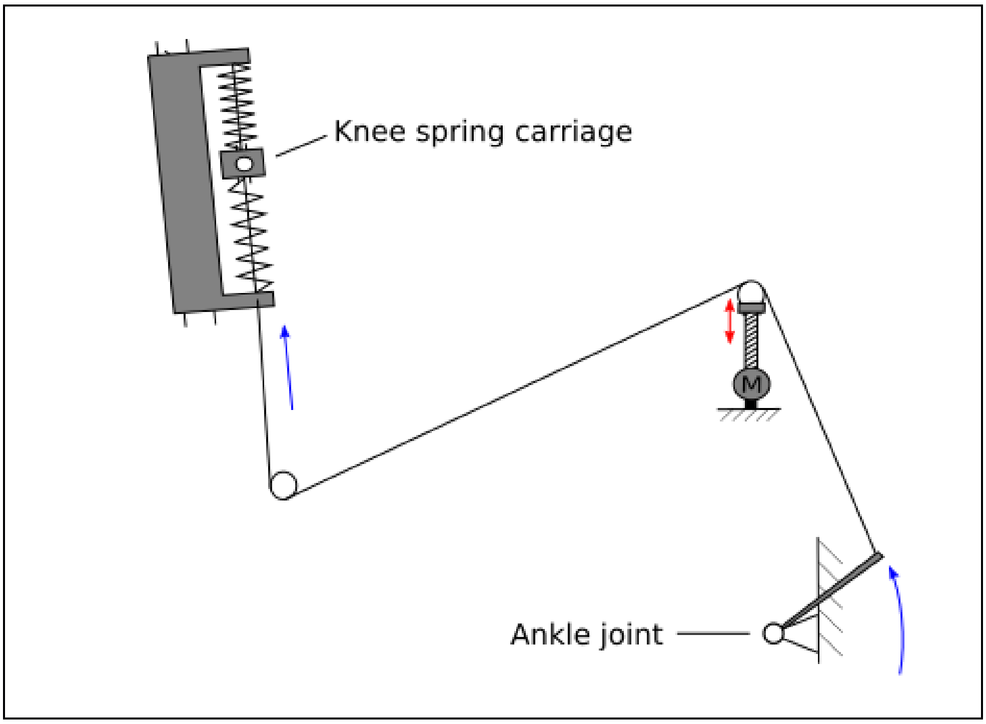

Figure 2.7: Schematic of the energy transfer mechanism, inspired from [5]. The red arrow represents the motion of the pulley when (dis-)activating the energy transfer.

CHAPTER 3

MULTIBODY MODELLING OF THE PROSTHESIS

To fulfil the objectives of the thesis, the main tool that was used is a multibody dynamic model of the CYBERLEGs-Beta prosthesis. It was developed using *Robotran*, which is a symbolic generator of multibody models. The principle of *Robotran* is described in Appendix E.

In the real prosthesis, there is energy being possibly transferred from the knee to the ankle, as explained in section 2.3. However, the energy transfer is still in development and subject to changes [4]. This is why it was decided to disregard its modelling in the present thesis. Consequently, the ankle and the knee do not communicate to each other in the multibody model, and both mechanisms can be separately modelled and analysed.

In the following sections, the ankle and the knee models are described and compared to the real mechanisms.

3.1 Modelling of the ankle

A first remark about this model is the fact that it is in two dimensions, i.e. does not take into account any motion that is not parallel to the sagittal plane. This is justified because there is no degree of freedom outside this plane.

The mere principle of *Robotran* is to divide mechanisms into a base, some bodies and some joints. The housing of the prosthesis was defined as the non-moving base of the model. The ankle was then divided into six bodies and five moving joints. The different bodies are shown in Figure 3.1 and are:

- The **foot**: including the plate, the fake foot, both springs and their shafts.
- The **crank**: including the two cranks as well as the bevel gear on their axis.
- The **connecting rod**: simply including both connecting rods.
- The **MACCEPA spring slider**: just including the MACCEPA spring slider.
- The **parallel spring slider**: including the parallel spring slider and the rod that links it to the housing.
- The **motor rotor**: including the motor rotating parts and the bevel gear at its output.

The five moving joints are shown in Figure 3.1 and are:

- The **ankle joint**: the motion of the foot with respect to the limb.
- The **MACCEPA joint**: the motion of the cranks. Constrained to the motor motion through the bevel gears.
- The **motor joint**: the motion of the motor rotor. Pilots the MACCEPA joint.
- The **moment arm joint**: the joint between the cranks and the connecting rods. The only free joint of the mechanism.
- The **MACCEPA spring joint**: the translation of the MACCEPA spring slider.
- The **parallel spring joint**: the motion of the parallel spring slider.

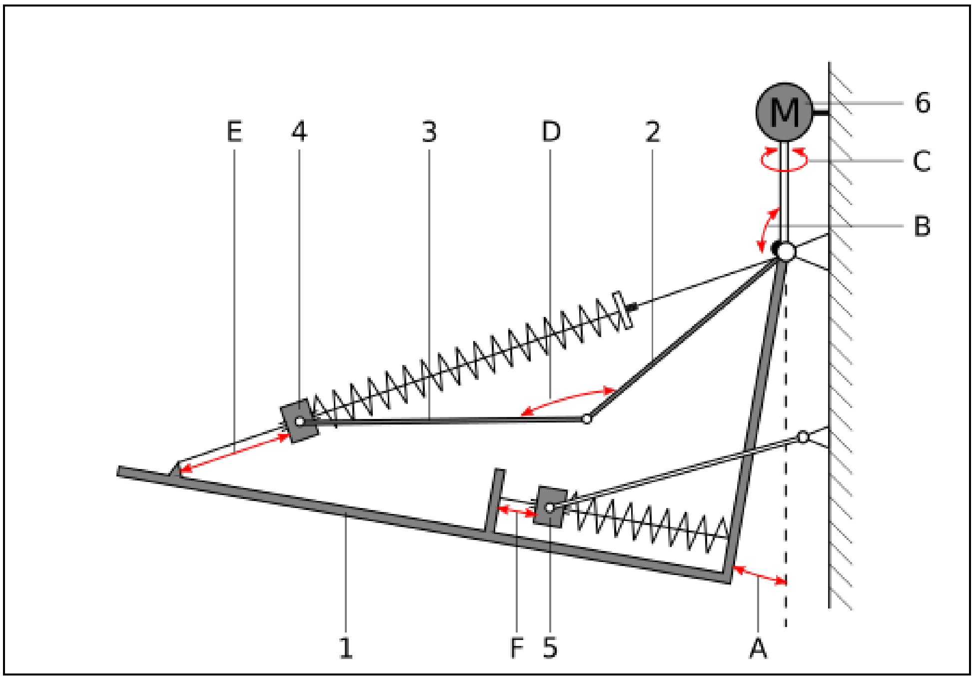

Figure 3.1: The different bodies and joints in the ankle model. **Bodies**: 1: Foot. 2: Crank. 3: Connecting rod. 4: MACCEPA spring slider. 5: Parallel spring slider. 6: Motor rotor. **Joints**: A. Ankle joint. B. MACCEPA joint. C. Motor joint. D. Moment arm joint. E. MACCEPA spring joint. F. Parallel spring joint.

The masses, centres of mass and moments of inertia of each bodies were either measured or approximated using the corresponding CAD files.

The magnitude of the forces in the spring joints were computed using the following formula:

$$F_{spring} = -K_{spring} \cdot (x - L_0) + B_{spring} \cdot \dot{x} \tag{3.1}$$

With x, being the position of the spring slider and L_0, the free length of the spring. The values of K_{spring}, the stiffness of the springs, are provided by the springs datasheets. $B_{spring} \cdot \dot{x}$ is the term that models the viscous damping in the springs and includes all other frictions in the joint as well, like the one coming from the bearings. As all springs only work in compression, the computed force is brought to zero if going into traction.

The losses for the motor and the gearing box, are modelled using the efficiency ratio coming from the corresponding datasheets.

The ankle multibody model is shown in Figure 3.2. The bodies and the joints previously described can be found in the schematic. The mechanism has two degrees of freedom for six joints. Four constraints were then added to the model. It is clear that the parallel spring joint is entirely dependent on the ankle joint. A rod cut was added to bring this constraint. The rod cut models the actual rod between the parallel spring slider and the housing. Also, the MACCEPA spring joint and the moment arm joint are dependent on the MACCEPA joint. A ball cut was added to ensure that the kinematic of the MACCEPA spring slider is equal to the one of the tip of the connecting rod. The model being in two dimensions, this brings two constraints (and not three). The last constraint was added by forcing the kinematic of the MACCEPA joint to be equal to the one of the motor joint (divided by the gear ratio, though).

There are two more elements in the model, but they are of little importance. The first one is a non-moving joint representing the angle between the foot and the MACCEPA spring shaft. The other is a joint between the base and the motor rotor body. This joint is constrained to be the exact opposite of the motor joint. That way, the rotor also moves with respect to the housing.

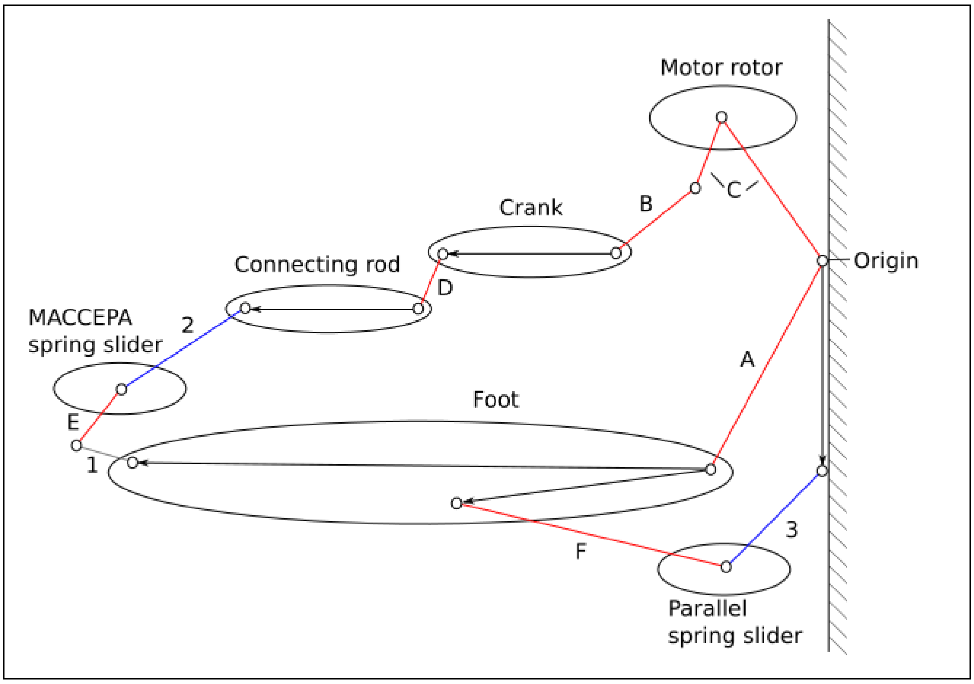

Figure 3.2: Multibody model of the ankle mechanism. **Joints**: A. Ankle joint. B. MACCEPA joint. C. Motor joint. D. Moment arm joint. E. MACCEPA spring joint. F. Parallel spring joint. **Other elements**: 1. Fixed angle between the foot and the MACCEPA spring shaft. 2. Ball cut that constraints the MACCEPA slider joint (E) and the moment arm joint (D) to the MACCEPA joint (B). 3. Rod cut that constraints the parallel spring joint (F) to the ankle joint (A).

3.2 Modelling of the knee

The model of the knee mechanism lies in two dimensions as well, i.e in the sagittal plane. The extension and baseline springs, that go by pairs in the real prosthesis are reduced to a single spring for each pair (with a doubled stiffness, logically).

The non-moving base of the model is once again the housing of the prosthesis. The rest of the model is composed of four bodies and four moving joints. They are shown in Figure 3.3. The four bodies are:

- The **knee pyramid**: including the upper-leg pyramid adapter and the piece moving around the knee joint.

- The **carriage**: including the spring carriage, the extension springs and the baseline springs.
- The **spring slider**: including the spring slider and the connecting rod that links it to the knee pyramid.
- The **motor rotor**: including the motor rotating parts, the gearbox and the spindle.

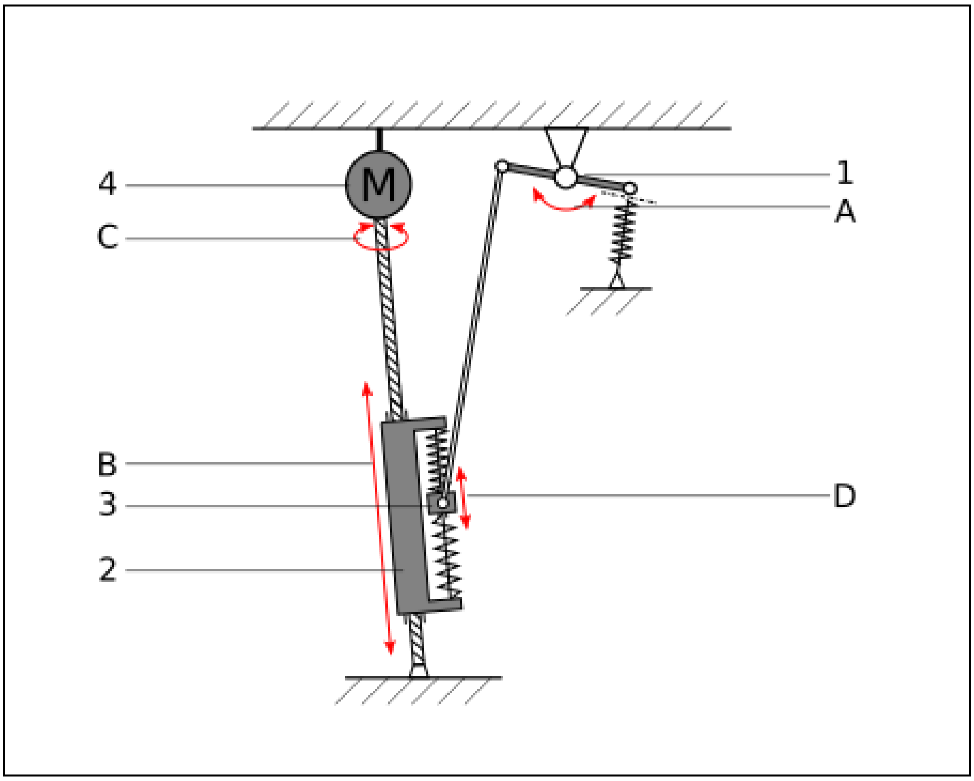

Figure 3.3: The different bodies and joints in the ankle model. **Bodies**: 1: Knee pyramid. 2: Carriage. 3: Spring slider. 4: Motor rotor. **Joints**: A. Knee joint. B. Carriage joint. C. Motor joint. D. Springs joint.

The four moving joints are:

- The **knee joint**: the motion of the leg with respect to the thigh.
- The **carriage joint**: the motion of the carriage along the spindle. Constrained to the motor motion through the spindle.
- The **motor joint**: the motion of the motor rotor. Pilots the carriage joint.
- The **springs joint**: the translation of the slider between the baseline and extension springs.

Most considerations that were made for the ankle are also applied to the knee model. The springs have also been modelled using Equation 3.1. The force produced by the extension springs is added to the one produced by the baseline springs. The gearbox and motor efficiencies are taken into account as well.

The multibody model of the knee is shown in Figure 3.4. The bodies and joints described above can be observed in this schematic. The mechanism also has two degrees of freedom, but for four joints. Two constraints have thus been added to the model. The first constraint simply links the carriage joint to the motor joint through the transmission ratio, which is the combination of the gear ratio and the spindle thread. The second constraint is the rod that represents the real connecting rod between the knee pyramid and the spring slider. The distance between the spring slider and the attachment point of the rod on the knee is maintained constant by the model.

Another important element of the model is the weight acceptance mechanism modelling. It is represented by a force that is applied to the knee pyramid. This force is calculated using the current position and velocity of the knee joint. If this position is above 10°, the spring begins to work in compression. The force is then computed using Equation 3.1 as for the other springs. The weight acceptance mechanism can be engaged or disengaged in the real prosthesis. This was modelled by using a simple boolean that multiplies the computed force.

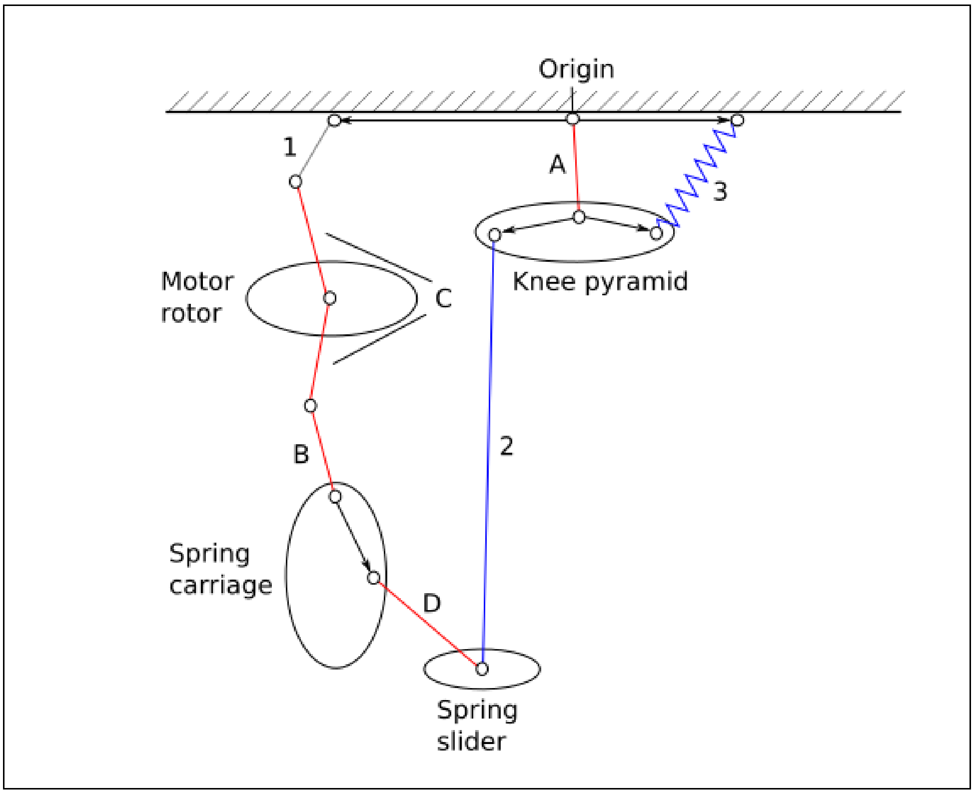

Figure 3.4: Multibody model of the knee mechanism. **Joints**: A. Knee joint. B. Carriage joint. C. Motor joint. D. Springs joint. **Other elements**: 1. Inclination angle between the motor axis and the limb axis. 2. Rod cut that constraints the springs joint (C) to the knee joint (A) and the carriage joint (B). 3. Link force that models the Weight Acceptance mechanism.

The last two elements of the model are details. There is a non-moving joint that represents the inclination angle between the motor axis and the limb axis. The other is a joint placed before the motor rotor, that is equal to the opposite of the motor joint in order to make the motor moving with respect to the base.

CHAPTER 4 QUASI-STATIC AND DYNAMIC MODEL ANALYSIS

In this chapter, the quasi-static and dynamic behaviour of the mechanisms are analysed. First, the quasi-static analysis sets all joints velocities and accelerations to zero and observes the forces and torques in the joints depending solely on their position. Then, the dynamic analysis imposes the same positions but takes the corresponding velocities and accelerations into account. The goal of the dynamic analysis is to determine the order of magnitude of the dynamical effects in the joints for a certain stride duration. Then, the relevant differences between both analysis will be highlighted. The quasi-static analysis is based on [5]. On the other hand, as explained earlier, the dynamic analysis and its comparison with the quasi-static analysis is one of the contribution of this thesis.

The prosthesis is designed to match the Winter's healthy limb dynamic [50][4]. David Winter's healthy gait refers to normative data about the torques and trajectories of the joints of a human walking at a normal speed [51]. In this thesis, this data is used for the ankle and the knee. The Winter's torque and angle in function of the stride progression for the ankle joint are shown in Figure 4.1 and in Figure 4.2 for the knee. More details about the biomechanics of the gait can be found in Appendix D.

Winter's data takes the dynamic of the lower limb and the contact with the environment into account. Also, the weight of the prosthesis is comparable to the weight of a human leg [50]. Therefore, all the following torques were included into the Winter's torques in the simulations: torques due to the motion of the prosthesis, torques due to gravity, torques due to the contact foot-ground and torques coming from the thigh. This justifies the choice of the housing of the prosthesis as non-moving base for the multibody models. Indeed, the dynamic of this housing is included in the Winter's torque and therefore only the internal motions of the mechanisms need to be explicit in the model.

To reproduce the Winter's kinematic in the simulations (position, velocity and acceleration), the ankle and knee joints are driven as if a motor was controlling them. The torques in these joint resulting from the simulations represent the torques that such a motor should apply to maintain this kinematic. These are the torques that were compared with the Winter's torques.

In both simulations, as the electromechanical behaviours of the motors are not yet taken into account, the motor joints are directly driven in position. These positions were obtained using the results of [5].

The dynamical analysis of the system is done by also considering the velocities and accelerations of each joint. Therefore, a stride duration must be chosen. It was fixed to 1s which corresponds to a natural cadence (120 steps per minute, 60 strides per minute) [51].

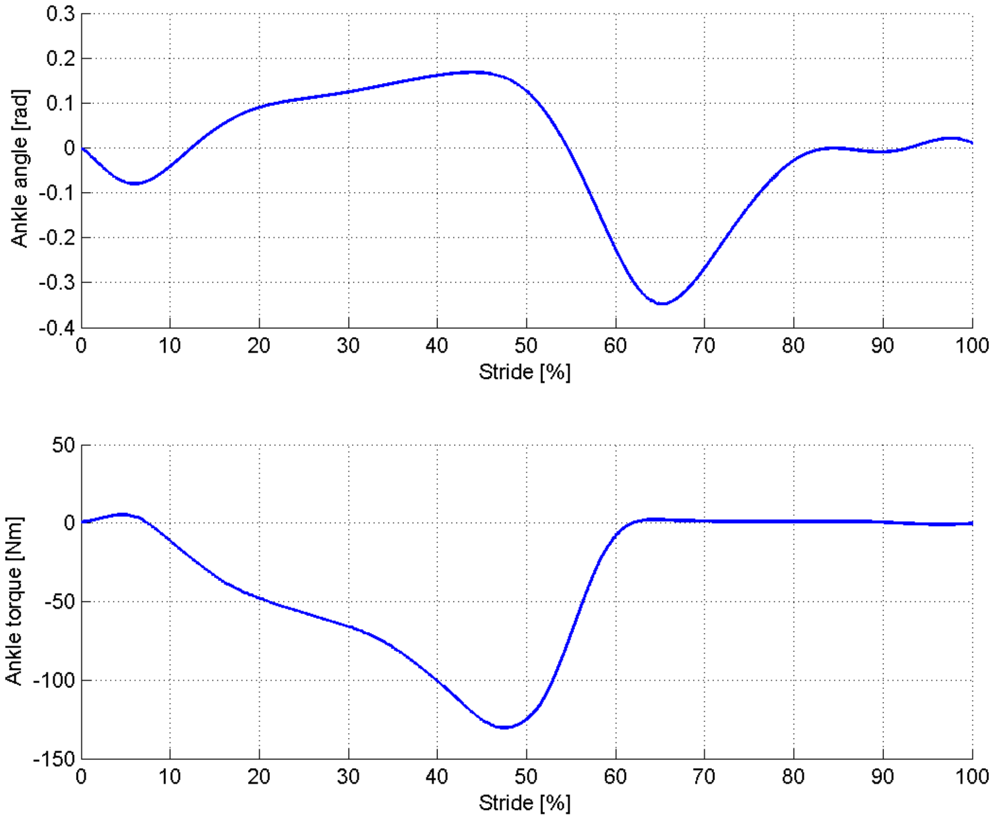

Figure 4.1: Winter's angle and torque for a healthy ankle.

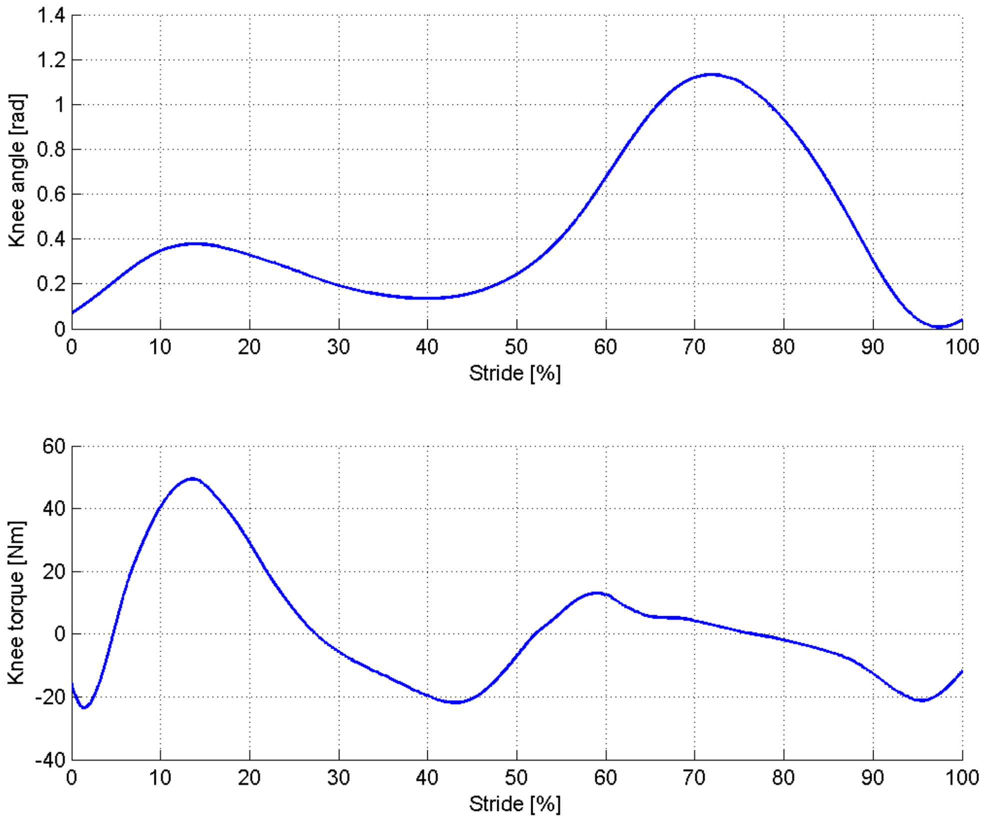

Figure 4.2: Winter's angle and torque for a healthy knee.

To understand the analysis performed in the next sections, it is useful to describe how *Robotran* decomposes the dynamic joint equations. This description is done in Appendix E. Both mechanisms have at least one kinematic loop. Therefore, to close these loops, algebraic constraints were added, as explained in chapter 3. As a reminder, here is the *Robotran* dynamic equation for joint i in such a closed-loop system:

$$M_i(q,t)\ddot{q}_i + c_i(q,\dot{q},t,F_{ext},L_{ext},g) = \mathcal{Q}_i + J_i^T\lambda(q,t) \tag{4.1}$$

with

- $M(q,t)$, the mass matrix of the system.
- $\ddot{q}$, the acceleration vector of the system.
- $c(q,\dot{q},t,F_{ext},T_{ext},g)$, the term that contains the Coriolis, centrifugal and gravity terms as well as the external forces and torques.
- $\mathcal{Q}$, the generalized joint forces vector.
- J, the Jacobian matrix of the constraints, see Appendix E .
- λ, the Lagrange multipliers associated to each constraint, see Appendix E .

In a nutshell, the term $M_i(q,t)\ddot{q}_i$ represents the forces or torques due to the acceleration of the bodies. $\mathcal{Q}_i$ is the force or torque brought by either a spring, an actuator or in the case of the ankle and knee joints, the Winter's torque. If the joint is free, this term is zero. The term $J_i^T\lambda(q,t)$ represents the forces or torques applied on joint i due to the constraints [52]. These algebraic constraints are there either to close a kinematic loop or to link a joint to another (representing a mechanical transmission). Each constraint is associated with a Lagrange multiplier λ. Multiplying this λ with the corresponding Jacobian term gives the force or torque in any joint due to this constraint. Finally, $c(q,\dot{q},t,F_{ext},T_{ext},g)$ contains the rest of the forces and torques.

In the specific case of the quasi-static analysis, the velocities, accelerations and all time-dependent terms are equal to zero. Gravitational terms are included in Winter's torque. Therefore, the joint equation becomes:

$$c_i(q,F_{ext},L_{ext}) = \mathcal{Q}_i + J_i^T\lambda(q) \tag{4.2}$$

From now, the analysis differs for each mechanism. They are thus separately handled in the following sections.

4.1 Ankle

4.1.1 Quasi-static analysis

In the quasi-static model, the torques applied to the ankle joint come from two sources. Either from the MACCEPA spring or the parallel spring. They are contained in the $J^T\lambda(q)$ part of the joint equation. $c(q,F_{ext},T_{ext})$ is null here because there is no external forces or torques. Therefore, the ankle joint equation can be rewritten from Equation 4.2 as:

$$0 = T_{ankle} + J_{a,r}\lambda_r(q) + J_{a,b}\lambda_b(q) \tag{4.3}$$

With $J_{a,r}$, the Jacobian term linking the connecting rod constraint of the parallel spring to the ankle joint and $J_{a,b}$, the Jacobian term linking the ball cut constraint of the MACCEPA spring to the ankle joint. The mathematical development of all the Jacobian terms as well as their geometrical meaning can be found in Appendix B.2.

The quasi-static equation of the parallel spring joint is:

$$0 = F_{para} + J_{p,r}\lambda_r(q) \tag{4.4}$$

With F_{para}, the force provided by the parallel spring and $J_{p,r}$, the Jacobian term linking the rod cut constraint to the parallel spring joint. The quasi-static equation of the MACCEPA spring joint is quite similar and is given by:

$$0 = F_{MACCEPA} + J_{M,b}\lambda_b(q) \tag{4.5}$$

With $F_{MACCEPA}$, the force provided by the MACCEPA spring and $J_{M,b}$, the Jacobian term linking the ball cut constraint to the MACCEPA spring joint.

By isolating $\lambda_r(q)$ in Equation 4.4 and $\lambda_b(q)$ in Equation 4.5 and substituting them in Equation 4.3, the ankle joint equation can be rewritten as:

$$T_{ankle} = \kappa_r \cdot F_{para} + \kappa_b \cdot F_{MACCEPA} \tag{4.6}$$

with $\kappa_r = J_{a,r}/J_{p,r}$ and $\kappa_b = J_{a,b}/J_{M,b}$. This equations clarifies the fact that the ankle torque is the sum of the contributions from the MACCEPA spring and the one from the parallel spring. Imposing the right positions in order to make T_{ankle} equal to the Winter's healthy ankle torque, Figure 4.3 is obtained.

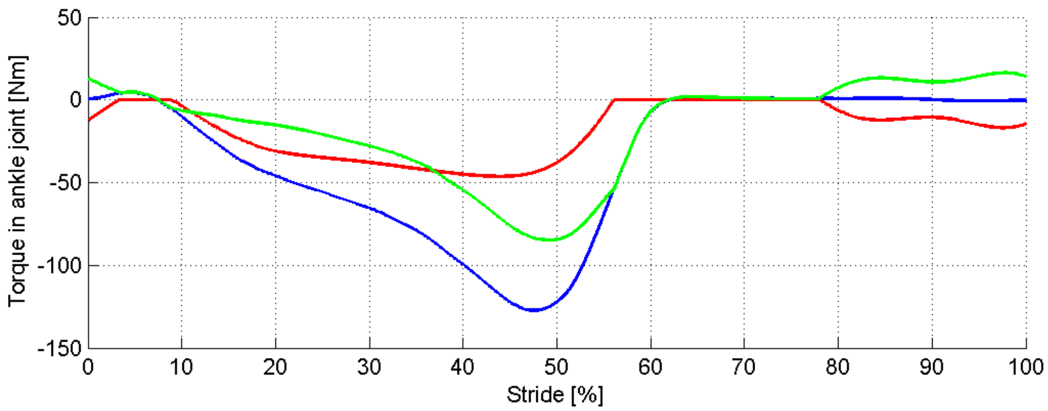

Figure 4.3: Evolution of the torque in the ankle joint. The blue line is the Winter's torque T_{ankle}. The red line is the parallel spring contribution $\kappa_r \cdot F_{para}$. The green line is the MACCEPA spring contribution $\kappa_b \cdot F_{MACCEPA}$.

This Figure illustrates nicely how the parallel spring helps to reduce the peak torque of the MACCEPA.

The relationship between the motor torque and the force in the MACCEPA spring has already been calculated [50] and is given by :

$$T_{motor} = \rho \cdot [B\,cos(\alpha) + A\,[1 - (\frac{B}{A}\,sin(\alpha))^2]^{1/2}] \cdot \frac{B\,sin(\alpha)\,F_{MACCEPA}}{A[1 - (\frac{B}{A}\,sin(\alpha))^2]^{1/2}]} \tag{4.7}$$

With A, the length of the connecting rod, B, the length of the crank and α, the angle between the crank and the MACCEPA spring shaft, as shown in Figure 4.4. ρ is the transmission ratio between the motor and the MACCEPA joint. With $A = B$, it gets simplified to:

$$T_{motor} = 2 \cdot \rho \cdot A \cdot sin(\alpha) \cdot F_{MACCEPA}$$

Therefore, the following quasi-static relationship between the torque motor and the ankle joint torque concludes this analysis:

$$T_{motor} = \frac{\kappa_M}{\kappa_b} \cdot (T_{ankle} - \kappa_r F_{para}) \qquad (4.8)$$

With $\kappa_M = 2 \cdot \rho \cdot A \cdot sin(\alpha)$. If this relationship holds when the dynamic effects are taken into account, then it could be used to control the motor. This is covered in the next section.

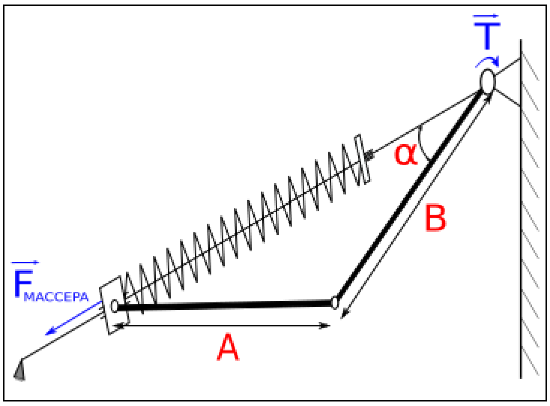

Figure 4.4: Schematic of the MACCEPA system.

4.1.2 Dynamic analysis

In the dynamic analysis, the velocities and accelerations are considered different from zero and correspond to a stride duration of one second. The equation of the ankle joint is rewritten as:

$$M(q,t)\ddot{q} + c(q,\dot{q},t) = T_{ankle} + J_{a,r}\lambda_r(q) + J_{a,b}\lambda_b(q) \qquad (4.9)$$

Using the same positions that produce the Winter's torque in T_{ankle} in the quasi-static analysis, Figure 4.5 is obtained.

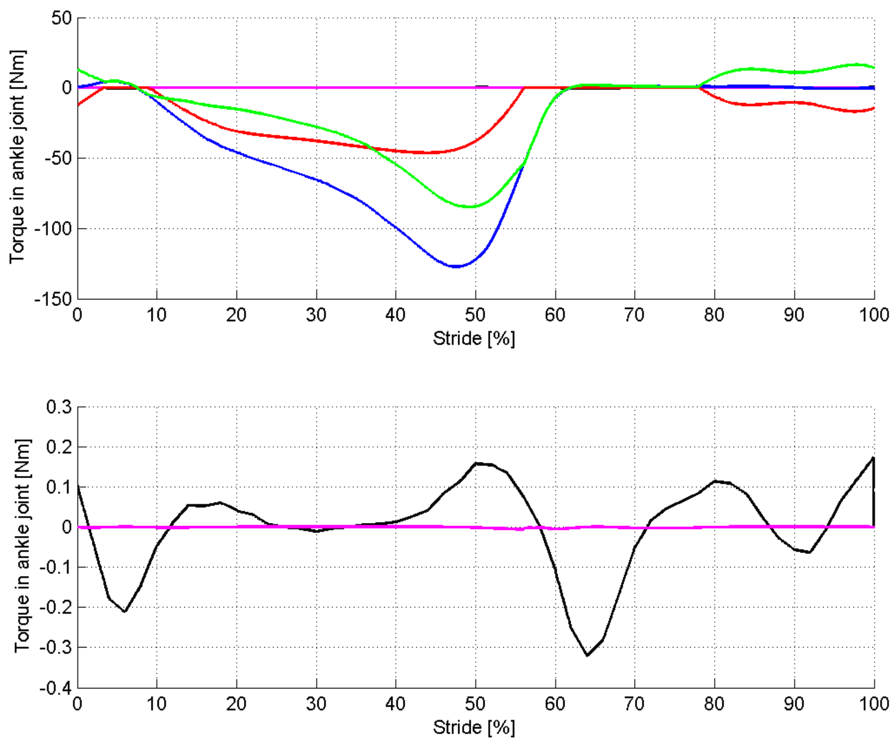

Figure 4.5: Evolution of the torque in the ankle joint. The blue line is the Winter's torque. The red line is the parallel spring contribution. The green line is the MACCEPA spring contribution. The second graphs zooms on $M(q,t)\ddot{q}$ and $c(q,\dot{q},t)$. The black line is $M(q,t)\ddot{q}$ and the magenta line is $c(q,\dot{q},t)$.

So, for a stride duration of one second, the torques due to $M(q,t)\ddot{q}$ and $c(q,\dot{q},t)$ are two orders of magnitude smaller than the torques coming from the springs. Therefore, if the user performs a normal gait, these terms can be neglected in this joint for any calculation. The same process will now be applied on all the others joints.

In the parallel spring joint, the equation is:

$$M(q,t)\ddot{q} + c(q,\dot{q},t) = F_{para} + J_{p,r}\lambda_r(q) \quad (4.10)$$

These terms are expressed in Figure 4.7. $M(q,t)\ddot{q}$ and $c(q,\dot{q},t)$ are four orders of magnitude smaller than the spring force. Therefore, F_{para} and $J_{p,r}\lambda_r(q)$ are confounded in the graph. $M(q,t)\ddot{q}$ and $c(q,\dot{q},t)$ can also be neglected for a stride duration of one second.

In Figure 4.8, the same exercise is made for the MACCEPA spring joint. A similar result is obtained as $M(q,t)\ddot{q}$ and $c(q,\dot{q},t)$ are also four orders of magnitude smaller than the MACCEPA spring force. The equation of this joint is given by:

$$M(q,t)\ddot{q} + c(q,\dot{q},t) = F_{MACCEPA} + J_{M,b}\lambda_b(q) \quad (4.11)$$

As $M(q,t)\ddot{q}$ and $c(q,\dot{q},t)$ are quite small as well, $F_{MACCEPA}$ appears confounded with $J_{M,b}\lambda_b(q)$. It means that for both spring mechanisms (parallel and MACCEPA), the torque transmitted to the ankle joint is only due to the springs.

Finally, in the motor joint, the equation can be written as:

$$M(q,t)\ddot{q} + c(q,\dot{q},t) = T_{motor} + J_{m,b}\lambda_b(q) \quad (4.12)$$

These different terms are shown in Figure 4.6

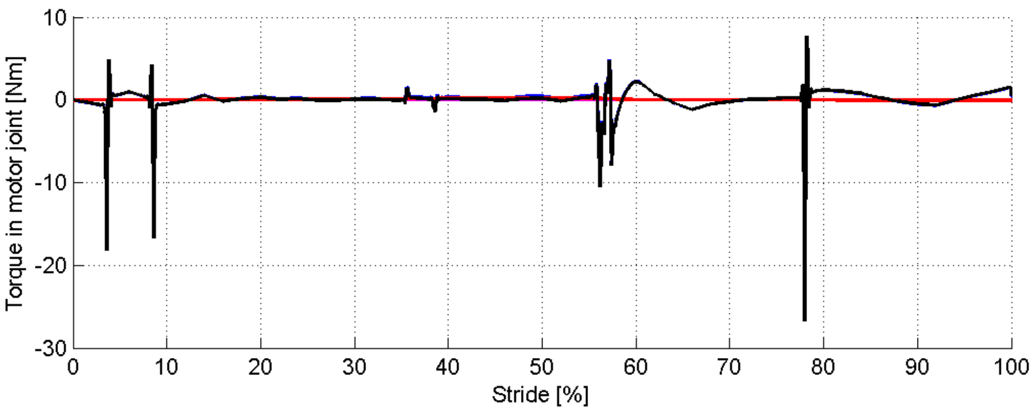

Figure 4.6: Evolution of the torque in the motor joint. The blue line is the torque provided by the motor T_{motor}, almost confounded with the red line $J_{p,r}\lambda_r(q)$. The black line is $M(q,t)\ddot{q}$ and the magenta line is $c(q,\dot{q},t)$.

$c(q,\dot{q},t)$ is also negligible here. However, the torque due to the accelerations is quite large. In fact, it can go up to a hundred times the load torque (due to the MACCEPA spring and represented by $J_{m,b}\lambda_b(q)$). Nevertheless, this is the result of the *inverse dynamics* module of *Robotran* in which the accelerations were imposed. The real motor is in reality not able to pull out such changes of angular momentum because of the large rotor inertia.

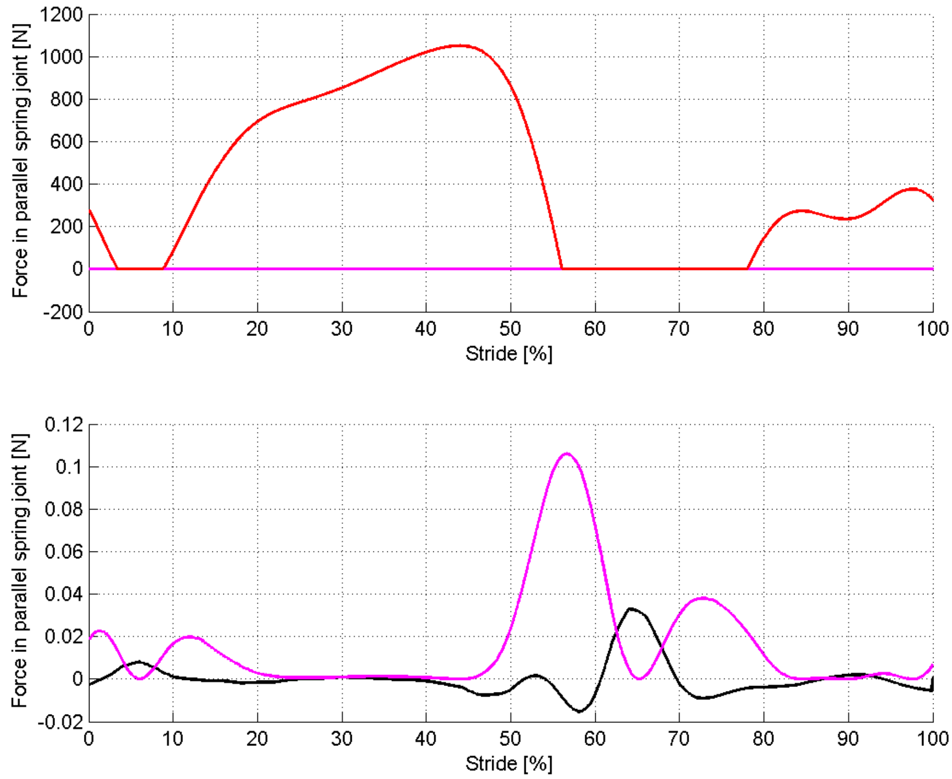

Figure 4.7: Evolution of the force in the parallel spring joint. The blue line is the spring force F_{para}, confounded with the red line $J_{p,r}\lambda_r(q)$. The second graphs zooms on $M(q,t)\ddot{q}$ and $c(q,\dot{q},t)$. The black line is $M(q,t)\ddot{q}$ and the magenta line is $c(q,\dot{q},t)$.

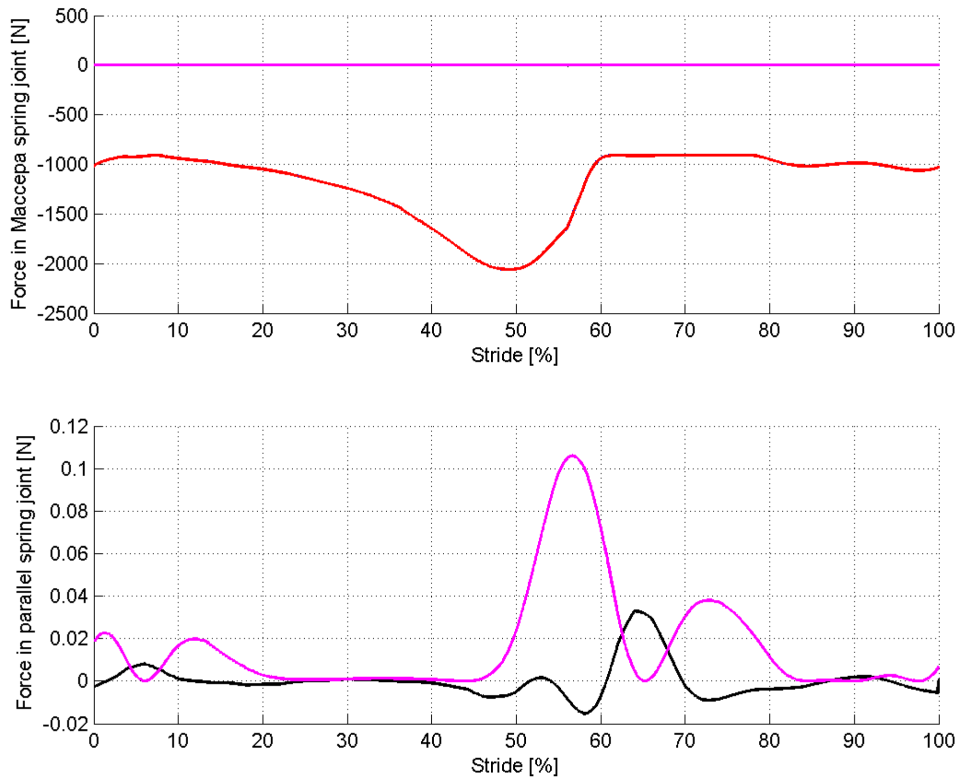

Figure 4.8: Evolution of the force in the MACCEPA spring joint. The blue line is the spring force $F_{MACCEPA}$, confounded with the red line $J_{M,b}\lambda_b(q)$. The second graphs zooms on $M(q,t)\ddot{q}$ and $c(q,\dot{q},t)$. The black line is $M(q,t)\ddot{q}$ and the magenta line is $c(q,\dot{q},t)$.

In chapter 5, an analysis of the capacities of the real motor regarding this trajectory is done. And these capacities are taken into account in the simulations done for the low-level controller described in the last chapters. In those, $M(q,t)\ddot{q}$ has the same order of magnitude than the load on the motor. The latter can thus not be neglected.

All in all, the only change due to dynamic effects in the quasi-static Equation 4.8 is the presence of the rotor inertial term. No dynamic effects in the MACCEPA spring joint means that $J_{m,b}\lambda_b(q)$ can be replaced by $\kappa_M \cdot F_{MACCEPA}$. The dynamic version of Equation 4.8 can then be written as:

$$T_{motor} = \frac{\kappa_M}{\kappa_b} \cdot (T_{ankle} - \kappa_r F_{para}) + M(q,t)\ddot{q} \tag{4.13}$$

The only significant term in $M(q,t)\ddot{q}$ being the acceleration of the motor rotor times its extended moment of inertia Θ_M, the equation can finally be simplified to:

$$T_{motor} = \frac{\kappa_M}{\kappa_b} \cdot (T_{ankle} - \kappa_r F_{para}) + \Theta_M \ddot{q}_{motor} \tag{4.14}$$

(With Θ_M taking the rotor moment of inertia into account, plus the moments of inertia of the gears and the cranks as seen by the motor (i.e. divided by ρ^2)).

4.2 Knee

4.2.1 Quasi-static analysis

In the quasi-static model, the torques applied on the knee joint come from two sources: from the weight acceptance mechanism and from the baseline and extension springs through the connecting rod. The weight acceptance torque comes from the external force applied on the knee pyramid, this term is thus contained in $c(q, F_{ext})$. The torque resulting from the baseline and extension springs force is contained in $J^T\lambda(q)$.

Therefore, the knee joint equation becomes from Equation 4.2:

$$T_{WA} = T_{knee} + J_{k,r}\lambda_r(q) \tag{4.15}$$

with T_{WA}, the torque resulting from the weight acceptance force, T_{knee}, the knee torque, $J_{k,r}$, the Jacobian term linking the rod cut constraint to the knee joint and $\lambda_r(q)$, the Lagrange multiplier associated with the rod constraint. In that case, its physical meaning is the force in the connecting rod divided by its length. As for the ankle, an explanation of these Jacobian terms can be found in Appendix B.2.

The quasi-static springs joint equation is:

$$0 = F_{springs} + J_{s,r}\lambda_r(q) \tag{4.16}$$

with $F_{springs}$, the sum of the extension and baseline springs forces and $J_{s,r}$, the Jacobian term linking the rod cut constraint to the springs joint.

Isolating $\lambda_r(q)$ in Equation 4.16, replacing the result in Equation 4.15 and finally isolating T_{knee} gives:

$$T_{knee} = T_{WA} - \kappa \cdot F_{springs} \tag{4.17}$$

with $\kappa = J_{k,r}/J_{s,r}$.

This equation highlights the fact that the resulting torque in the knee joint is indeed the sum of the weight acceptance torque and the torque resulting from the extension and baseline springs force. By setting T_{knee} to the Winter's torque for a healthy knee, Figure 4.9 is obtained for a whole stride. Once again, it can be observed that the parallel spring of the weight acceptance mechanism helps to reduce the peak torque of the SEA system.

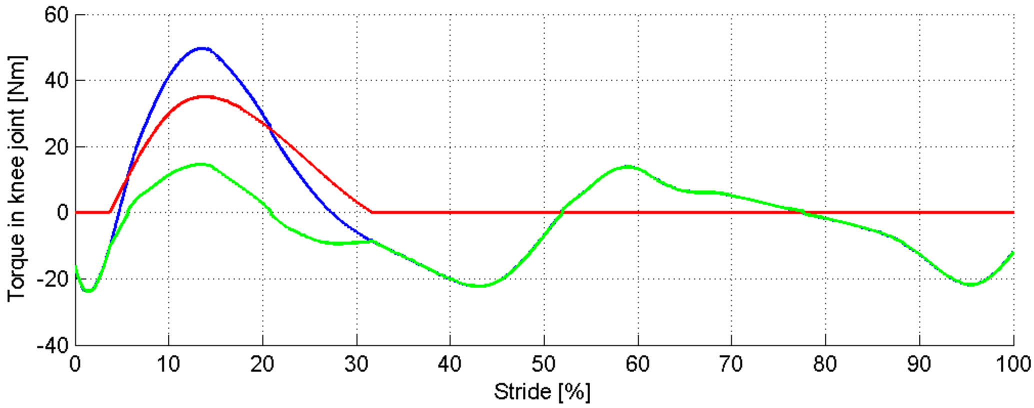

Figure 4.9: Evolution of the torque in the knee joint. The blue line is the Winter's torque. The red line is the weight acceptance torque. The green line is the torque coming from the baseline and extension springs.

The activation and deactivation of the weight acceptance mechanism appears quite clearly on the Figure. The torque that it produces sticks to zero when the mechanism is disengaged.

With the accelerations being 0, it appears clearly that the force in the carriage joint is equal to the force in the springs joint. The load torque applied on the motor is thus equal to this springs force multiplied by the transmission ratio between the carriage translation and the motor rotation:

$$T_{motor} = \rho \cdot F_{springs} \tag{4.18}$$

with ρ, this transmission ratio (gearbox and spindle combined). This finally leads to Equation 4.19, which links the desired knee joint torque to the motor torque output:

$$T_{motor} = \frac{\rho}{\kappa} \cdot (T_{WA} - T_{knee}) \tag{4.19}$$

If this relationship holds or not when the dynamical effects are taken into account is the subject of the next section.

4.2.2 Dynamic analysis

Here, the velocities and accelerations correspond to a stride duration of one second. The knee joint dynamical equation becomes:

$$M(q,t)\ddot{q} + T_{WA} = T_{knee} + J_{k,r}\lambda_r(q) \tag{4.20}$$

No body is attached to the knee pyramid through a normal joint. This means that there can neither be a Coriolis term nor a centrifugal term included in $c(q, \dot{q}, t, F_{ext}, L_{ext}, g)$. Therefore it stays equal to $c(q, F_{ext}) = T_{WA}$ in this equation. In Figure 4.10, all terms of this equation are shown.

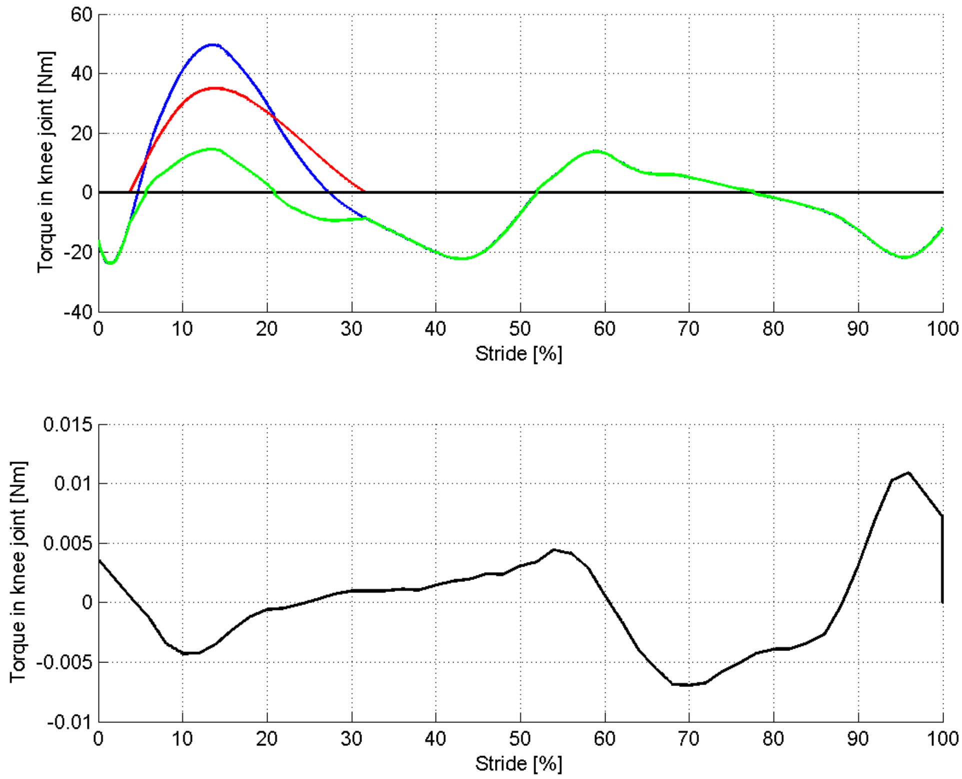

Figure 4.10: Evolution of the torque in the knee joint. The blue line is the Winter's torque T_{knee}. The red line is the Weight Acceptance torque T_{WA}. The green line is the torque coming from the Baseline and Extension springs $J_{k,r}\lambda_r(q)$. The black line is $M(q,t)\ddot{q}$. The second graphs zooms on $M(q,t)\ddot{q}$.

It can be observed that the contribution of $M(q,t)\ddot{q}$ to the knee joint torque is three orders of magnitude smaller than the other terms and plays thus no relevant role in the knee joint equation.

The springs joint dynamical equation becomes:

$$M(q,t)\ddot{q} = F_{springs} + J_{s,r}\lambda_r(q) \tag{4.21}$$

$c(q,\dot{q},t,F_{ext},L_{ext},g)$ is zero in this joint equation because there are no external forces or torques and there are no centrifugal and Coriolis forces because the spring joint is on the same axis than the carriage joint.

The contribution of each of these terms on the joint force are shown in Figure 4.11. It is observed that $M(q,t)\ddot{q}$ is also really small compared to the other terms. It is therefore negligible.

In the motor joint, the joint dynamic equation becomes:

$$M(q,t)\ddot{q} = T_{motor} - \rho \cdot J_{c,r}\lambda_r(q) \tag{4.22}$$

with $J_{c,r}$, the Jacobian term linking the rod constraint to the carriage joint. $c(q,\dot{q},t,F_{ext},L_{ext},g)$ is null for the same reasons than in the springs joint. The carriage moving on the same axis as the springs, $J_{c,r} = J_{c,s}$. By isolating λ_r in Equation 4.20 and replacing it in Equation 4.22, the joint equation can then be rewritten as:

$$T_{motor} = \frac{\rho}{\kappa} \cdot (T_{WA} - T_{knee}) + M\ddot{q} \tag{4.23}$$

As only the motor acceleration times the rotor extended moment of inertia is relevant in $M\ddot{q}$, the equation can finally be changed to:

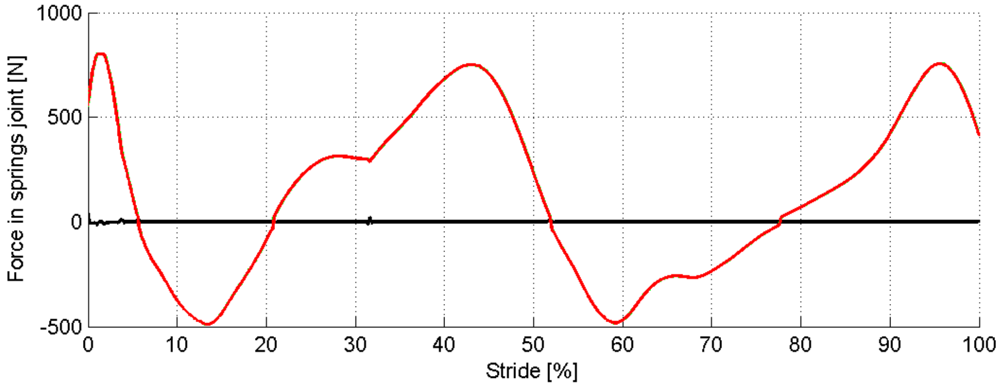

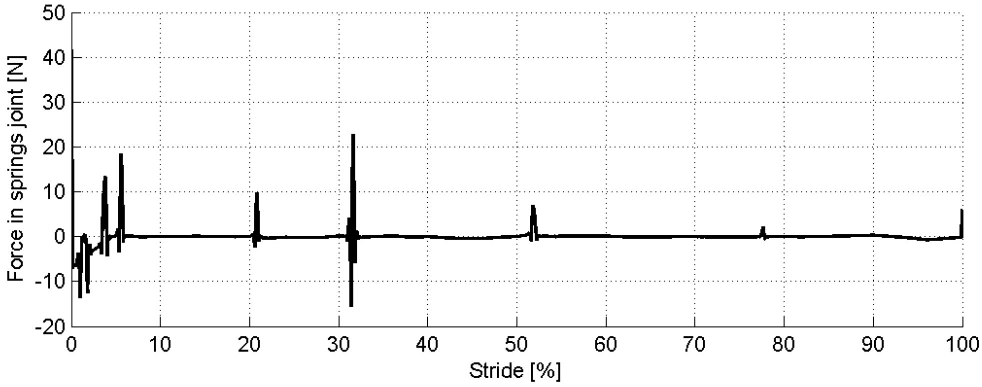

Figure 4.11: Evolution of the forces in the springs joint. The red line is the joint force $F_{springs}$. The green line is the force transmitted to the knee pyramid through the connecting rod $J_{s,r}\lambda_r(q)$, confounded with the red line because they are almost equal. The black line is $M(q,t)\ddot{q}$. The second graphs zooms on $M(q,t)\ddot{q}$

$$T_{motor} = \frac{\rho}{\kappa} \cdot (T_{WA} - T_{knee}) + \Theta_M \ddot{q}_{motor} \tag{4.24}$$

Θ_M is the extended motor rotor inertia, i.e. the motor moment of inertia plus the moment of inertia of the gearbox and the spindle as well as the mass of the carriage (as seen by the motor).

The contribution of the terms of Equation 4.24 are shown in Figure 4.12.

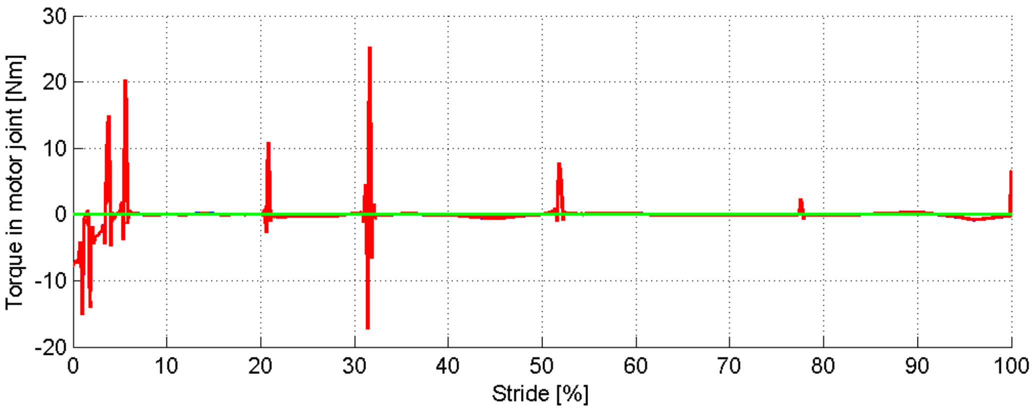

Figure 4.12: Evolution of the torques in the motor joint. The confounded blue and red lines are the motor torque T_{motor} and $\Theta_M \ddot{q}_{motor}$ respectively. The green line is the load torque $T_{load} = \frac{\rho}{\kappa} \cdot (T_{WA} - T_{knee})$.

The motor accelerations that are demanded are far too high, the resulting $\Theta_M \ddot{q}_{motor}$ is three orders of magnitude higher than $T_{load} = \frac{\rho}{\kappa} \cdot (T_{WA} - T_{knee})$. This problem will be addressed in chapter 5.

CHAPTER 5

ACTUATOR DIMENSIONING

In chapter 4, the trajectories of the motor and the joints constrained to them (through a gearbox or a spindle) were imposed in order to perfectly match the Winter's torque at the ankle/knee joints. In fact, this torque is the ideal output of the system but it is clear that it might not be perfectly matched when it comes to use a real motor. Indeed, is was observed in chapter 4 that the motor accelerations could be huge and unreachable by a actual DC motor. Such changes of the angular momentum of the rotor require tremendous torques. These torques are out of reach for the motors currently in use by the real prosthesis.

To investigate on this problem, the electromechanical model of the real motors were added to the current models. It is based on the conventional equations for DC motors, which are:

$$U(t) = L\,\frac{d}{dt}i(t) + R\,i(t) + k\phi\,\dot{q}(t) \tag{5.1}$$

$$T_{em}(t) = k\phi\,i(t) \tag{5.2}$$

With $U(t)$, the voltage applied to the motor, L, the terminal phase-to-phase inductance, R, the terminal phase-to-phase resistance, $i(t)$, the current flowing through the rotor conductors, $k\phi$, the torque constant of the motor, $\dot{q}(t)$, the angular velocity of the rotor and $T_{em}(t)$, the electromechanical torque produced by the motor. L, R and $k\phi$ are characteristic parameters of the motors and found in their datasheets (see Appendix F).

No viscous damping (K_v) is considered in the rotor joint because it can be neglected for such small machines. Therefore, the electrical time constant is considered really smaller than the mechanical time constant as shown in Equation 5.3:

$$\frac{L}{R} = \tau_e \ll \tau_m = \frac{J}{K_v} \sim \infty \tag{5.3}$$

Therefore, in order to lighten the computation loads of the simulations, Equation 5.1 can be simplified to:

$$U(t) = R\,i(t) + k\phi\,\dot{q}(t) \tag{5.4}$$

Then, a simple PI controller for the motor position was added to this model. The reference positions were the ones used in chapter 4. The controller gains were tuned to find the best results. The goal of these simulations is to check, whether or not, the motors are able to approach the desired trajectory in a satisfying manner and if the output torques in the ankle/knee joint are acceptable or not.

5.1 Ankle motor

The motor currently in use for the ankle mechanism is the *Maxon EC-4pole 30*, with a diameter of 30mm and a power of 200W. Its datasheet can be found in Appendix F. It is coupled to a gearbox with a reduction ratio of 33:1 and then to a bevel gear system with reduction 10:1 to redirect its rotating axis from the vertical axis to the ankle axis.

The result of the simple PI control is shown in Figure 5.1:

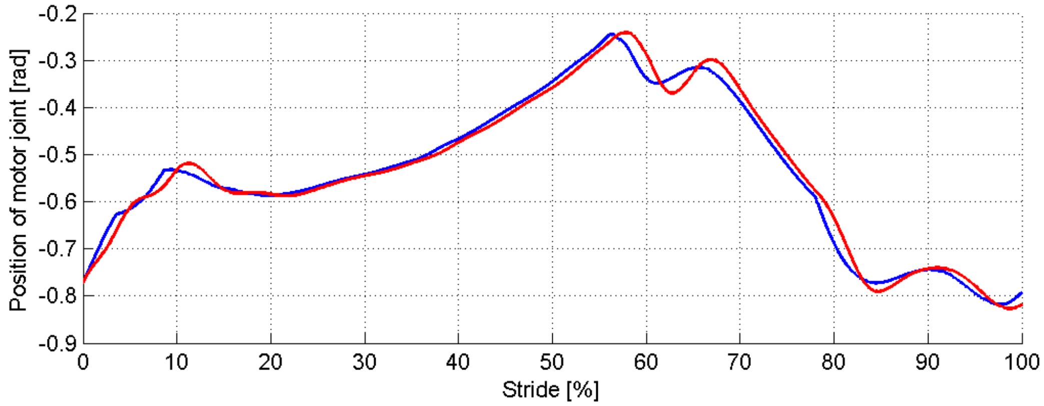

Figure 5.1: Evolution of the position of the motor joint. The blue line is the reference position used in chapter 4. The red line is the position tracking the reference.

It looks like the motor is able to track the desired position with this position controller. The resulting torque in the ankle joint is also quite close to the Winter's torque, as seen in Figure 5.2:

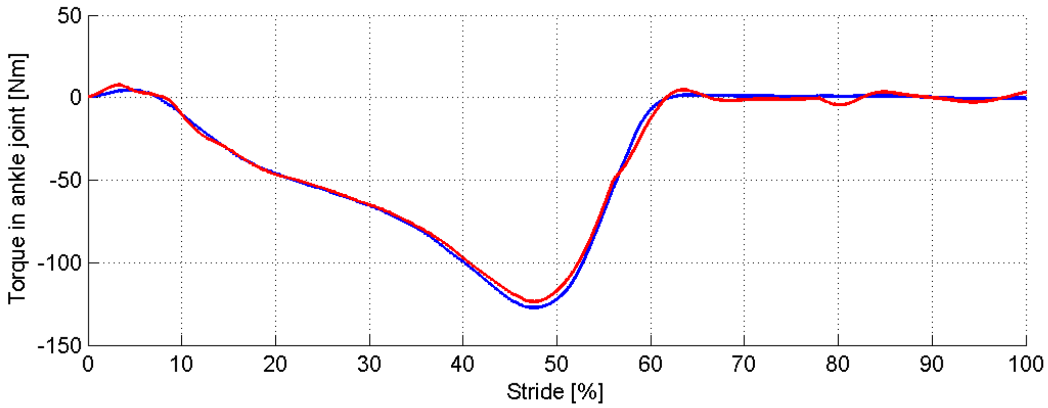

Figure 5.2: Evolution of the torque in the ankle joint. The blue line is the Winter's torque. The red line is the output torque of the model.

Figure 5.3 compares the torque in the motor joint to the one as simulated in chapter 4. It can be seen that the very high accelerations are filtered by the motor capacities.

A good visual tool to analyse the capacities of the motor is the operating range graph [53]. This graph has the angular speed of the rotor on the vertical axis and the developed electromechanical torque in abscissa. The characteristic curve of the DC motor is drawn on it. This curve is a line going through the no-load speed on the vertical axis and through the stall torque on the horizontal axis. Derived from Equation 5.1 and 5.2, the equation of the line is:

$$\dot{q} = \frac{1}{k\phi}(U_N - \frac{R}{k\phi}T_{em}) \tag{5.5}$$

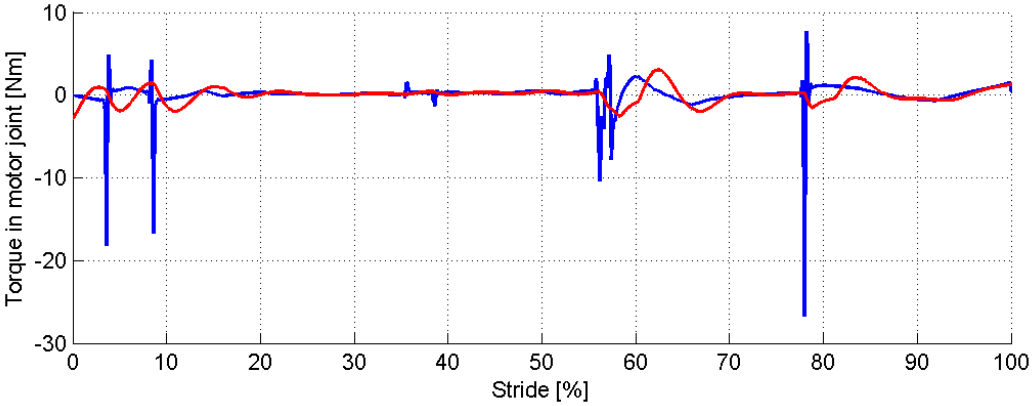

Figure 5.3: Evolution of the torque in the motor joint. The blue line is the torque from chapter 4. The red line is the output torque of the model.

With U_N, the nominal tension of the motor. The same line is drawn for negative velocities and negative torques. Then, the angular velocity of the motor in function of the developed electromechanical torque during the simulation is drawn on the graph. Two vertical lines representing five times the nominal torque (positive and negative) are drawn. Five times because a motor is allowed to operate up to this torque if it does not last longer than a certain period of time depending on the thermal behaviour of the motor. For the ankle motor, this period is equal to 2.11s (see Appendix F), which is far higher than any possible overload duration because the stride lasts for 1s. This graph is shown in Figure 5.4.

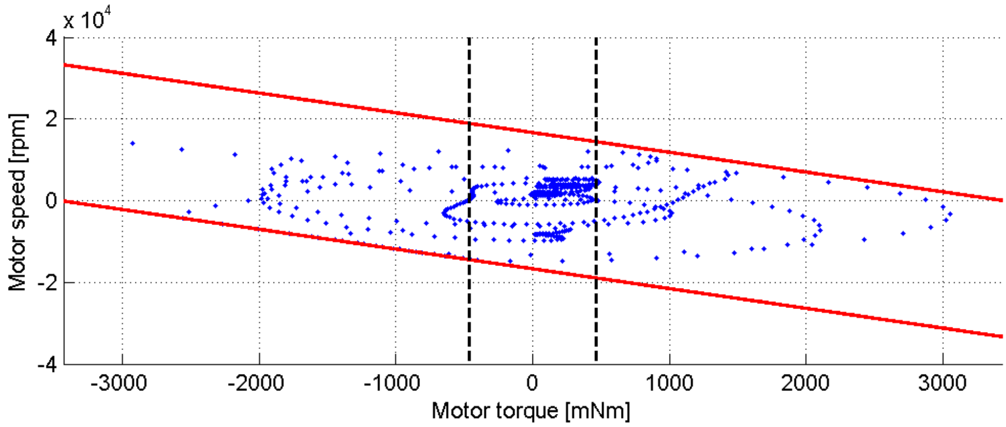

Figure 5.4: Operating range of the motor during a stride. The red lines are the positive and negative characteristic curves of the DC motor. The blue points are the angular velocity in function of the developed electromechanical torque during the simulation with the simple PI controller. The black dashed lines are five times the positive and negative nominal torque.

On this graph, it appears clearly that the gains of the controller are too high. Indeed, the torque produced by the motor is most of the time under five times the nominal torque. However, the motor gets sometimes overloaded. This is not acceptable because the motor might heat up too much. There are two solutions to this. Either diminish the gain and get a worse tracking of the position or improve the control method in order to have such a good tracking of the position but with smaller gains. These two solutions can be achieved without changing the motor or the transmission system. The control methods will be described later in chapter 6.

5.2 Knee motor

The current knee motor is the *Maxon EC-i 40*, with a diameter of 40mm and a power of 70W. It is coupled to a gearbox with a transmission ratio of 5.8:1 and then to a spindle with a pitch thread of 2mm to drive the translation motion of the spring carriage (see Appendix F).

The result of the PI control on the motor position is displayed in Figure 5.5. It appears clearly that the motor cannot track the reference position. The controller output is saturated to the nominal voltage and the angular velocity is therefore maximum at all time. This maximal velocity is obviously not sufficient to follow the trajectory in an efficient way. This bad tracking results in a bad output torque in the knee joint as well. This is shown in Figure 5.6.

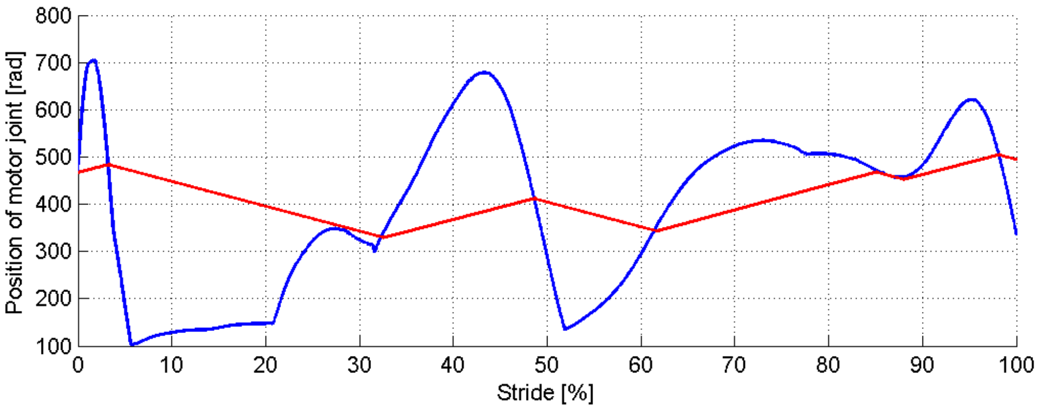

Figure 5.5: Evolution of the position of the motor joint. The blue line is the reference position used in chapter 4. The red line is the position tracking the reference.

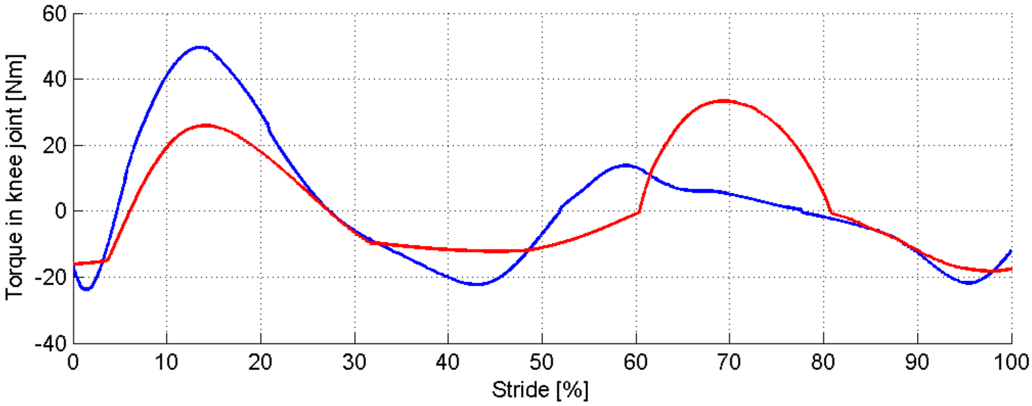

Figure 5.6: Evolution of the torque in the knee joint. The blue line is the Winter's torque. The red line is the output torque of the model.

Figure 5.7 shows the torque in the motor joint compared to the one obtain in chapter 4. It appears that the motor torque stays in the right range, the nominal torque being $0.160\,Nm$. Comparing with Figure 5.6, it appears clearly that this torque is mostly due to the load torque coming from the springs. Indeed, the accelerations are low here because of the velocity being always saturated.

Figure 5.8 is the operating range graph of the motor. It shows the velocities (in blue) being saturated to $\pm\frac{1}{k\phi}(U_N - \frac{R}{k\phi}T_{em})$ (the red lines). This is why changing the gains of the controller will not help, because the voltage already gets stuck to its nominal value. Testing another control method is pointless as well. As the torques stays far under the admissible limit, the solution appears to either reduce the transmission ratio, change the motor or both.

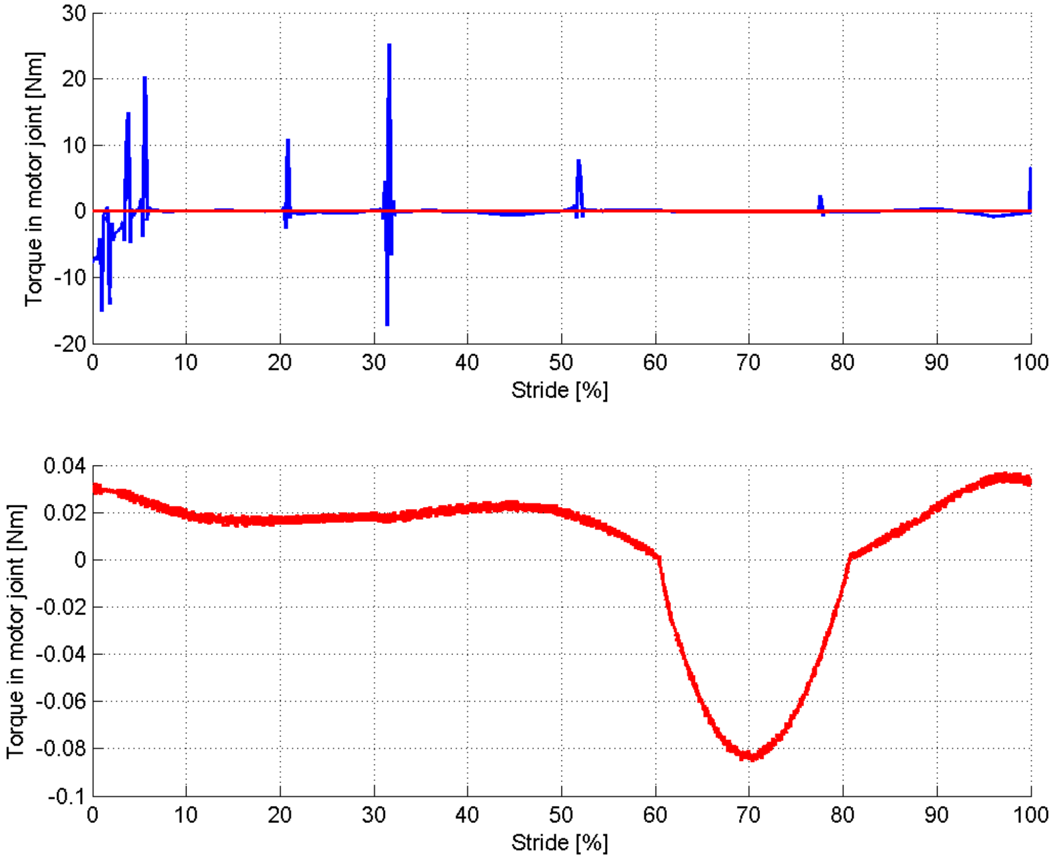

Figure 5.7: Evolution of the torque in the motor joint. The blue line is the torque from chapter 4. The red line is the output torque of the model. The second graph zooms on this realistic motor torque

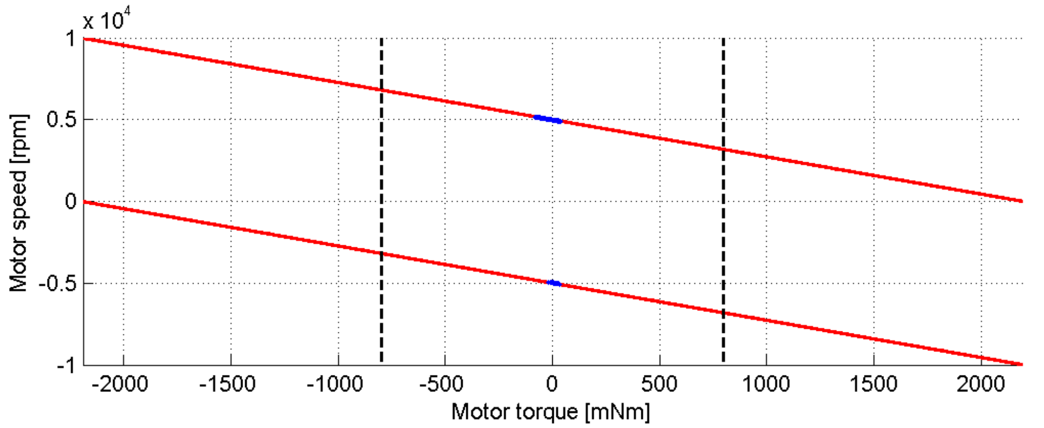

Figure 5.8: Operating range of the motor during a stride. The red lines are the positive and negative characteristic curves of the DC motor. The blue points are the angular velocity as a function of the developed electromechanical torque during the simulation with the simple PI controller. The black dashed lines are five times the positive and negative nominal torque.

A new motor/gearbox/spindle system was researched. While doing so, the two main criteria were an equivalent mass and power in order to conserve the soul of the prosthesis. Indeed, an important goal of the CYBERLEGs-Beta project is to design a energy-efficient and light device.

A new transmission system was chosen. The references can be found in Appendix F. The spindle has a 4mm thread pitch while there is no gearbox. This results in a higher spindle inertia for the rotor but the acceleration torques stay acceptable. This new system was tested with the current motor and with another motor with a power of 80W (only 10W higher than the current one). They have been tested with really high gains to figure out their maximum capacities. Figures 5.9 and 5.10 compare the results by looking at the motor position tracking and the torque in the knee joint.

The 80W motor can give a better position tracking than the old motor. The latter is not able to track the position during the beginning of the weight acceptance phase and at the end of the stance phase. Indeed, its maximum velocity is slightly below the required velocity to track the position at these moments. This results in a worse output torque in the knee joint. The new motor uses more power but 80W is still pretty comparable to the 70W of the old motor. It brings the missing velocity and was therefore selected. The whole new actuation system composed of the motor and the spindle will be used in the control methods considerations in the chapter 6.

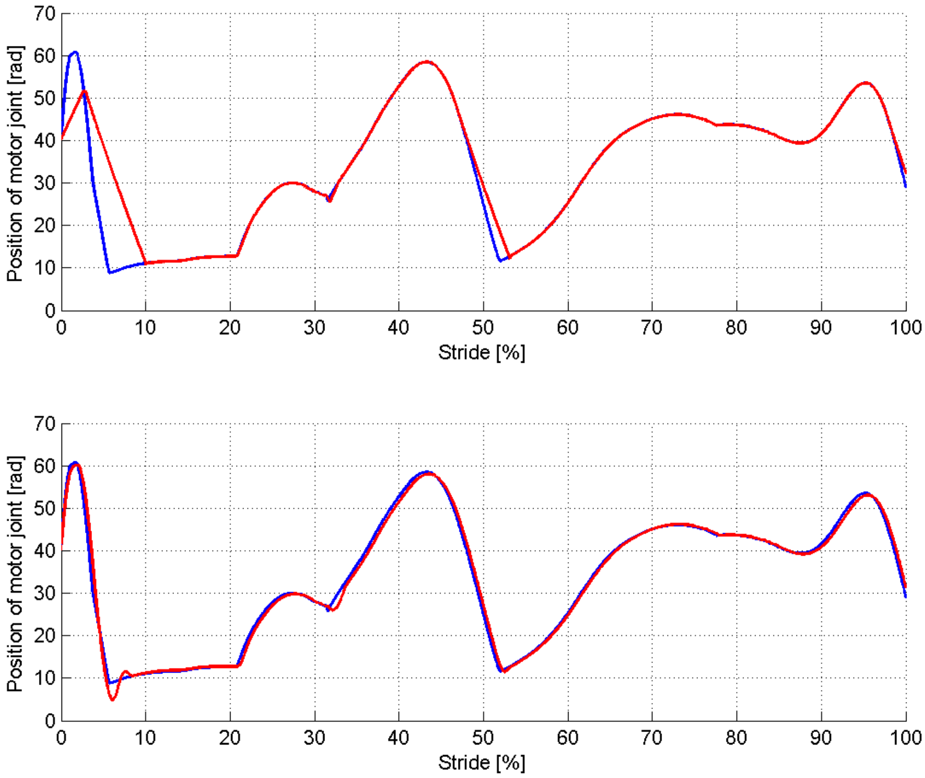

Figure 5.9: Evolution of the position of the motor joint. The top graph is the 70W motor and the second graph is the 80W motor. The blue line is the reference position used in chapter 4. The red line is the position tracking the reference.

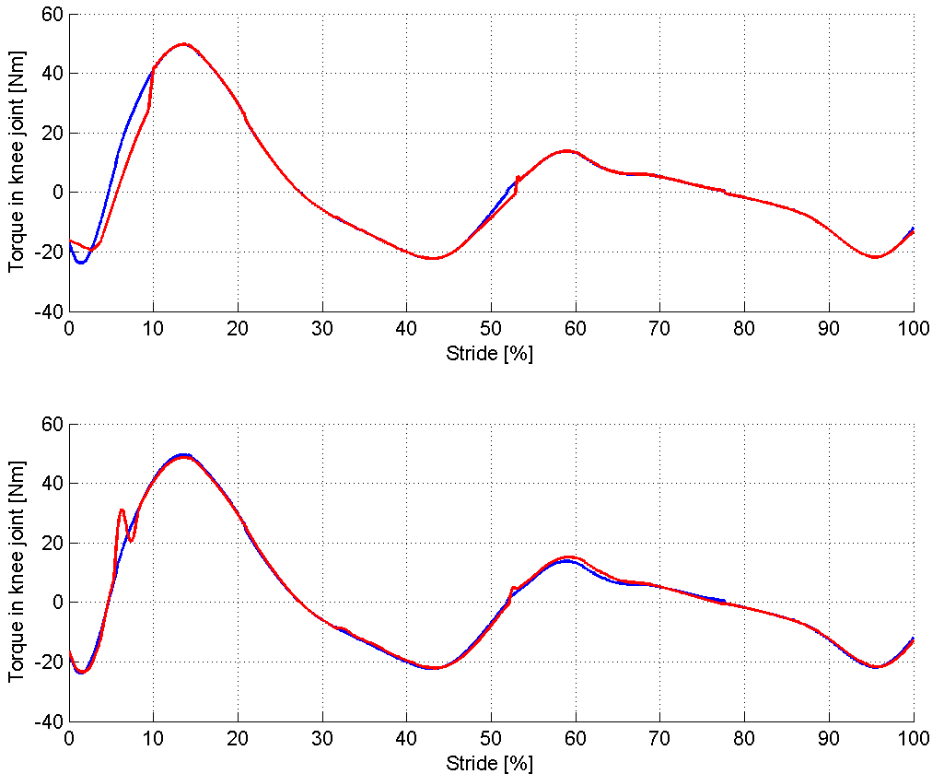

Figure 5.10: Evolution of the torque in the knee joint. The top graph is the 70W motor and the second graph is the 80W motor. The blue line is the Winter's healthy knee torque . The red line is the output torque.

CHAPTER 6

LOW-LEVEL CONTROL

Currently, the prosthesis control is composed of two layers. The high-level controller is based on an intention detection system [4]. Sensors coupled with an algorithm coming from experimental results are able to determine in which phase of the gait is the user. For each phase corresponds a setpoint with a defined set of commands. A finite state machine determines when to switch between these setpoints using the sensors inputs. The commands are specific positions for the carriage in the knee mechanism and the MACCEPA in the ankle mechanism. These positions were experimentally determined [4]. The others commands are booleans enabling or disabling the weight acceptance and energy transfer mechanisms. The second layer is the low-level controller. It tracks the desired positions in a closed-loop.

One objective for the CYBERLEGs-Beta prosthesis is to use a continuous input for the low-level controller. This input could be the result of a bioinspired high-level controller. The second goal of this thesis was to design a low-level controller able to track such a continuous input.

In a nutshell, this chapter will present a system containing the low-level controller, the motors and the prosthesis acting as a black box. The inputs of this black box is the command coming from the virtual high-level controller, i.e. the desired torques in the ankle and knee joints, as well as two booleans stating whether the weight acceptance and energy transfer mechanisms must be engaged or not. The desired torques could be the Winter's healthy gait torques but could also be the torques needed to climb stairs or to perform sit-to-stand. They must stay in the reachable range of the mechanisms though.

Both mechanisms have two degrees of freedom. It means that the torques in the ankle and knee joint not only depend on the motors dynamic but on the current position of these joints as well. A measurement of both angles must therefore be provided to the controller. In the real prosthesis, encoders are placed on the ankle and knee joints to produce this information. Encoders can also provide the positions of the motors to the system. A schematic of the black box is shown in Figure 6.1.

N.B.: from now, the symbols designating a command will have a tilde on them, e.g. $\tilde{T}_{ankle}$. Meanwhile, estimations of values will use a hat, e.g. $\hat{T}_{load}$.

This whole system is composed by the low-level controller, the motors and the prosthesis mechanisms. The low-level controller converts the control inputs and the angle measurements into the electrical voltages that are applied to the motors. From these voltages, the motors develop an electromechanical torque. The prosthesis mechanisms finally convert these torques into the output torque in the ankle and knee joints.

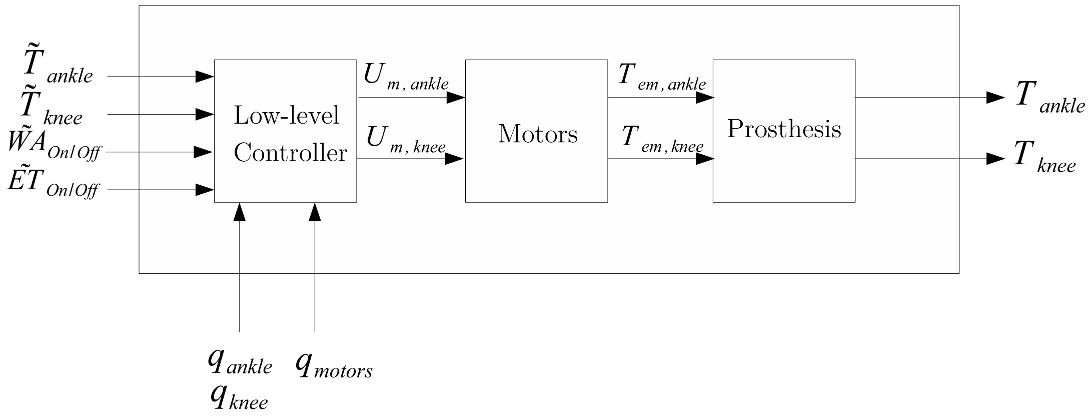

Figure 6.1: Schematic of the whole system.

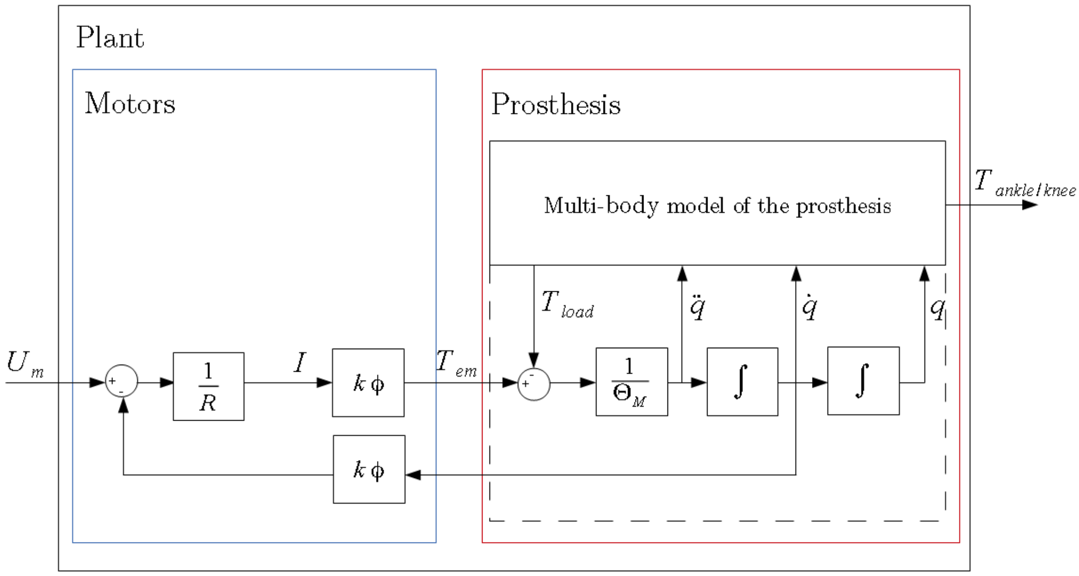

Figure 6.2: Block diagram representing the model of the plant. U_m is the voltage applied on the motor. R is the phase-to-phase terminal resistance of the motor. $k\phi$ is the torque constant of the motor. T_{em} is the electromechanical torque developed by the motor. T_{load} is the load torque on the motor joint. $\ddot{q}, \dot{q}$ and q are the acceleration, the velocity and the position of the motor joint respectively. $T_{ankle/knee}$ is the output torque in the ankle/knee joint.

The different low-level controller designs were tested on the multibody models augmented by the electromechanical model of the motors, as described in chapter 5. Those models constitute the plant of the controlled system. Their block diagram is drawn in Figure 6.2.

As explained in chapter 5, the electrical time constant is neglected in the motor model. Therefore, the term $L\,di/dt$ is not present. Note that in the Figure, the multibody *Robotran* model is extended by the dashed lines. The application of the load torque on the motor joint and the double integration of its acceleration are normally also part of the multibody model. There are just explicit in the Figure to make further explanations easier.

The two methods that have been tested are position control (in section 6.2) and torque control (in section 6.3).

6.1 Motor position estimation

Before using position control, the position inputs must be calculated. Indeed, the position commands are currently based on experimental results. This is why an estimator of the motor desired position in function of the desired ankle/knee torque and the current position of the ankle/knee joint must be implemented. A measurement of the current motor position is also provided. Its principle is summarized in Figure 6.3. Such an estimator is obviously dependent on the mechanism geometry. It is thus explained in two different sections, starting with the ankle mechanism.

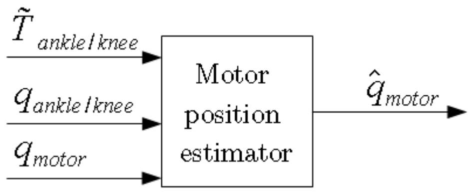

Figure 6.3: Schematic of the estimator.

6.1.1 Estimation in the ankle mechanism

The principle of the estimator is simple. First, using the measurements of the positions of the motor and the ankle joint, it computes the other positions using the geometrical relationships between the other generalized coordinates. Then, it can use these positions to calculate the Jacobian matrix of the constraints $J_{i,k} = \partial h_i / \partial q_k$ (see Appendix E). The position of the parallel spring joint can also provide an estimation of the force in the parallel spring. Using $J_{i,k}$, F_{para} and the desired torque in the ankle joint $\tilde{T}_{ankle}$, the desired force in the MACCEPA spring joint can be obtained by using the results of the dynamic analysis of chapter 4. Finally, this force is converted into a desired position for the motor joint. This process is summarized in Figure 6.4.

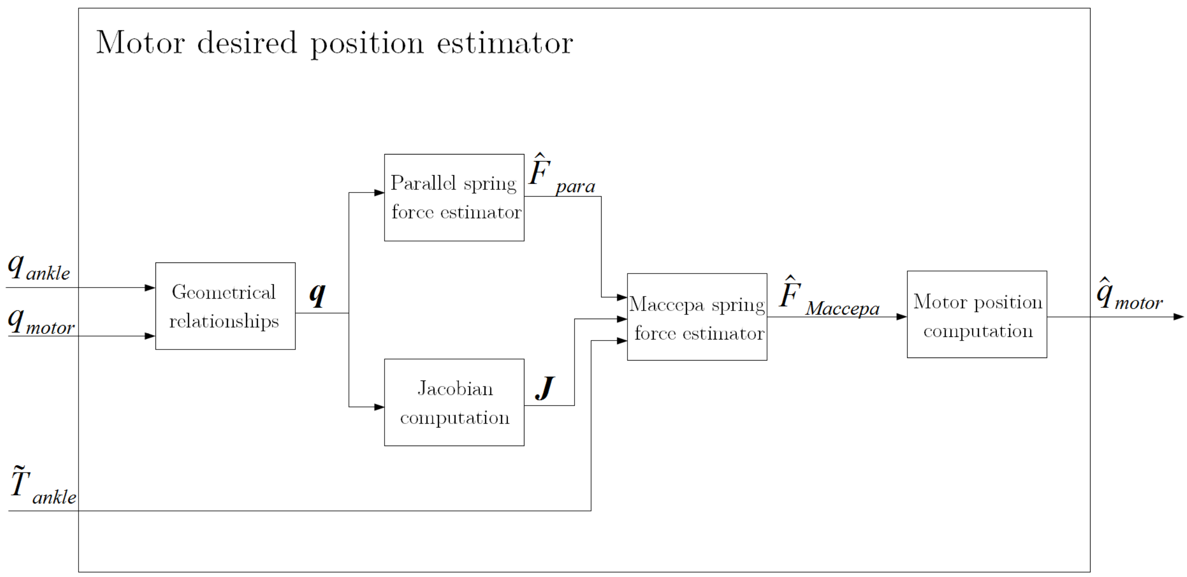

Figure 6.4: Schematic of the whole estimator.

The first step of the process is the computation of the current positions of the MACCEPA spring joint, the moment arm joint and the parallel spring joint. Indeed, the system has two degrees of freedom, so the measurements of the positions of the ankle and motor joint can provide other joints positions.

This is done using the geometrical relationships between the joints. They are developed in Appendix B.1. In a second time, the force in the parallel spring is estimated using the following simple formula (neglecting friction):

$$\hat{F}_{para} = K_{para} \cdot q_{para} \tag{6.1}$$

Then, some terms of the Jacobian are computed. With them, κ_r and κ_b are obtained.

After that, the desired force in the MACCEPA spring can be estimated with Equation 4.6 developed in chapter 4:

$$\hat{F}_{MACCEPA} = \frac{1}{\kappa_b}(\tilde{T}_{ankle} - \kappa_r \cdot \hat{F}_{para}) \tag{6.2}$$

When $\hat{F}_{MACCEPA}$ is known, the desired position of the MACCEPA spring joint can be deduced from it, by simply using the stiffness of the spring:

$$\hat{q}_{MACCEPA} = \frac{\hat{F}_{MACCEPA}}{K_{MACCEPA}} \tag{6.3}$$

Finally, the angle of the motor is computed using the geometric relationship between it and the MACCEPA spring joint position [4].

$$\hat{\alpha} = acos(\frac{L_0 + \hat{q}_{MACCEPA}}{2\,A}) \tag{6.4}$$

with A, the length of the connecting rod, $B = A$, the length of the crank, L_0, the rest length of the MACCEPA spring and $\hat{\alpha}$, the desired angle of the MACCEPA.

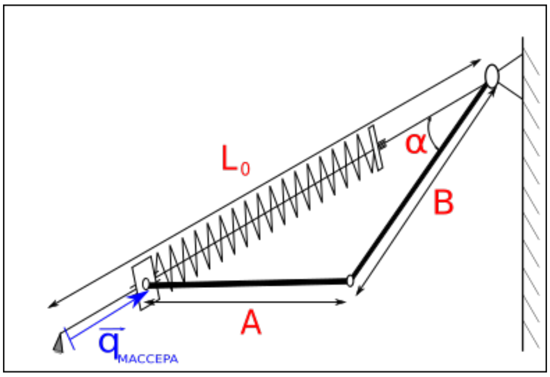

Figure 6.5: Schematic of the MACCEPA system.

The problem of the *arccos* function is that it is symmetrical about the y-axis and always returns the absolute value of the desired angle. However, it might need to return the negative value of the angle because the torque in the ankle joint is a function of the sine of that angle, as seen in Equation 4.1.1. Its sign is therefore important. It is equal to the sign of the contribution of the MACCEPA spring in the ankle joint, i.e. the desired torque in the ankle joint minus the contribution of the parallel spring. The following sign function can thus be defined:

$$\kappa_b \cdot \hat{F}_{MACCEPA} = \kappa_r \cdot \hat{F}_{para} - \tilde{T}_{ankle} \tag{6.5}$$

$$sign(\kappa_b \cdot \hat{F}_{MACCEPA}) = sign(\hat{\alpha}) \tag{6.6}$$

Finally, the desired position of the motor is deduced from α using the transmission ratio of the gears system:

$$\hat{q}_{motor} = \rho \cdot \hat{\alpha} \tag{6.7}$$

Figure 6.6 shows the result of the estimator for a stride using the Winter's data. It compares two results. One is from an experiment where the Winter's torque and motor position are artificially perfectly tracked. The other comes from an experiment using closed-loop control (with small instabilities around the desired motor position). The purpose of this Figure is to highlight the influence of instabilities on the result of the estimator.

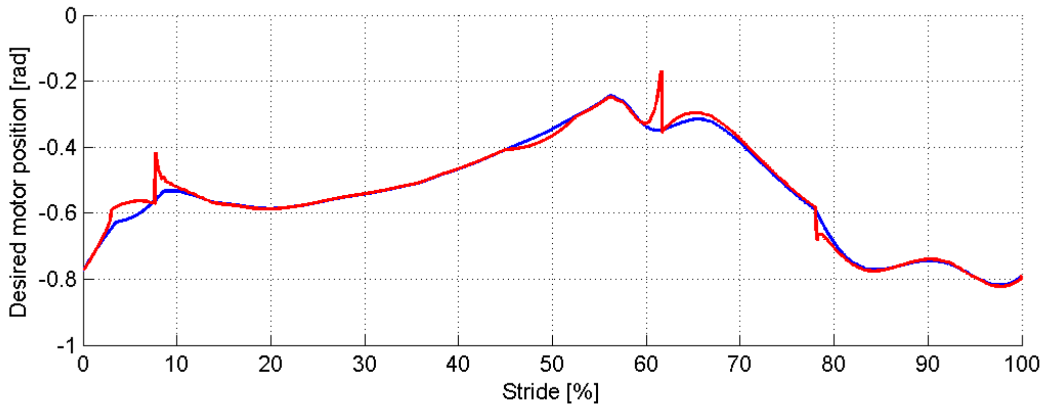

Figure 6.6: Evolution of the estimated desired motor position. The blue line is the output of the estimator when the trajectory is artificially perfect. The red line is the output of the estimator with a closed-loop trajectory.

The peaks and error zones correspond to the moment when the mechanism is in the singularity position, i.e. when $\alpha = 0$. In that case, κ_b is the division of two values extremely closed to zero. Numerical errors coupled to the instabilities due the control leads to extremely high values for $\hat{F}_{MACCEPA}$. These values are limited by the estimator to prevent them from becoming absurdly high. Nevertheless, these peaks are filtered by the real motor dynamic and do not really influence its torque output. This will be seen in section 6.2.

6.1.2 Estimation in the knee mechanism

The principle of this estimator is quite the same than the estimator for the ankle motor. First, using a geometrical relationship, it computes the position of the springs joint using the positions of the knee joint and the motor joint. Then, using these, it can compute the Jacobian matrix of the constraints (see Appendix B.2). The torque in the knee joint created by the weight acceptance mechanism can also be calculated in function of the position of this knee joint. All those elements combined can provide the desired force in the extension/baseline springs. This force can finally be transformed into the desired position of the motor using the stiffness of the springs and the transmission ratio of the motor. The schematic of the estimator is displayed in Figure 6.7.

The relationship between the knee joint, the motor joint and the springs joint is a bit complex [5] and can be found in Appendix B.1.

The computation of κ and the weight acceptance torque are explained in Appendix B.3. With these, the force in the springs joint can be calculated using Equation 6.8:

$$\hat{F}_{springs} = \frac{1}{\kappa}(\hat{T}_{WA} - \tilde{T}_{knee}) \tag{6.8}$$

With $\hat{F}_{springs}$, $\hat{q}_{springs}$ can be obtained with:

$$\hat{q}_{springs} = \begin{cases} \hat{F}_{springs}/K_{BL}, & \text{if } \hat{F}_{springs} > 0 \\ \hat{F}_{springs}/K_{EX}, & \text{otherwise} \end{cases} \tag{6.9}$$

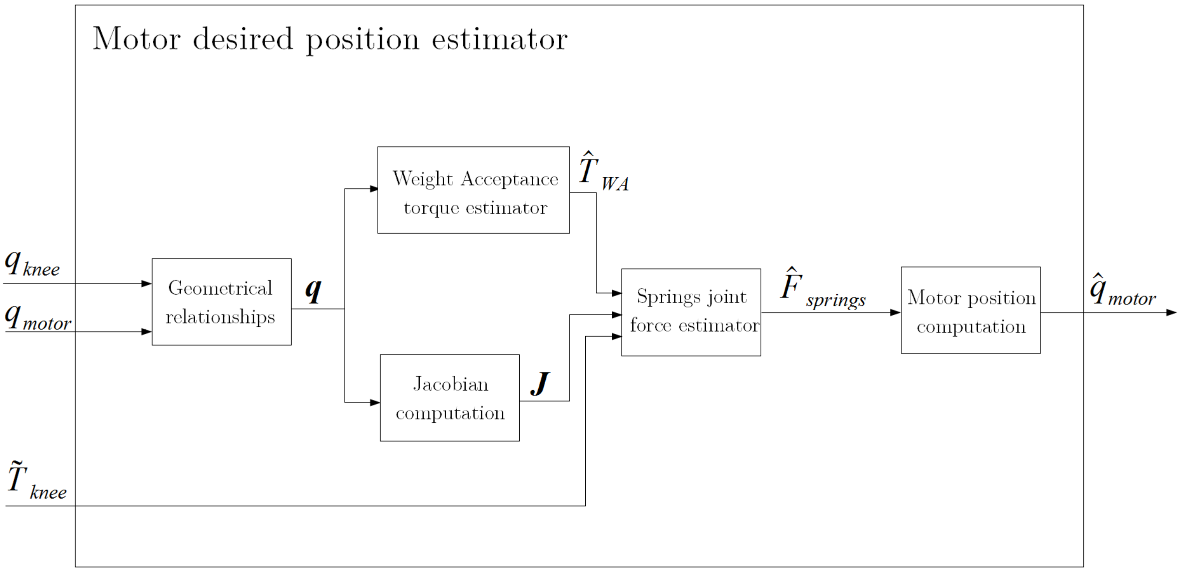

Figure 6.7: Schematic of the whole estimator.

Then, the desired position of the motor is easily found using the transmission ratio:

$$\hat{q}_{motor} = \rho \cdot \hat{q}_{springs} \tag{6.10}$$

Figure 6.8 shows the output of this simulator. It compares two results in the same manner than Figure 6.6. Here, the instabilities do not generate any trouble. The estimation stays satisfying during the whole stride. The two graphs are almost confounded in the Figure. This is mostly due to the fact that the knee mechanism does not encounter any singularity during a stride.

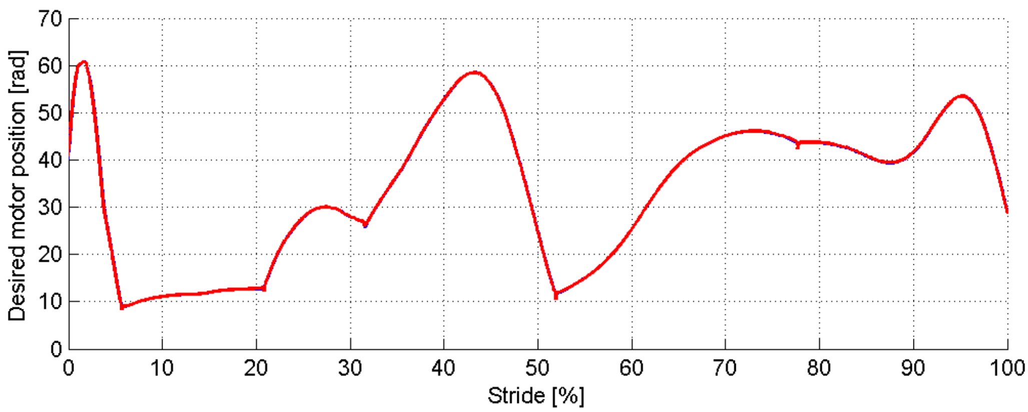

Figure 6.8: Evolution of the estimated desired motor position. The blue line is the output of the estimator when the trajectory is artificially perfect. The red line is the output of the estimator with a closed-loop trajectory. Both lines are almost confounded.

6.2 Position control

As explained earlier, the first low-level control technique investigated is a PID-controller tracking the position of the motor. In the current low-level controller, this position loop is coupled with a velocity and then to a current loop. These last two loops are performed by a commercial controller, i.e. the *ESCON* from *Maxon*. In this chapter, they are bypassed and the output of the controller is directly applied to the motor. This allows to use the results of the dynamic analysis of the prosthesis performed in chapter 4. Indeed, these results can be used to estimate the load torque applied to the motor and then feedforward this value to the motor command. This will be explained later.

In this control system, the reference positions are the one calculated with the estimators described in section 6.1. The global schematic of the basic control system (just the PID position loop) is shown in Figure 6.9.

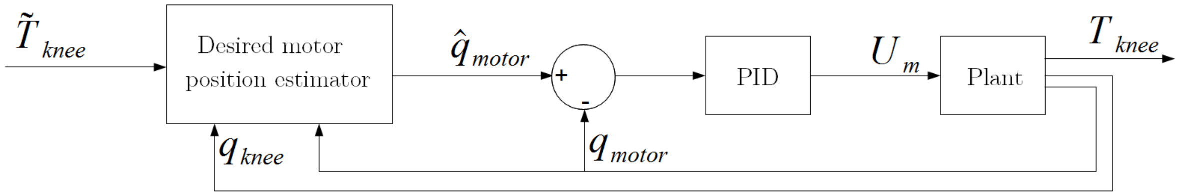

Figure 6.9: Schematic of the position PID control.

However, as seen in chapter 5, just by using this method, a good tracking is impossible to get without high gains. These large gains result in high voltages and currents in the motor. Therefore, it makes sense to try to diminish these gains while keeping a good tracking of the position.

The first thing that was done is quite common in DC motor control [54]. A compensation term for the back-electromotive force was added, as shown in Figure 6.10. This supposes a good estimation of the torque constant $k\phi$. This term is summed with the command. If the estimation of $k\phi$ is good enough, the back-emf will be compensated. This makes the controller work on a simplified equivalent plant [54]. This equivalent system is shown in Figure 6.11.

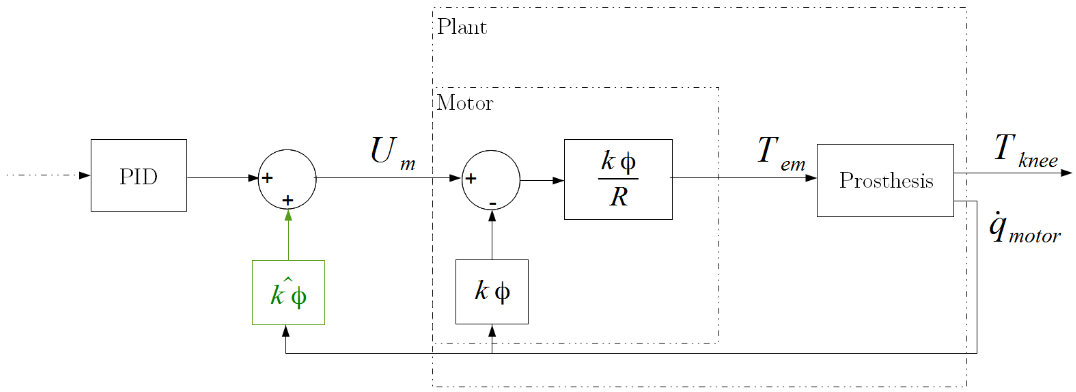

Figure 6.10: Addition of the compensation of the back electromotive force. The compensation term is in green in the schematic.

Because the plant seen by the controller is made simpler, the synthesis of the controller becomes easier and its performances are enhanced [54].

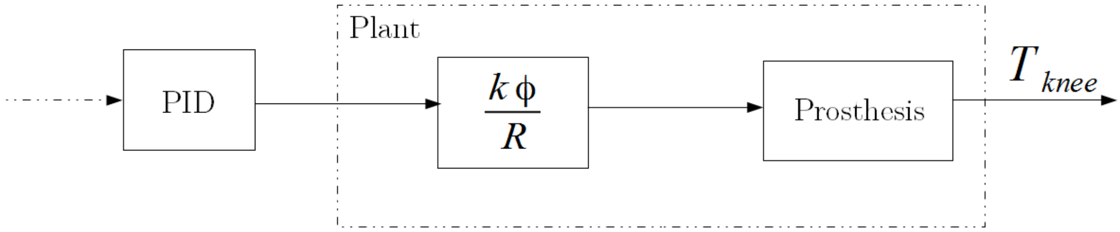

Figure 6.11: Simplified plant as seen by the controller with a good estimation of $k\phi$.

The second thing that was added to the control is the feedforward of the estimated load torque. The load torque is computed using Equation 6.11 for the ankle motor and Equation 6.12 for the knee motor. These equations are the result of the analysis of the multibody model (see chapter 4).

$$\hat{T}_{l,ankle} = \frac{\rho_{ankle} \cdot \kappa_M}{\kappa_b} \cdot (\hat{T}_{ankle} - \kappa_r F_{para}) \tag{6.11}$$

$$\hat{T}_{l,knee} = \frac{\rho_{knee}}{\kappa} (T_{WA} - \hat{T}_{knee}) \tag{6.12}$$

They can easily be computed using the values calculated during the estimation of the desired motor position. Then, the value is multiplied by $R/k\phi$ to be physically equivalent to a voltage and then summed to the command, as displayed in Figure 6.12. A comparison between the estimated load torque and the real load torque for the knee mechanism can be found in Figure 6.14.

If the estimation of the load is perfect, the controller works on an even more simplified plant, as shown in Figure 6.13. The transfer function of this equivalent plant is equal to:

$$G(s) = \frac{k\phi \cdot R}{Js^2} \tag{6.13}$$

The whole system block diagram finally obtained is shown in Figures 6.16 and 6.15. It will be the base for the test performed in the next sections. This control method has been tested on both ankle and knee mechanisms. Its performances have been compared to the ones obtained without any feedforward and without any feedback. The criteria of a good performance are the quality of the output torque in the ankle/knee joint, the tracking of the desired motor position and finally, the gains of the controller necessary to obtain such tracking.

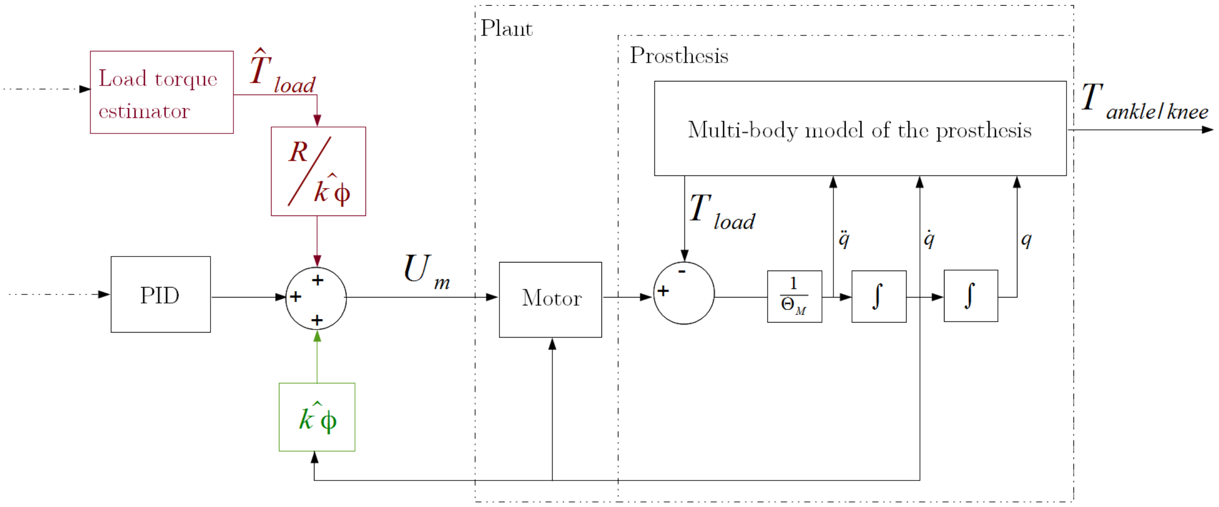

Figure 6.12: Addition of the compensation of the load torque. The compensation term is in red in the schematic.

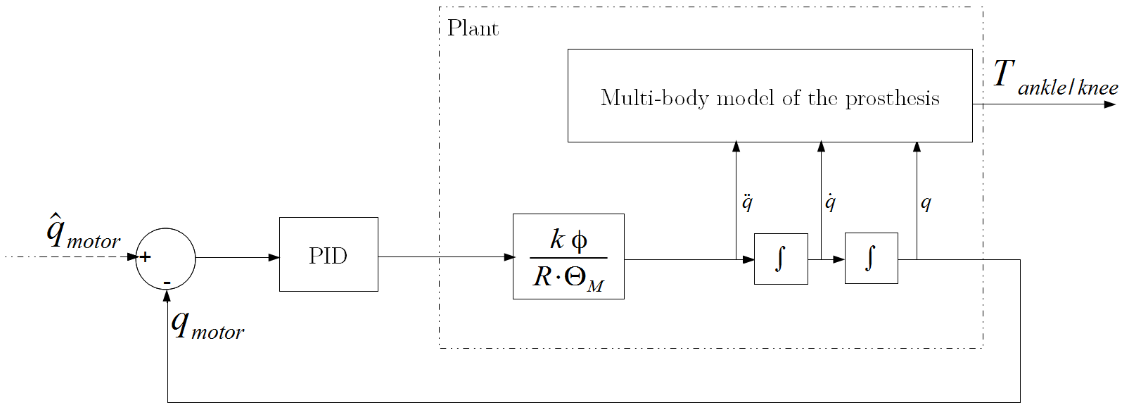

Figure 6.13: Simplified plant as seen by the controller with the addition of the compensation of the load torque.

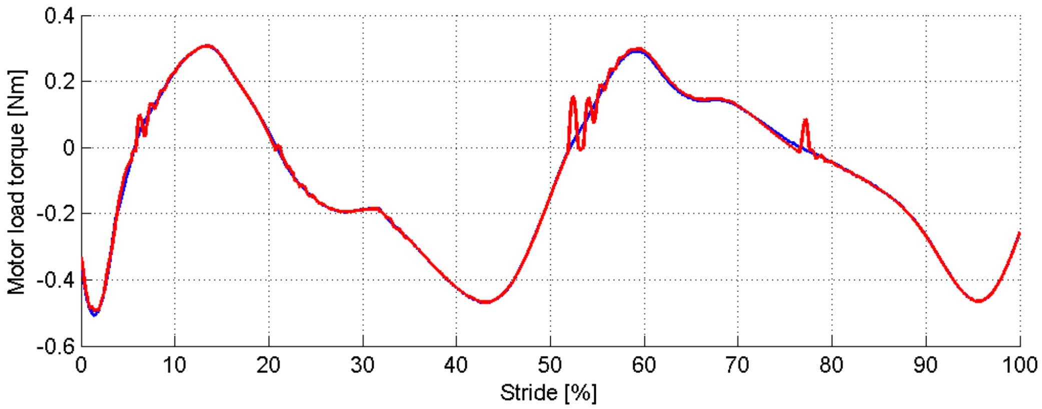

Figure 6.14: Comparison of the estimated load torque and the real load torque in a closed-loop simulation with feedforward of the estimated load torque. The real load torque is in red. The estimation of the load torque is in blue.

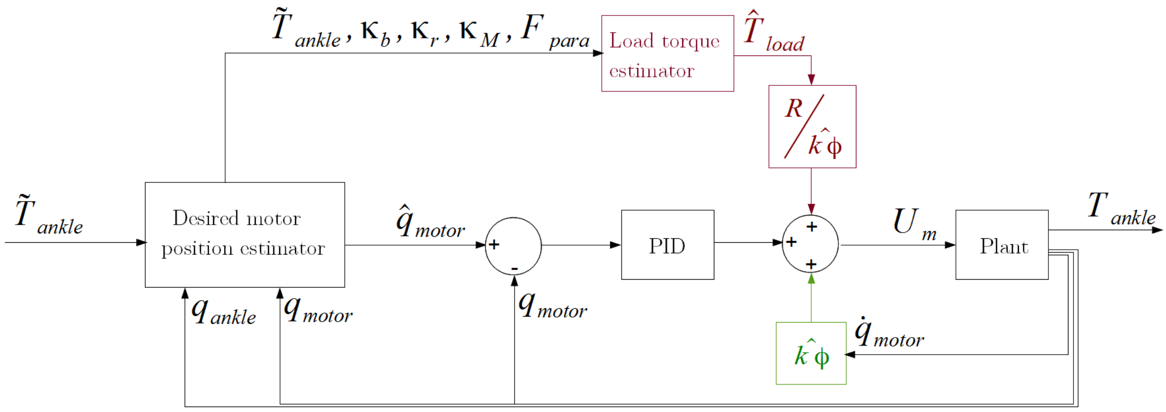

Figure 6.15: Control diagram of the ankle with the controller using feedback on the position and feedforward on the load torque.

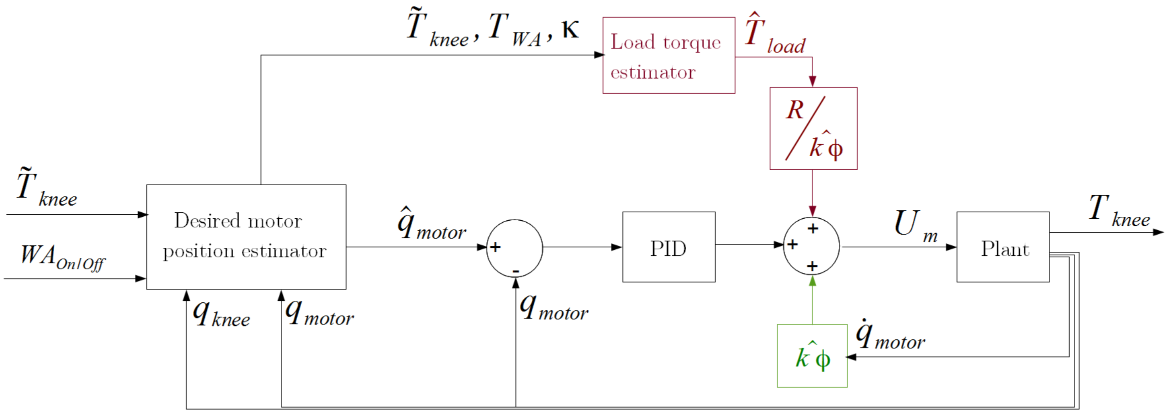

Figure 6.16: Control diagram of the knee with the controller using feedback on the position and feedforward on the load torque.

6.2.1 Knee control

A reminder here: all the control methods are tested on the new motor/gearbox/spindle system described in chapter 5. Indeed, it makes no sense to test them on the current system because this one is unable to track the desired positions.

6.2.1.1 Feedforward and feedback

By using the control method with feedback and feedforward of the load torque, the results shown in Figure 6.17 are obtained. The good tracking of the desired position result in a satisfying output torque.

6.2.1.2 Feedback only

The contribution of the load torque feedforward can be demonstrated by showing the position tracking without it and by using the same gains for the controller. The results are shown in Figure 6.18.

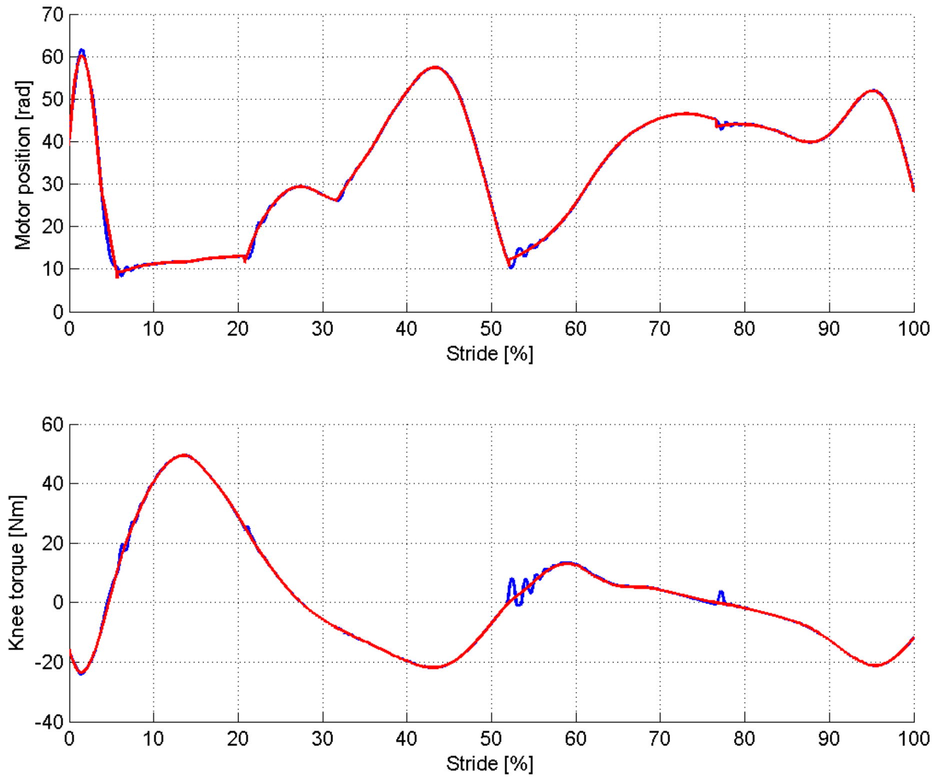

Figure 6.17: **Top graph**: tracking of the motor position with feedback of the position and feedforward of the load torque. The desired position is in red and the real position of the motor is in blue. **Second graph**: torque output for the same simulation. The Winter's healthy knee torque is in red and the real output torque is in blue.

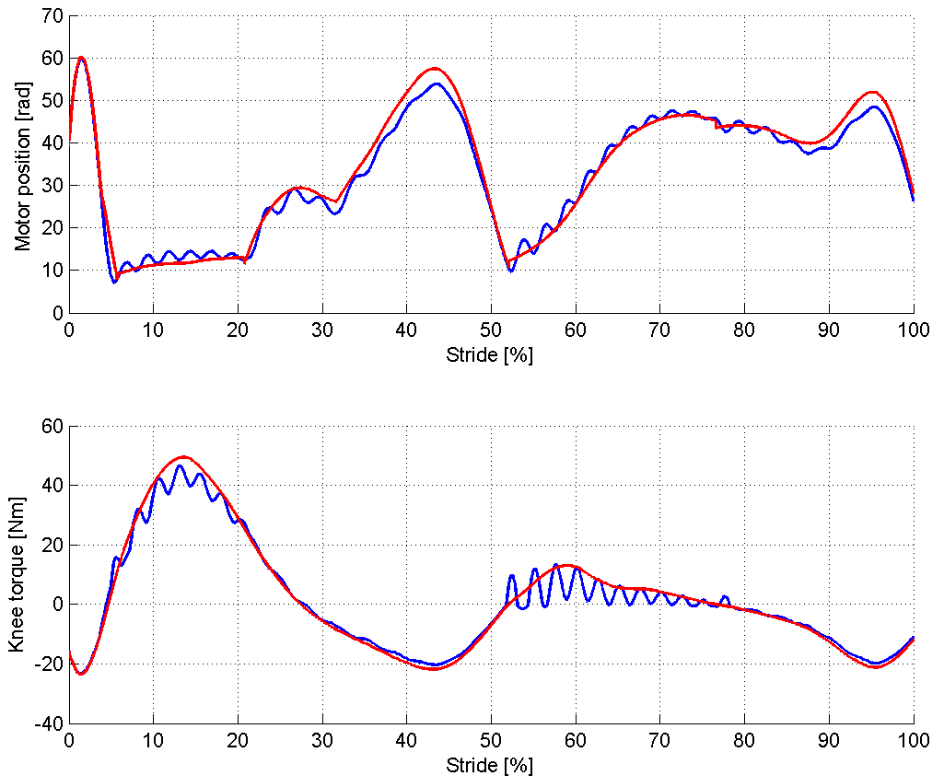

Figure 6.18: **Top graph**: tracking of the motor position with feedback of the position but no feedforward of the load torque. The desired position is in red and the real position of the motor is in blue. **Second graph**: torque output for the same simulation. The Winter's healthy knee torque is in red and the real output torque is in blue.

The position tracking is not as good and this results in a worse output torque in the knee joint. In fact, the gains of the controller must be one order of magnitude higher to obtain a position tracking similar to the one with the feedforward.

6.2.1.3 Feedforward only

Another test was made by only using the feedforward of the load torque and no feed back. The systems works then in open-loop. The corresponding block diagram in shown in Figure 6.19. The results are shown in Figure 6.20.

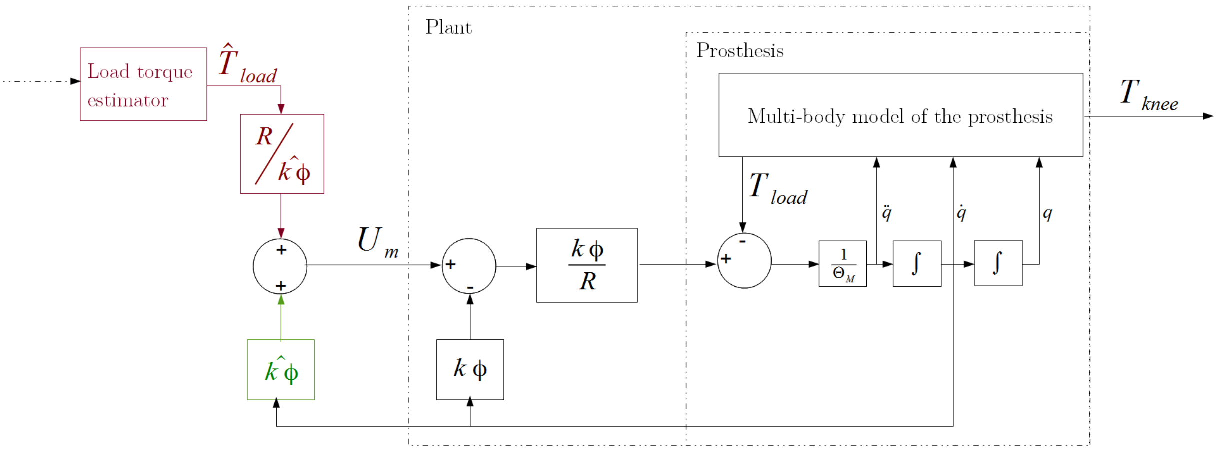

Figure 6.19: Schematic of the system without feedback.

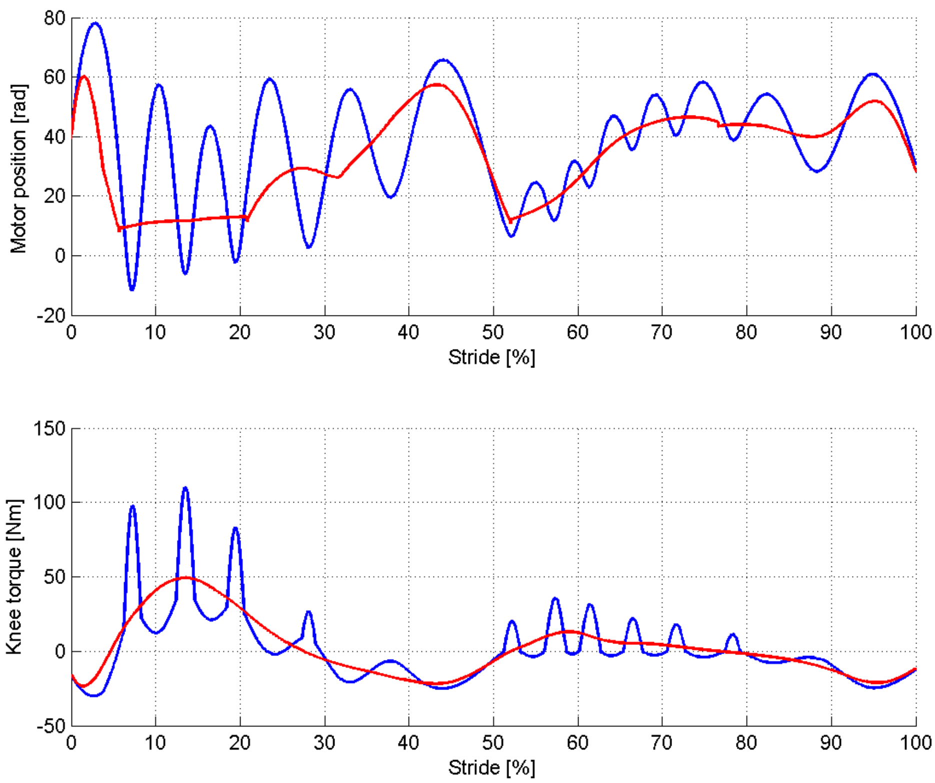

Figure 6.20: **Top graph**: tracking of the motor position with feedforward of the load torque but no feedback of the position. The desired position is in red and the real position of the motor is in blue. **Second graph**: torque output for the same simulation. The Winter's healthy knee torque is in red and the real output torque is in blue.

It is observed that the position is vaguely tracked but there are large oscillations around it.

The torque output behaves consequently in the same way. As deduced from the block diagram in Figure 6.19, if the load torque and the torque constant $k\phi$ are well estimated, then it results in the term $\Theta_M \ddot{q}$ being equal to zero. However, in reality, this term is one order of magnitude larger than the load torque. So, to make a system without feedback work, there are two possibilities: either compensate this inertial term as well or diminish it. The latter can be done either by lowering the global inertia of the system rotor/gearbox/spindle or by reducing the accelerations, i.e. with a longer stride duration. As an example, Figure 6.21 shows the result without feedback but with this global inertia divided by 10.

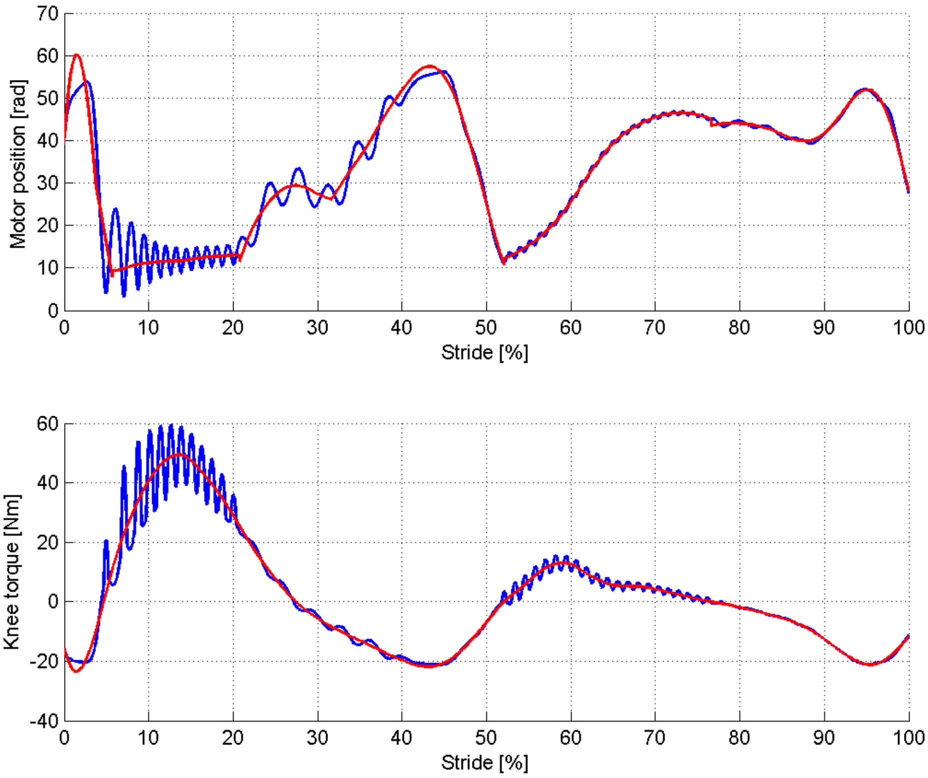

Figure 6.21: **Top graph**: tracking of the motor position with feedforward of the load torque but no feedback of the position. The global inertia of the rotor/gearbox/spindle system is divided by ten as an example. The desired position is in red and the real position of the motor is in blue. **Second graph**: torque output for the same simulation. The Winter's healthy knee torque is in red and the real output torque is in blue.

Despite the remaining oscillations, the result here is far better. Nevertheless, to reduce the global inertia or making the stride longer is not realistic. And to compensate the acceleration demands a measurement of it, or to numerically differentiate the measurement of the velocity. By looking at the results given by just adding feedback and a PID controller, it does not seem justified to either add a new sensor for the acceleration or to add the heavy computation of the differentiation of the velocity.

In conclusion, the whole system including the feedback and the feedforward parts is a satisfying low-level controller. If the torque input is in the reachable range in function of the knee angle, then this controller will be able to track it.

6.2.2 Ankle control

For the ankle, the results are really similar and will thus not be explained here to avoid redundancy. The results graphs for the three control types are shown in Figure 6.22, 6.23, and 6.24.

The feedforward of the load torque look justified, even if its impact is less impressive than for the knee mechanism. In fact, the gains just need to be multiplied by four in order to have a position tracking similar to the one with feedforward. This is due to the ratio between load torque and $\Theta_M \ddot{q}$ being lower here.

This ratio is also the reason why not having feedback on the motor position looks worse here, as seen in the last figure. Therefore, it is imperative to use feedback for the ankle.

In conclusion, this low-level controller is able to track the desired torque without any problem and can therefore be coupled to a bioinspired mid-level or high-level controller that provides a continuous command for the ankle torque.

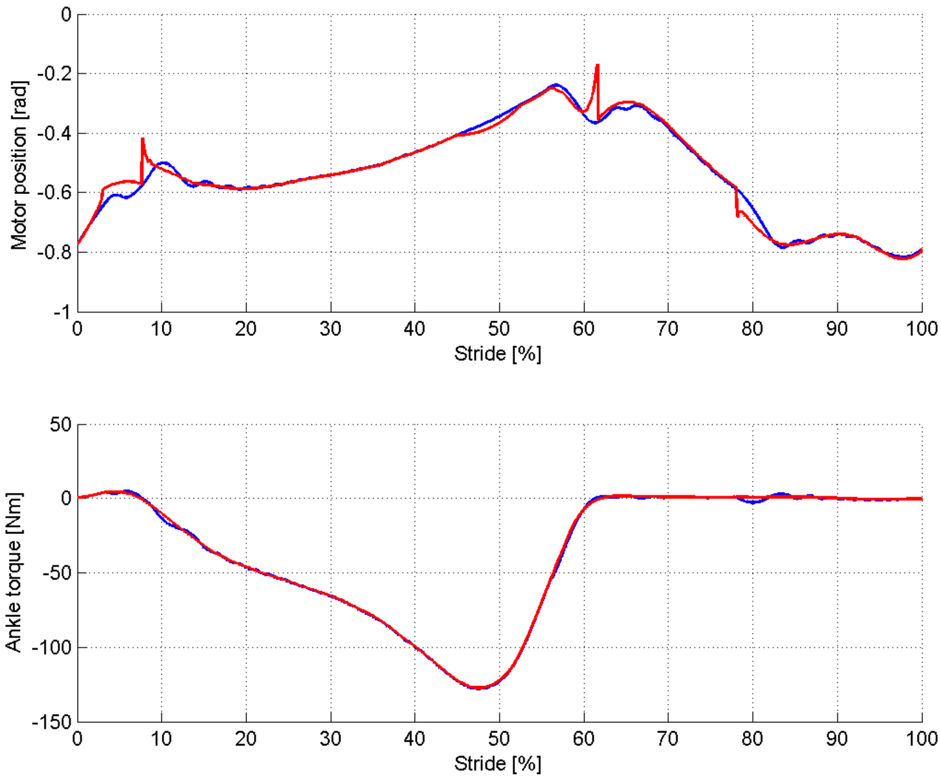

Figure 6.22: **Top graph**: tracking of the motor position with feedback of the position and feedforward of the load torque. The desired position is in red and the real position of the motor is in blue. **Second graph**: torque output for the same simulation. The Winter's healthy ankle torque is in red and the real output torque is in blue.

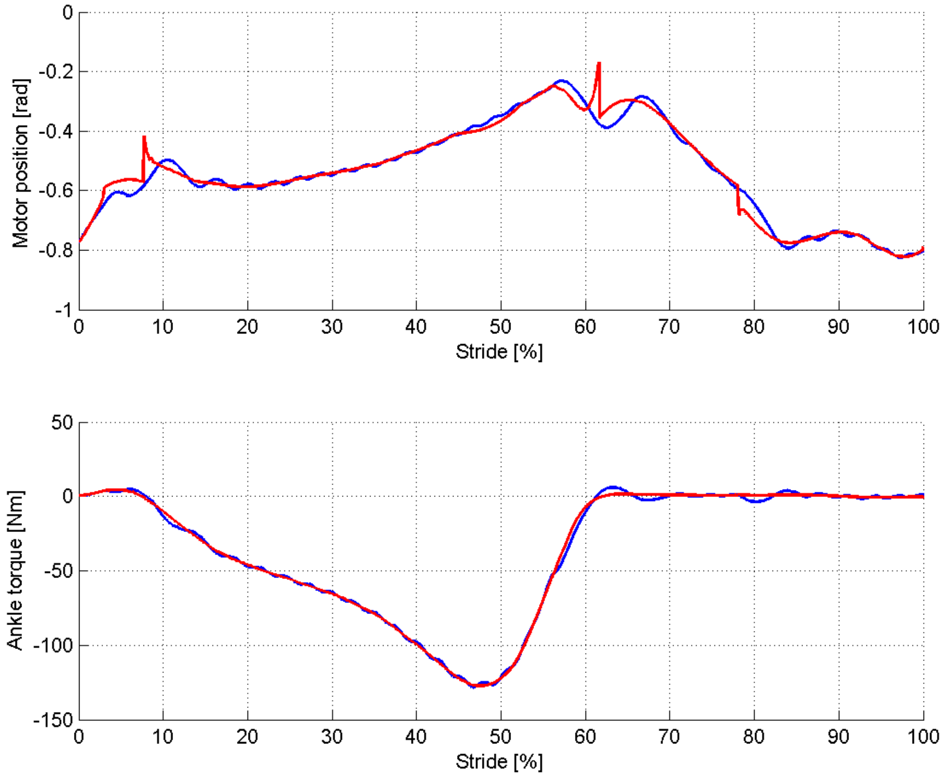

Figure 6.23: **Top graph**: tracking of the motor position with feedback of the position but no feedforward of the load torque. The desired position is in red and the real position of the motor is in blue. **Second graph**: torque output for the same simulation. The Winter's healthy ankle torque is in red and the real output torque is in blue.

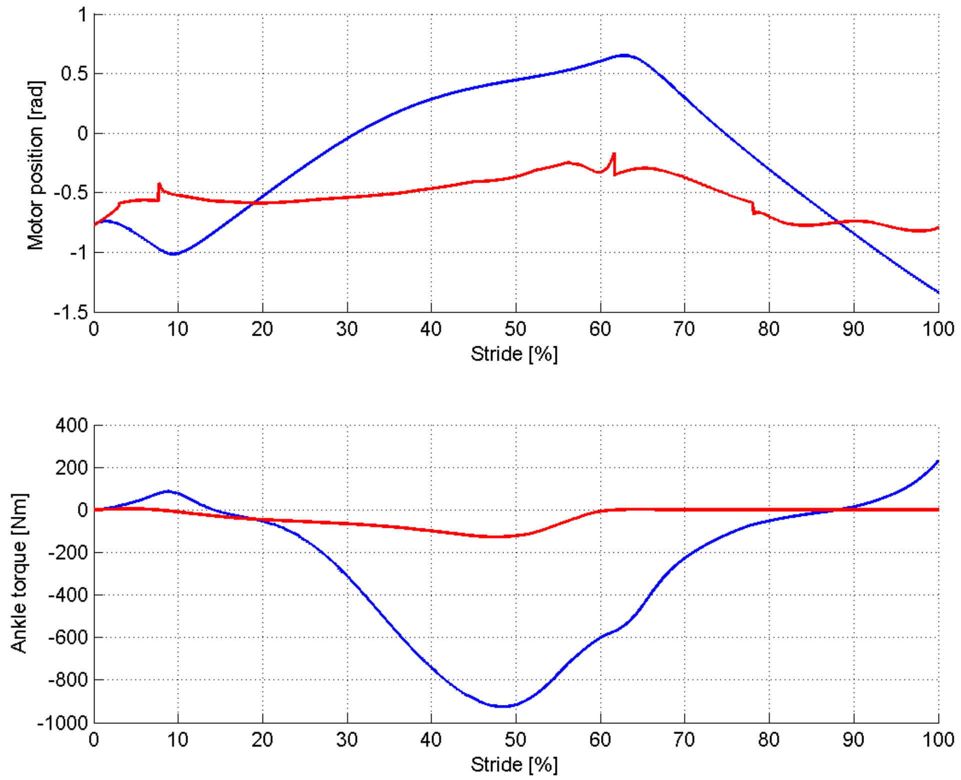

Figure 6.24: **Top graph**: tracking of the motor position with feedforward of the load torque but no feedback of the position. The desired position is in red and the real position of the motor is in blue. **Second graph**: torque output for the same simulation. The Winter's healthy ankle torque is in red and the real output torque is in blue.

6.3 Torque control

Another idea that was proposed to control the motor was torque control, i.e. directly control the error between the actual value of the output torque with the desired torque in the ankle or knee joint. The block diagram of this method is shown in Figure 6.25.

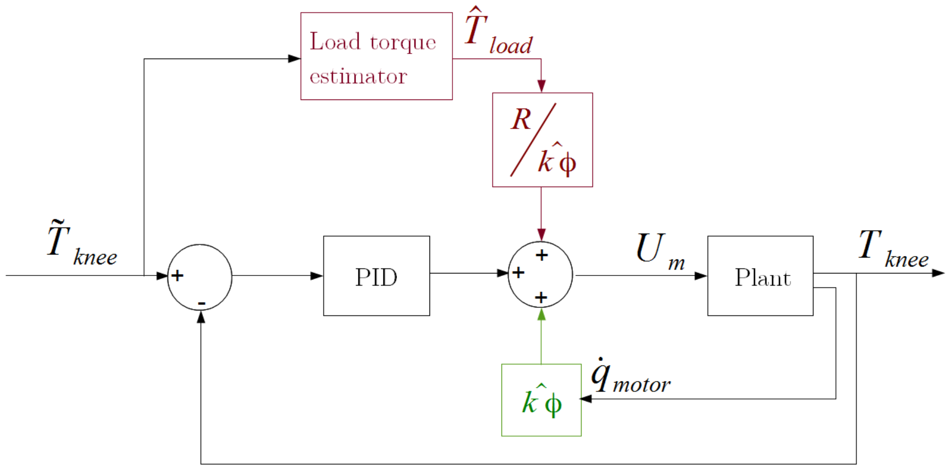

Figure 6.25: Schematic of torque control for the knee mechanism.

Such control has been tested on the knee mechanisms, with and without feedforward of the load torque. The results are shown in Figure 6.26 and 6.27.

It appears in the Figures that just a loop with the torque is not sufficient to fully control the output torque. Indeed, with this controller, the motor kinematic is not fully constrained and is free to oscillate at its natural frequency. This is also visible in the Figures because the moment when the slider switches between the extension and the baseline spring (different stiffness) is visible. The feedforward does not seem to help.

Therefore, in order to get a good tracking of the desired torque, another loop stabilizing this kinematic must be added. In the end, such a method would bring nothing compared to the position method described in the last chapter and to the current low-level controller that also contains various loops. It was not further investigated in this thesis.

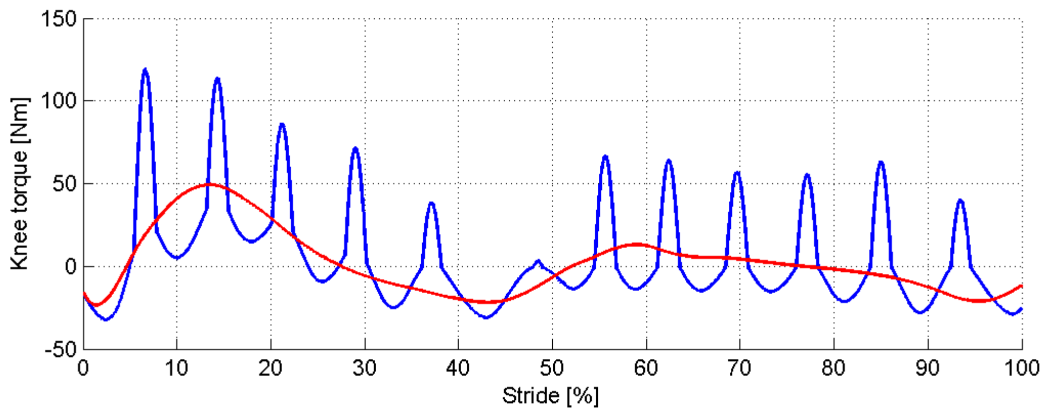

Figure 6.26: Tracking of the knee torque without feedforward of the load torque. The Winter's healthy knee torque is in red and the real position of the motor is in blue.

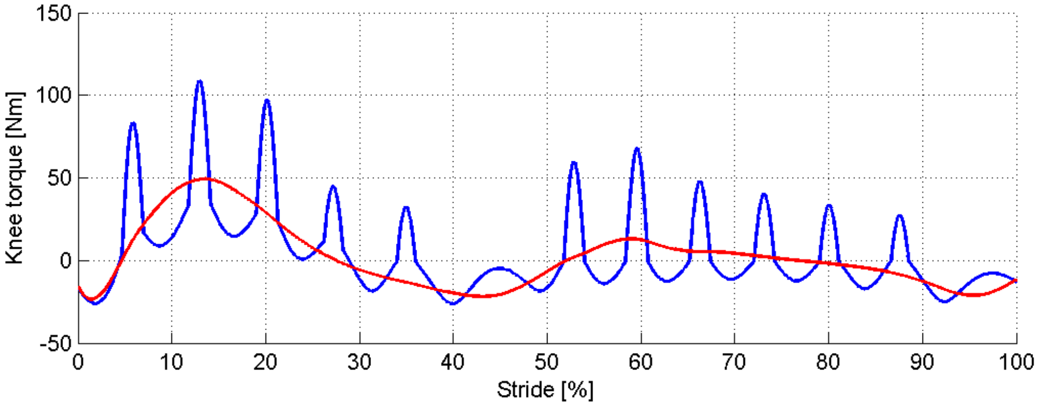

Figure 6.27: Tracking of the knee torque with feedforward of the load torque. The Winter's healthy knee torque is in red and the real position of the motor is in blue.

CONCLUSION

In this thesis, the CYBERLEGs-Beta prosthesis has been described. Then, its multibody modelling was explained. Thanks to this model, the dynamical effects in the prosthesis joints have been identified as negligible. Indeed, they are always two or three orders of magnitude lower than the others forces and torques. This difference excludes any invalidation of the model coming from an eventual error in the estimation of the parts masses and moments of inertia. This result is quite satisfying because it allows the already existing quasi-static model to be used for control without worrying about inertial, centrifugal and Coriolis forces. Except, of course, for the inertial effects due to the accelerations of the rotors of the motors.

From this analysis, a new motor/gearbox/spindle system was dimensioned for the knee mechanism. Indeed, the transmission ratio of the current system is currently too high. By using a slightly more powerful motor and a transmission ratio ten times lower, the system is able to provide the kinematic needed to obtain the Winter's knee torque in a healthy gait.

Then, four estimators were implemented. The two first estimate the desired motor position in function of the desired torque in the ankle and knee joints and the measurement of the position of these joints. The two others estimate the load torques that are currently applied to both motors. These load torques can then be used to improve the control of the actuators.

Finally, position and torque control were analysed as low-level control techniques for the motors. Position control with feedforward of the load torque and feedback on the motor position appeared to provide the best results.

Among all the things that can be done in order to continue this project, the first is to test the controller with the joint torques corresponding to stair climbing and sit-to-stand motion. Indeed, it was tested with steps, ramps and periodic torque inputs and gave satisfying results. However, it would be a great step to prove that the controller also works for these motions, because they are one of the goals of the prosthesis .

The next step would be to test the low-level controller on the real prosthesis to validate it. A mid-level bioinspired locomotion controller could be "plugged" on it and command him the reference torques for the ankle and knee joints. However, to test it on the knee mechanism, the knee motor system must be modified, as stated above.

Finally, stepping back a little, it appears that the method used in this thesis to design the low-level controller can also be adapted to another active prosthesis if a multibody or analytical model is provided. All these active prostheses try to reduce their power consumption and a good low-level control method can help on this subject.

BIBLIOGRAPHY

[1] Kathryn Ziegler-Graham. Estimating the prevalence of limb loss in the united states - 2005 to 2050,. *Archives of Physical Medicine and Rehabilitation*, 2008.

[2] Advanced Amputee Solution. Amputee statistics you ought to know.

[3] Michael R. Tucker, Jeremy Olivier, Anna Pagel, and Hannes Bleuler. Control strategies for active lower extremity prosthetics and orthotics: a review. *Journal of NeuroEngineering and Rehabilitation*, 2015.

[4] Louis Flynn, Bram Vanderborght, Dirk Lefeber, and Joost Geeroms. CYBERLEGs Beta-prosthesis active knee system. *Robotics and Multibody Mechanics*, 2015.

[5] S. Heins, L. Flynn, J. Geeroms, D. Lefeber, and R. Ronsse. Static and multi-body modelling of the CYBERLEGs Beta-prosthesis, an active transfemoral prosthesis with knee to ankle energy transfer [in preparation].

[6] J. C. H. Goh, S. E. Solomonidis, W. D. Spence, and J. P. Paul. Biomechanical evaluation of SACH and uniaxial feet. *Prosthetics and orthotics international*, 1984.

[7] Francesco Paradisi, Anna Sofia Delusse, and Stefano Brunelli. The conventional non-articulated SACH or a multiaxial prosthetic foor for hypomobile transtibial amputees ? *The Scientific World Journal*, 2015.

[8] Anthony Staros. SACH (Solid-Ankle Cushion-Heel) Foot. *Orthopedic & prosthetic appliance journal*, 1957.

[9] Yadan Zeng. Design and testing of a passive prosthetic ankle with mechanical performance similar to that of a natural ankle. Master's thesis, Marquette University, 2013.

[10] Rino Versluys, Pieter Beyl, Van Damme Michael, and Anja Desomer. Prosthetic feet: State-of-the-art review and the importance of mimicking human ankle-foot biomechanics. *Disability and Rehabilitation*, 2009.

[11] Brian J. Hafner, Joan E. Sanders, Joseph Czerniecki, and John Fergason. Energy storage and return prostheses: Does patient perception correlate with biomechanical analysis? *Clinical Biomechanics*, 2002.

[12] Össur. Vari-flex with evo. Technical report, Össur Head Office, 2014.

[13] Branko Brackx, Van Damme Michaël, Arnout Matthys, and Bram Vanderborght. Passive ankle-foot prosthesis prototype with extended push-off. *International journal of advanced robotic systems*, 2015.

[14] Pierre Cherelle, Arnout Matthys, Victor Grosu, and Bram Vanderborght. The AMP-Foot 2.0: Mimicking intact ankle behavior with a powered transtibial proshtesis. Technical report, Vrije Universiteit Brussel, 2013.

[15] Pierre Cherelle, Arnout Matthys, Victor Grosu, and Bram Vanderborght. Design and validation of the ankle mimicking prosthetic AMP-Foot 2.0. *IEEE*, 2014.

[16] Alan R. De Asha, Ramesh Munjal, Jai Kulkarni, and John G. Buckley. Impact on the biomechanics of overground gait of using an 'echelon' hydraulic ankle–foot device in unilateral trans-tibial and trans-femoral amputees. *Clinical Biomechanics*, 2014.

[17] Hugh M. Herr and Alena M. Grabowski. Bionic ankle-foot prosthesis normalizes walking gait for persons with leg amputation. *The Royal Society*, 2011.

[18] Össur. Proprio foot. Technical report, Össur Head Office, 2016.

[19] Matthew M. Williamson and Gill A. Pratt. Series elastic actuators. *IEEE*, 1995.

[20] Matthew M. Williamson. Series elastic actuators. Master's thesis, Massachusetts Institute of Technology, 1995.

[21] Samuel K. Au and Hugh M. Herr. Powered ankle-foot prosthesis. *IEEE*, 2008.

[22] Nikos G. Tsagarakis, Irene Sardellitti, and Darwin G. Caldwell. A new Variable Stiffness Actuator: Design and modelling. *IEEE*, 2011.

[23] Christophe Everarts, Bruno Dehez, and Renaud Ronsse. Variable stiffness actuator applied to an active ankle prosthesis: Principle, energy-efficiency and control. *IEEE*, 2012.

[24] Ronald Van Ham, Bram Vanderborght, Björn Verrels, and Dirk Lefeber. MACCEPA: The mechanically adjustable compliance and controllable equilibrium position actuator used in the controlled passive walking biped veronica. 2006.

[25] Bram Vanderborght, Nikos G. Tsagarakis, Claudio Semini, and Ronald Van Ham. MACCEPA 2.0: Adjustable compliant actuator with stiffening characteristic for energy efficient hopping. *IEEE*, 2009.

[26] Louis Flynn, Bram Vanderborght, Dirk Lefeber, and Joost Geeroms. Sliding-bar MACCEPA for powered ankle prosthesis. *Journal of Mechanisms and Robotics*, 2014.

[27] Maarten Weckx, Glenn Mathijssen, Si Mhand Benali Idris, and Raphaël Furnemont. A two-degree of freedom variable stiffness actuator based on the MACCEPA concept. *Actuators*, 2014.

[28] Ontario. Total knee replacement. *Ontario Health technology assessment Series*, 2005.

[29] Julie Wiest. *What's new in prosthetic knees ?* 2002.

[30] Össur. Locking knee. Technical report, Össur Head Office, 2016.

[31] WillowWood. Alignment and assembly fot the geoflex knee. Technical report, Ohio Willow Wood, 2011.

[32] OttoBock. 3r33/3r17 technical specifications. Technical report, Otto Bock HealthCare GmbH, 2011.

[33] Össur. Balance knee control. Technical report, Össur Head Office, 2015.

[34] Michelle M. Lusardi, Milagros Jorge, and Caroline C. Nielsen. *Orthotics and prosthetics in rehabilitation.* Elsevier Saunders, 2007.

[35] Felix Nicolas. Andando en cinta con protesis transfemoral. https://www.youtube.com/watch?v=lJZXNID1U0s.

[36] Bill Dupes. Prosthetic knee systems.

[37] J Thiele, B Westebbe, M Bellman, and M Kraft. Designs and performance of microprocessor-controlled knee joints. *Biomed Tech*, 2014.

[38] Ernesto C. Martinez-Villalpand and Hugh Herr. Agonist-antagonist active knee prosthesis : a preliminary study in level-ground walking. *Journal of Rehabilitation Research and Development*, 2009.

[39] Össur. Mauch knee. Technical report, Össur Head Office, 2015.

[40] OttoBock. 3r106-pro, 3r106-pro technical specifications. Technical report, Otto Bock HealthCare GmbH, 2013.

[41] Össur. Rheo knee 3. Technical report, Össur Head Office, 2016.

[42] OttoBock. C-leg technical specifications. Technical report, Otto Bock HealthCare GmbH, 2016.

[43] Randyhanger. Bilateral above knee amputee climbing stairs naturally. https://www.youtube.com/watch?v=LJAcv7nTqz8.

[44] OttoBock. C-LEG Standing Up and Sitting Down.

[45] Marko B.Popovic. *Biomechanics and Robotics*. Pan Stanford, 2014.

[46] OttoBock. 3r60-pro technical specifications. Technical report, Otto Bock HealthCare GmbH, 2015.

[47] OttoBock. 1c30 trias technical specifications. Technical report, Otto Bock HealthCare GmbH, 2015.

[48] Arnout Matthys, Pierre Cherelle, Van Damme Michael, and Bram Vanderborght. Concept and design of the HEKTA (harvest energy from the knee and transfer it to the ankle). *IEEE*, 2012.

[49] Louis Flynn, Bram Vanderborght, Dirk Lefeber, and Joost Geeroms. Ankle-knee prosthesis with powered ankle and energy transfer for CYBERLEGs Alpha-prototype. *IEEE*, 2013.

[50] Louis Flynn, Bram Vanderborght, Dirk Lefeber, and Joost Geeroms. Ankle-knee prosthesis with powered ankle and energy transfer : Development of the cuberlegs alpha-prosthesis. *Robotics and Autonomous Systems*, 2015.

[51] David A. Winter. *Biomechanics and motor control of human movement*. John Wiley and sons, 2005.

[52] P. Fisette and J.C Samin. Symbolic modeling of multibody systems. www.robotran.be.

[53] Maxon. Motors operating range. http://www.maxonmotor.com/maxon/view/content/maxon-Knowledge.

[54] Rik de Doncker, Duco W.J. Pulle, and André Veltman. *Advanced Electrical Drives : analysis, modeling and control*. Springer, 2011.

[55] Alice Boone. Experimental tests on a powered-ankle foot prosthesis. Master's thesis, Université Catholique de Louvain, 2015.

[56] CYBERLEGs. The CYBERnetic LowEr-limb coGnitive ortho-prosthesis.

[57] N. Docquier, A. Poncelet, and P. Fisette. ROBOTRAN: a powerful symbolic generator of multibody models. Université Catholique de Louvain.

[58] A. Parri, T. Yan, N. d'Elia, and F. Vannetti. Control of an active pelvis orthosis for gait assistance in the elderly. *GNB2014*, 2014.

[59] Sivangi Raychoudhury. Three dimensional kinematics of human metatarsophalangeal joint during locomotion. Master's thesis, University of Manchester, Faculty of engineering and physical science, 2014.

[60] Christopher L Vaughan, Brian L Davis, and Jeremy C O'Connor. *Dynamics of human gait*. Kiboho publishers, 1992.

[61] *Gait Analysis in the Science of Rehabilitation*. William & Wilkins, 1981.

[62] P.R.Khuman. Human gait. 2012.

[63] Marko Ackermann and Fabio G. Cozman. Automatic knee flexion in lower limb orthoses. *ABCM*, 2009.

[64] Chris A. McGibbon and David E. Krebs. Discriminating age and disability effects in locomotion : neuromuscular adaptations in musculoskeletl pathology. *Journal of Applied Physiology*, 2004.

Appendices

APPENDIX A — PROSTHESIS DATA

A general schematic of the prosthesis can be found in Figure A.2. It comes from [5]. All the parameters associated with this schematic and used in this thesis are in Table A.1. This table and the values come from [5] as well. The table is put in the next page for reading convenience with the schematic.

Parameter	Description	Value
θ_{WA}	WA spring compression limit angle	10 deg
K_{WA}	Weight acceptance spring stiffness	200 kN/m
L^0_{WA}	Weight acceptance spring rest length	0.038 m
K_{BL}	Baseline spring stiffness (2 springs)	10.7 kN/m
L^0_{BL}	Baseline spring rest length	0.064 m
K_{EX}	Extension spring stiffness (2 springs)	89 kN/m
L^0_{EX}	Extension spring rest length	0.032 m
C_k	Length of the WA lever arm	0.03 m
A_k	Length of the FA lever arm	0.03 m
B_k	Length of the rigid bar	0.15 m
Y_{WA}	Vertical distance between the knee joint and the WA axis	0.155 m
X_c	Horizontal distance between the knee joint the carriage axis	0.035 m
γ_c	Orientation of the carriage axis	5 deg
α_k	Angle of the FA lever arm when $\theta_k(t) = 0$ deg	20 deg
D	Length of the carriage	0.95 m
Z_0	Zero-position of the carriage	0.224 m
L_{sh}	Length of the shank	0.4 m
(p_{1x}, p_{1y})	Position of the first pulley's center	(0.005; 0.095)
(p_{2x}, p_{2y})	Position of the second pulley's center	(0.025; p_{2y})
R_p	Radius of the pulleys	0.01 m
K_{cable}	Stiffness of the cable	130 kN/m
θ_{para}	Parallel spring compression limit angle	-3.5 deg
K_{para}	Parallel spring stiffness	103 kN/m
L^0_{para}	Parallel spring compression rest length	0.025 m
K_{MAC}	MACCEPA spring stiffness	130 kN/m
(x^0_H, y^0_H)	Position $(x_H(t), y_H(t))$ when $\theta_a(t) = \theta_{\text{para}}$	(0.003; 0.046)
(x_R, y_R)	Position of the extremity of R_{para} fixed to the shank	(0.008; 0.045)
(x^0_F, y^0_F)	Position $(x_F(t), y_F(t))$ when $\theta_a(t) = \theta_{\text{para}}$	(0.028; 0.047)
R_{para}	Length of the rigid bar of the parallel spring system	0.03 m
A_M	Length of the drive side moment arm of the MACCEPA	0.05 m
B_M	Length of the spring side moment arm of the MACCEPA	0.05 m
P	Precompression of the MACCEPA spring	0.007 m
E	Length of the ET lever arm at the ankle joint	0.04 m
ζ_{ET}	Angle of the ET lever arm at the ankle	80 deg
φ_0	Zero-position of the MACCEPA lever arm with respect to the shank	143 deg

Figure A.1: Parameters of the CYBERLEGs-Beta prosthesis [5]

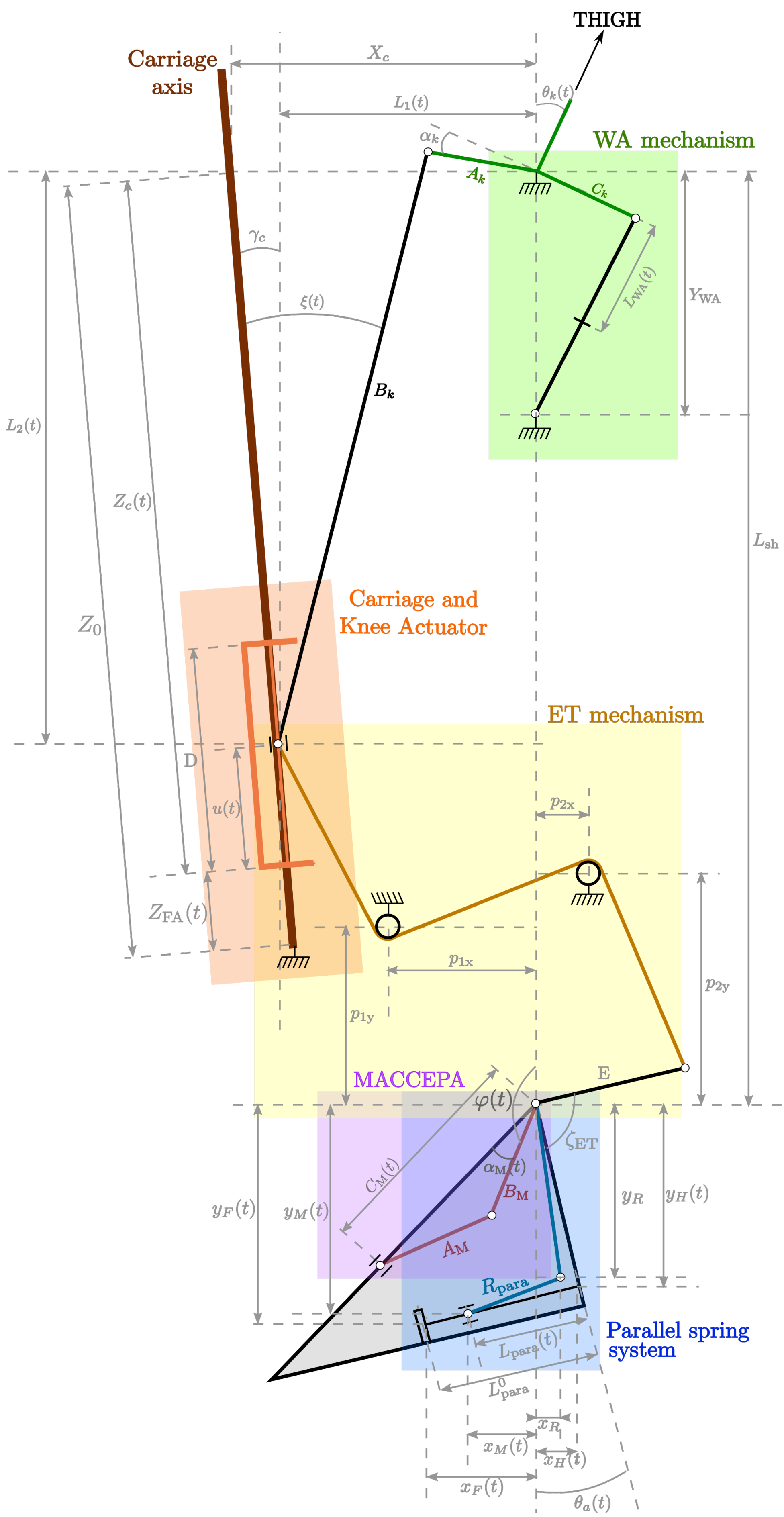

Figure A.2: Schematic of the CYBERLEGs-Beta prosthesis [5]

APPENDIX B

MATHEMATICAL APPENDIX

B.1 Geometrical relationships

In this section, the kinematic relationships between the different generalized coordinates of the mechanisms are explained.

B.1.1 Ankle

In the ankle, there are two degrees of freedom for six generalized coordinates (joints). Therefore, four kinematic relationships can be found. The denominations of Figure A.2 will be used here. The two degrees of freedom are defined as the ankle joint $\theta_a(t)$ ($-q_{ankle}(t)$) and the motor joint $q_{motor}(t)$.

The four dependent coordinates are the MACCEPA angle $\alpha_M(t)$ ($\alpha(t)$), the moment arm angle $q_{mom}(t)$ (angle between A_M and B_M), the MACCEPA spring translation $C_M(t)$ ($A_M + B_M - q_{MACCEPA}(t)$) and finally the parallel spring position $L_{para}(t)$ ($L^0_{para} - q_{para}(t)$).

The obvious relationships are:

$$\alpha_M(t) = q_{motor}(t)/\rho_a \tag{B.1}$$
$$C_M(t) = 2\,A_M(1 - cos(\alpha_M(t))) \tag{B.2}$$
$$q_{mom}(t) = \pi - 2\,\alpha_M(t) \tag{B.3}$$

ρ_a is the combined transmission ratio of the bevel gears and the gearbox. These relationships suppose $A_M = B_M$ because it is currently the case in the prosthesis. The relationship between $L_{para}(t)$ and $\theta_a(t)$ is a bit more complicated. It starts with finding the point H (see Figure A.2):

$$X_H(t) = L_H sin(\theta_a(t)); \tag{B.4}$$
$$Y_H(t) = -L_H cos(\theta_a(t)); \tag{B.5}$$

Then the X and Y differences between the point H and the point R (see Figure A.2) are defined:

$$X_H R(t) = X_H(t) - X_R; \tag{B.6}$$
$$Y_H R(t) = Y_H(t) - Y_R; \tag{B.7}$$

Then, point M (see Figure A.2) is found by solving:

$$(1+tan(\theta_a(t))^2)\chi(t)^2+(-2X_HR(t)-2Y_HR(t)\cdot tan(\theta_a(t)))\chi(t)+(Y_HR(t)^2-R_{para}^2+X_HR(t)^2) \tag{B.8}$$

The solution is always the positive one because the other does not make sense with the prosthesis geometry. Then $\psi(t)$ is found:

$$\psi(t)=\chi(t)\cdot tan(\theta_a(t)) \tag{B.9}$$

$\chi(t)$ and $\psi(t)$ are respectively the distance in x and y coordinates between the point H and the point M. Therefore:

$$X_M(t)=X_H(t)-\chi(t); \tag{B.10}$$

$$Y_M(t)=Y_H(t)-\psi(t); \tag{B.11}$$

When M is known, $L_{para}(t)$ is simply the distance between the point M and the point H, so:

$$L_{para}(t)=\sqrt{(X_M(t)-X_H(t))^2+(Y_M(t)-Y_H(t))^2} \tag{B.12}$$

It does not really make sense to write the entire exact relationship between $L_{para}(t)$ and $\theta_a(t)$ because it is too long.

B.1.2 Knee

In the knee, there are four generalized coordinates for two degrees of freedom. The two degrees of freedom are defined as the motor rotation q_{motor} and the knee joint rotation $\theta_k(t)$ ($q_{knee}(t)$).

The depending joints are the carriage motion $Z_c(t)$ ($q_{carriage}(t)$) and the springs slider motion $u(t)$ ($D-q_{slider}(t)$).

The relationship between the motor joint and the carriage joint is:

$$Z_c(t)=q_{motor}(t)/\rho_k \tag{B.13}$$

With ρ_k the combined transmission ratios of the gearbox and the spindle. The relationship between $u(t)$ and $\theta_k(t)$ is [5]:

$$u(t)=Z_c(t)-[(-A_k\cdot sin(\alpha_k-\theta_k(t))-B_k*cos(\xi(t)-\gamma_c))/cos(\gamma_c)] \tag{B.14}$$

with:

$$sin(\xi(t))=[X_c\cdot sin(\frac{\pi}{2}-\gamma_c)-A_k\cdot sin(\frac{\pi}{2}-\gamma_c+\alpha_k-\theta_k(t))]/B_k \tag{B.15}$$

B.2 Jacobian of the constraints

In this section, the Jacobian terms described in chapter 4 will be explained.

The first one is $J_{a,r}$. It links the rod constraint to the ankle joint. In *Robotran*, the constraints are associated with a Lagrange multiplier λ. For a connecting rod cut constraint, this multiplier is equal to the magnitude of the force, divided by the length of the rod. The connecting rod constraint is an algebraic equation imposing the distance between two points. It is usually written like $h(q) = 0$. The Jacobian term linking this constraint to the joint i is defined by $\partial h(q)/\partial q_i$ [52].

When *Robotran* generates the symbolic equations of the multibody model, it provides a symbolic expression for the Jacobian terms. For $J_{a,r}$, it is:

$$J_{a,r} = a \cdot b \tag{B.16}$$

Multiplying a times λ gives $a\lambda$, the horizontal component of the rod force. As λ is the force in the rod divided by its length, $a\lambda$ has indeed the dimension of a force. From there, multiplying $a\lambda$ with b (the lever arm between the ankle joint and the connecting rod) gives the torque produced by the rod force around the ankle joint. Hence, $J_{a,r}\lambda = a \cdot b \cdot \lambda$ is the torque due to the rod constraint in the ankle joint.

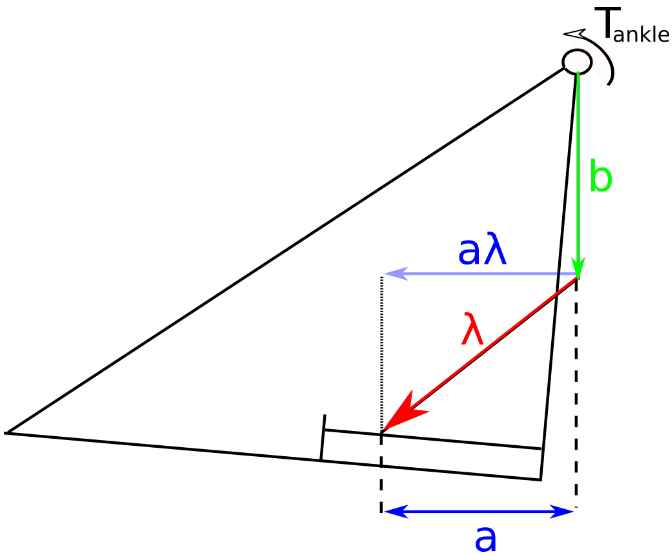

Figure B.1: Schematic of the parallel spring system in the ankle.

The same principle can be applied for $J_{p,r}$. However, the parallel spring joint is a prismatic joint. Therefore, λ gets transformed into a force and not a torque. $J_{p,r}$ has the dimension of a length this time.

Here $J_{p,r}$ is equal to:

$$J_{p,r} = a \cdot cos(\theta) + c \cdot sin(\theta) \tag{B.17}$$

$J_{p,r}\lambda$ has then the dimension of a force and its direction is the one of the parallel spring translation. Therefore, $J_{p,r}\lambda$ is indeed the force in the parallel spring joint due to the connecting rod constraint.

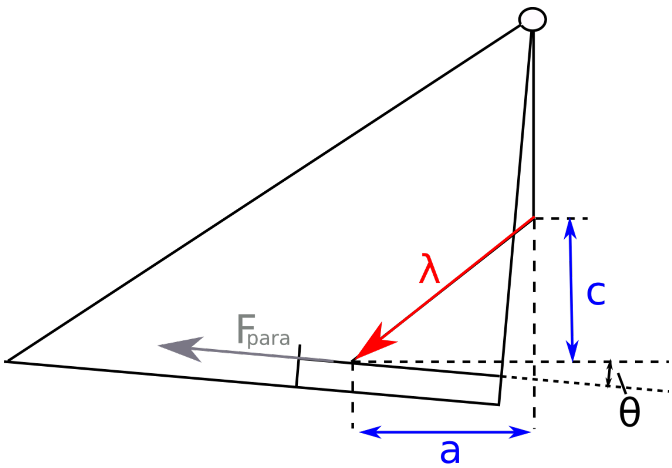

Figure B.2: Schematic of the parallel spring system in the ankle.

For $J_{k,r}$ and $J_{s,r}$ of the knee mechanism, the principle is exactly the same. $J_{k,r}\lambda$ transforms the force in the rod into a torque around the knee joint. And $J_{s,r}$ into a force along the spring prismatic joint.

For $J_{a,b}$ and $J_{M,b}$, it is almost the same. Except that a ball cut represents two constraints in two dimensions. Therefore, there are two Lagrange multipliers λ associated with this constraint. $J_{a,b}$ and $J_{M,b}$ have thus two components, one in the x direction and one in the y direction. But, in the end, it is the same principle. $J_{a,b}$ transforms the force due to the ball constraint into a torque around the ankle joint. And $J_{M,b}$ transforms it into a force along the MACCEPA spring joint.

B.3 Weight acceptance force

The weight acceptance mechanism is mainly composed of a spring. When the knee bends into its direction, the spring generates a counter-reaction. This force is calculated as a *link force* in *Robotran*. Then, this force is included in the $c(q, \dot{q}, t, F_{ext}, T_{ext}, g)$ as an external force. However, it must be transformed into a torque around the knee joint because this one is a revolute joint. This torque T_{WA} is also needed in the estimators of this thesis.

It is computed that way (see Figure A.2 for the symbols):

$$L_{WA}(t) = \sqrt{(C_k \cdot cos(\theta_k(t)) - X_{WA})^2 + (C_k \cdot sin(\theta_k(t)) + Y_{WA})^2} \tag{B.18}$$

The force in the weight acceptance spring is then:

$$F_{WA}(t) = K_{WA} \cdot (L_{WA}(t) - L^0_{WA}) \tag{B.19}$$

Defining:

$$\chi = (C_k \cdot cos(\theta_k(t)) - X_{WA})/L_{WA}(t) \tag{B.20}$$

$$\psi = (C_k \cdot sin(\theta_k(t)) + Y_{WA})/L_{WA}(t) \tag{B.21}$$

$T_{WA}(t)$ is finally:

$$T_{WA}(t) = -C_k \cdot F_{WA}(t) \cdot [\chi \cdot sin(\theta_k(t)) + \psi \cdot cos(\theta_k(t))] \tag{B.22}$$

APPENDIX C

THE CYBERLEGS PROJECT

CYBERLEGs (CYBERnetic LowEr-limb coGnitive ortho-prosthesis) is a collaborative research project funded by the European commission under the 7th Framework Programme. The project started on February 2012. It is composed by five partners from three different European countries :

- Italy: Scuola Superiore Sant'Anna and Rizzoli ortopedia
- Belgium: Université Catholique de Louvain and Vrije Universiteit Brussel
- Ljubljana: University of Ljubljana, faculty of Electrical Engineering

This chapter is mostly adapted from the CYBERLEGs website[56].

The scientific and technological global aim of CYBERLEGs project is the development of an artificial cognitive system for dysvascular transfemoral amputees lower-limb functional replacement and assistance in activities of daily living. To realize this, challenges are present like the development of a energy-efficient powered lower-limb prosthesis with energy transfer from knee to ankle joint or again the investigation of a recognition and prevention of falling.

At its end, the CYBERLEGs project will be a robotic system composed by an active leg prosthesis and a wearable active orthosis for assisting. It will allow the amputees to realize different actions like sit-to-stand and stairs climbing with a minimum energetic effort. The system will detect both intention of the user and the risk of fall with sensors.

After years, some results are obtained and are presented above.

First simulation of a walking biped

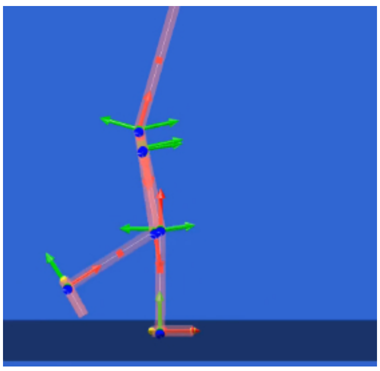

Figure C.1: Simulation of walking biped using *Robotran* [57]

To mimic the human gait, some researchers from UCL have simulated a healthy walking biped with the *Robotran* software developed by the UCL [57] and the *Matlab* environment. The model includes both the multibody model (see in Figure C.1) and the muscle dynamics. This biped is controlled by a reflex-based control layer. The model can then mimic the gait and will be modify to add in prosthesis devices.

CYBERLEGs prosthesis

Figure C.2: CYBERLEGs Beta-prosthesis

As the aim of the CYBERLEGs project is to provide a device for lower-limb amputees, a transfemoral prosthesis has been created, the CYBERLEGs Beta-prosthesis [4], displayed in Figure C.2. It is composed of an active knee and an active ankle with energy transfer between both modules.

The light-weight Active Pelvis Orthosis

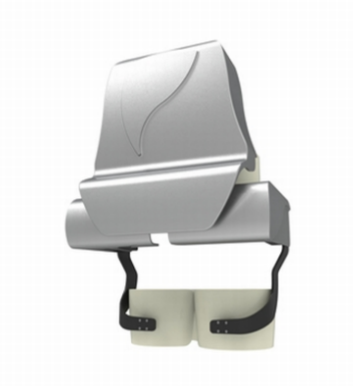

Figure C.3: The light-weight Active Pelvis Orthosis

The light-weight Active Pelvis Orthosis (APO) is a device used to provide gait assistance based on an adaptive oscillator controller, displayed in Figure C.3. An orthosis (or again an exoskeleton) for gait assistance is a mechanical device that the can be carried by the user. It closely fits the body and have a light weight (4.2 kg for the CYBERLEGs APO). Some tests are realized on non-amputee human but experiences on amputees have also started [58].

APPENDIX D

BIOMECHANICS OF THE GAIT

D.1 The gait analysis

Gait analysis is the term used to define the study of human walking. Human gait is the process of locomotion of a human to move from a start point to an end point. Walking is a repetition of a gait pattern named "stride" and begins when one foot touches the ground and ends when the same foot retouches the ground. It is thus a periodic movement of each foot from one position to the next. Therefore, descriptions of walking are normally confined to a single cycle, displayed in Figure D.1. In this Figure, the right foot touching the ground defines the gait starting point.

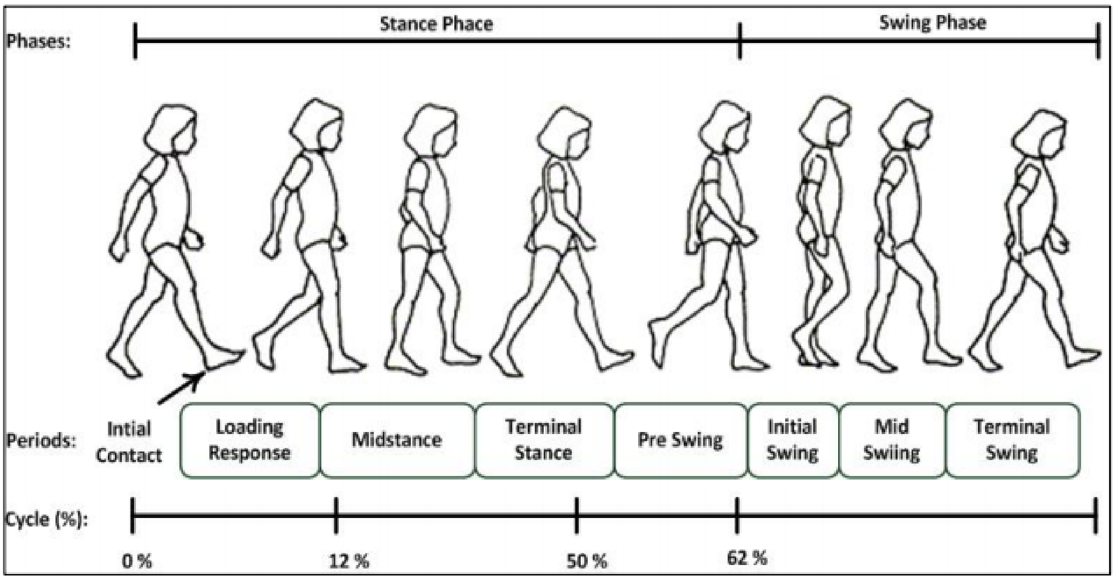

Figure D.1: The gait phase [59]

As seen in this Figure, the gait cycle is divided in two main phases : Stance phase and Swing Phase :
The Stance phase covers 60∼62% of the gait cycle. It is the part when the foot is in contact with the ground. The Swing phase is the second part of the cycle and lasts 38∼40% of this. During this phase, the foot does not touch the ground.

The gait cycle can also be divided in two different periods : the right step and the left step: The right step is the step when the right foot touches the ground and the left step when the left foot touches the floor. Each step starts when the corresponding foot begins to touch the ground. Then, the end of one step is the moment where the two feet are in contact with the ground.

With this definition, each step takes 50% of the gait cycle.

The first phase can be subdivided into five periods :

- The initial contact or heel strike. This period initiates the gait cycle and lasts up to 2% of the stride. It starts when the heel touches the ground.
- Loading response or double stance. It is the phase where the foot is flat and the toes of the opposite foot leave the ground. It ends at 12 % of the gait cycle. Here, the shift of the weight occurs from the left to the right.
- Mid-stance. In this period, the foot is entirely flat on the ground and the opposite foot leaves the ground completely. It is the first phase with single leg support. In this case, the total weight is supported by the right foot. It goes from 12% to 40% of the gait cycle.
- Terminal stance or heel-off. Here, the right heel rises off the ground and the left foot touches the ground. It takes 10% of the stride.
- Pre-swing or Toe-off. It is the final period of the stance and goes from 50% to 60∼62% of the gait cycle. It is the second double stance in the cycle. The second weight transfer occurs. The right heel is not in contact with the ground and the left foot is flat on the ground.

The swing phase follows the last part of the stance phase and is subdivided into three periods :

- The initial swing or acceleration. It is the first period in the swing phase. It follows directly the pre-swing phase. In this step, the toes leaves the ground. The other leg starts the second phase with single leg support. This phase ends when the total weight is on the left leg, at 70 % of the gait cycle.
- Mid-swing. Here, the right foot remains in the air until the tibia is vertical to the ground. The weight is then in front of the left foot. This phases ends at 85 % of the stride.
- Terminal swing or deceleration. It is the final phase of the gait cycle. The heel of the right foot touches the ground again.

The human walking can be seen like a cyclic pattern following the previous descriptions. It is displayed in Figure D.2.

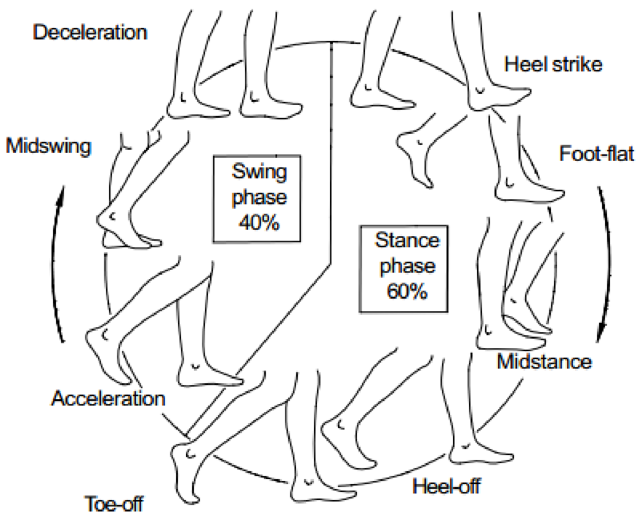

Figure D.2: Cyclic nature of human gait [60]

With this reference gait, the different movement of the knee and the ankle can be defined properly [61].

D.2 Knee analysis during walking

An analysis of the flexion angle of the knee is important to know how it behaves during the gait. To do that, each period of the gait must be analysed. First, the stance phase is considered in Figure D.3.
At the heel-strike or the initial contact, the knee is straight, and the flexion angle is approximately equal to zero.
During foot-flat period, the knee begins to flex. At the next period, mid-stance step, the knee reaches an angle of 20 degrees and then declines to zero at the heel-off period. When the toe lifts off the ground, the knee flexes again.

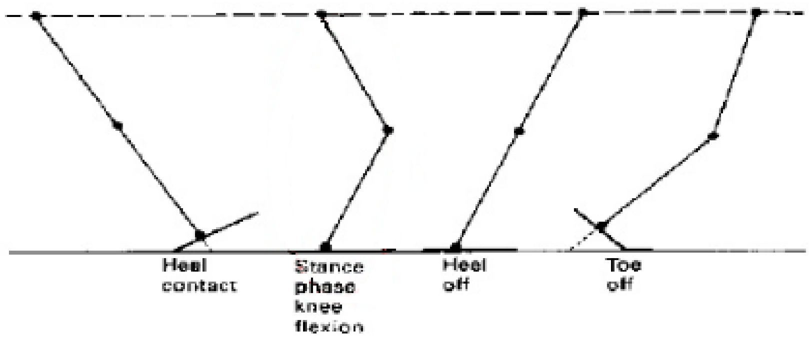

Figure D.3: Scheme of the knee movement during stance phase [62]

Secondly, the Swing phase starts. It is displayed in Figure D.4. This part is very important for the flexion angle because the maximum angle is reached. In the Figure, the first and second step represent the heel-off and the toe off in stance phase. During the third step, the knee continues to flex. The flexion angle reaches 60 degrees. During the mid-swing period, the gravity forces the knee to extend and finally, the flexion angle approximately equals zero at the terminal swing.

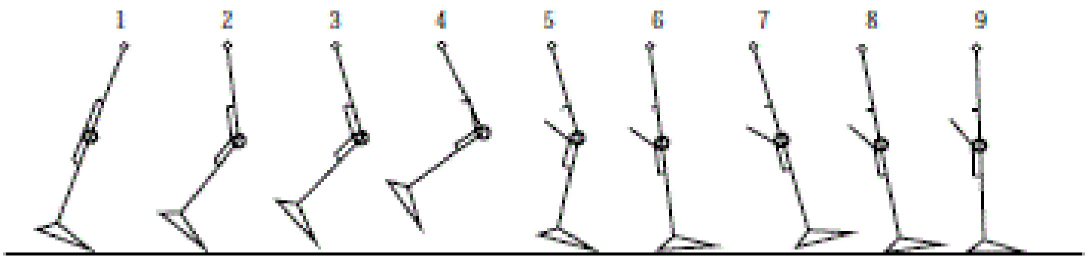

Figure D.4: Scheme of the knee movement during swing phase [63]

With these different phases when the knee flexes or extends, the graphical representation of the flexion angle in the sagittal plane is more understandable, displayed in Figure D.5. The first local maximum is achieved at mid-stance period and the second maximum at acceleration period. Concerning the knee power, two peaks are important. One during the foot-flat period and the second in the pre-swing period. These peaks are negative, this is why a knee dissipates energy at this time.

Finally, a lot of experiences have been made in order to get a reference set of data for a healthy human gait. This set is called Winter's data for a healthy gait. [51].

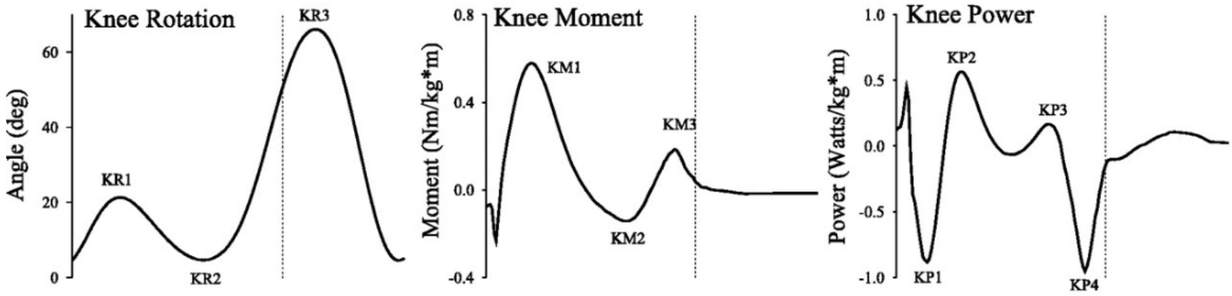

Figure D.5: Angle, moment and power knee during one stride [64]

D.3 Ankle analysis during walking

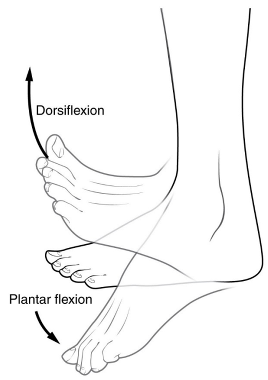

Figure D.6: Terms used for the ankle joint

The analysis of the ankle is made with the ankle joint. It is the joint at the end of the tibia. Three terms are used in function of flexion or extension of the ankle joint : plantarflexion, neutral position and dorsiflexion. The neutral position is the position where the tibia and the foot are perpendicular and then the ankle joint equals zero. The plantarflexion is used when the angle decreases. In opposite, the dorsiflexion is used when the angle increases. A schematic of this is displayed in Figure D.7.

With this definition, the analysis of this joint can be made during a gait cycle.
In Figure D.3, the stance phase is taken into account. During the initial contact, the ankle is a little bit flexed (approximately 2 degrees). Then, from the loading response to Heel-off, the ankle is in dorsiflexion. The ankle joint is positive. During the Toe-off, the ankle is in plantarflexion. At the end of this period, the ankle reaches the maximum plantarflexion (approximately 12 degrees).
The Figure D.4 shows the swing phase. In the acceleration period, the ankle joint is in plantarflexion and rises. During the mid-swing, the ankle joint reaches the neutral position and finally, this angle decreases a little bit during the deceleration period.
The graphical representation of this angle is shown in Figure D.7. In this Figure, the ankle power is globally positive. The peak of power represent 80 % of the power and it is positive. Then, the ankle is considered to consume energy.

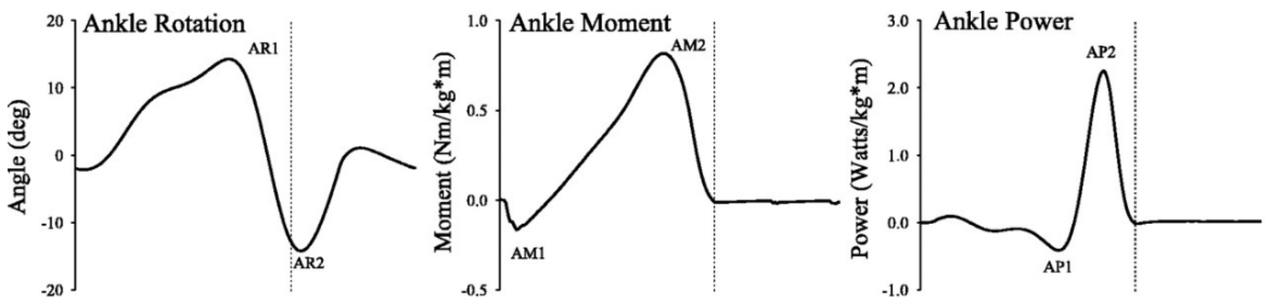

Figure D.7: Angle, moment and power ankle during one stride from [64]

APPENDIX E

ROBOTRAN

Robotran is a software able to model a multibody system (MBS). It was developed by the CEREM, the CEnter for Research in Energy and Mechatronics, which is part of the Institute of Mechanics, Materials and Civil Engineering at the Univeristé Catholique de Louvain. The modelling with *Robotran* allows to set up the equations of motion for a MBS system for a given set of system parameters and generalized coordinates. This chapter is mostly adapted from [57]. More details can be found on the website of *Robotran*.

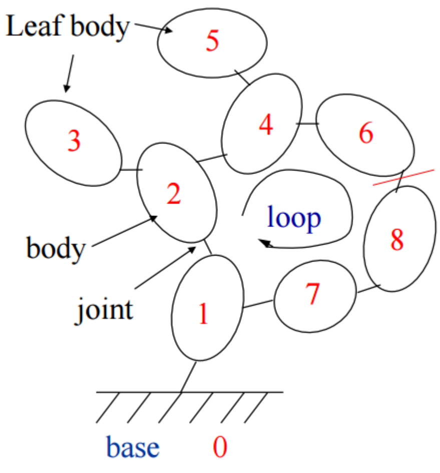

Figure E.1: Tree-like structure

To established the equation of motion, *Robotran* uses the relative joint coordinates(based on angles) and tree-like structure, displayed in Figure E.1. A tree-like structure is composed of a basis (considered like the initial body), bodies and joints. The bodies are rigid components connected by joints (pure rotation or pure translation) between them. Bodies at the end of the structure (bodies connected with only one other joint) are called "leaf bodies". In the structure, kinematic loops can appear. Cuts are used to close these loops. Indeed, if a joint is used to close them, it results in two ways to travel through the structure from the base to the leaves. And *Robotran* can not work in that case.

There are three different cuts used by *Robotran* : solid, rod and ball cuts. These cuts are shown in Figure E.2.

- The first procedure is the most general and consist in cutting a body of the loop in two parts: the original body and the shadow body. Six constraints must be satisfied. Three position constraints and three orientation constraints.

- The second kind of cut is the rod cut. It closes the loop with a connecting rod whose mass and inertia are ignored. In this case, only one constraint is sufficient to satisfy the loop kinematics, the distance between the extremities of the rod.

- The ball cut is the last one. This cut is like a spheric joint which can be considered ideal. That means there is no torque transmitted and no backlash in this joint. For this joint, three constraints must be satisfy : the three position constraints.

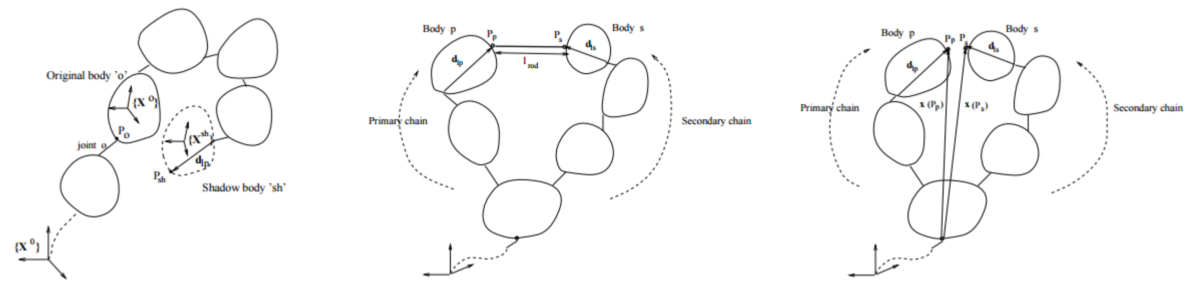

(a) Solid cut (b) Rod cut (c) Ball cut

Figure E.2: Cuts used in a closed loop [52]

After the tree-like structure established, the dynamic of these systems is considered. There are two types of dynamics used in *Robotran*. They are develop in the two following sections.

E.1 Direct dynamics

The motion of a multibody system can be predicted by the direct dynamic. It computes the generalized accelerations $\ddot{q}$ for a given configuration $(q, \dot{q})$ of the system on which forces(fr) and torques(tr) are applied. That can be written in a synthetic form (semi-explicit) :

$$M(q,\delta)\ddot{q} + c(q,\dot{q},\delta,fr,tr,g) = \mathcal{Q}(q,\dot{q}) \tag{E.1}$$

Or in explicit form :

$$\ddot{q} = f(q,\dot{q},\delta,fr,tr,\phi,\delta) \tag{E.2}$$

In the case of Equation E.1, variables are:

- M is the generalized mass matrix of the system [n*n]. It is symmetric and positive definite.
- c is a the non linear dynamical vector [n*1]. It contains the centrifugal, the gyroscopic, external forces, external torques and gravity terms.
- q is the relative generalized coordinates. It is a vector [n*1].
- $\mathcal{Q}$ represents the generalized joints forces (torques) [n*1]

To obtain this equation, *Robotran* uses the Newton-Euler algorithm.
However, this equation is not totally completed if any constraints is present in the system. This is the case where the multibody system contains loops. These loops imposes the generalized joint coordinates to satisfy algebraic constraint at any time, noted $h(q) = 0$. These constraints can also be physical phenomena like rolling without slipping. They are added in the motion equation with the Lagrange multiplier λ technique. The equation E.1 becomes:

$$\begin{aligned}
M(q,\delta)\ddot{q} + c(q,\dot{q},\delta,fr,tr,g) &= \mathcal{Q}(q,\dot{q}) + J\lambda && \text{(E.3)}\\
h(q) &= 0 && \text{(E.4)}\\
\dot{h}(q,\dot{q}) &= J(q)\dot{q} = 0 && \text{(E.5)}\\
\ddot{h}(q,\dot{q},\ddot{q}) &= J(q)\ddot{q} + \dot{J}\dot{q}(q,\dot{q}) = 0 && \text{(E.6)}
\end{aligned}$$

Here, J is the Jacobian constraints matrix [m*n]. It is calculated by the partial derivative of the constraints in function of the generalized coordinates $J = \frac{\delta h}{\delta q^t}$

E.2 Inverse dynamics

If the results of the simulation must be the forces or torques, the inverse dynamics is used. Indeed, it computes the generalized joint forces (torques) ϕ to be applied on each joint to get a given configuration $(q, \dot{q}, \ddot{q})$ of the system. It can be mathematically written like :

$$\phi = f(q, \dot{q}, \ddot{q}, \delta, fr, tr, \delta) \tag{E.7}$$

It is typically used in robotics to control actuators when following a desired trajectory. This equation is generated by Newton-Euler algorithm.
Like in the direct dynamics, if constraints are present in the system they are added in the equation with the Lagrange multiplier λ technique.

$$\begin{aligned} \phi = f(q, \dot{q}, \ddot{q}, \delta, fr, tr, \delta) + J\lambda h(q) &= 0 && \text{(E.8)} \\ \dot{h}(q, \dot{q}) &= J(q)\dot{q} = 0 && \text{(E.9)} \\ \ddot{h}(q, \dot{q}, \ddot{q}) &= J(q)\ddot{q} + \dot{J}\dot{q}(q, \dot{q}) = 0 && \text{(E.10)} \end{aligned}$$

APPENDIX F

MOTOR DATASHEETS

In this chapter, the following datasheets are displayed:

- The current ankle motor
- The current knee motor
- The proposed knee motor
- The proposed spindle
- The proposed screw nut
- The proposed flange bearing

EC-4pole 30 ∅30 mm, brushless, 200 Watt

High Power

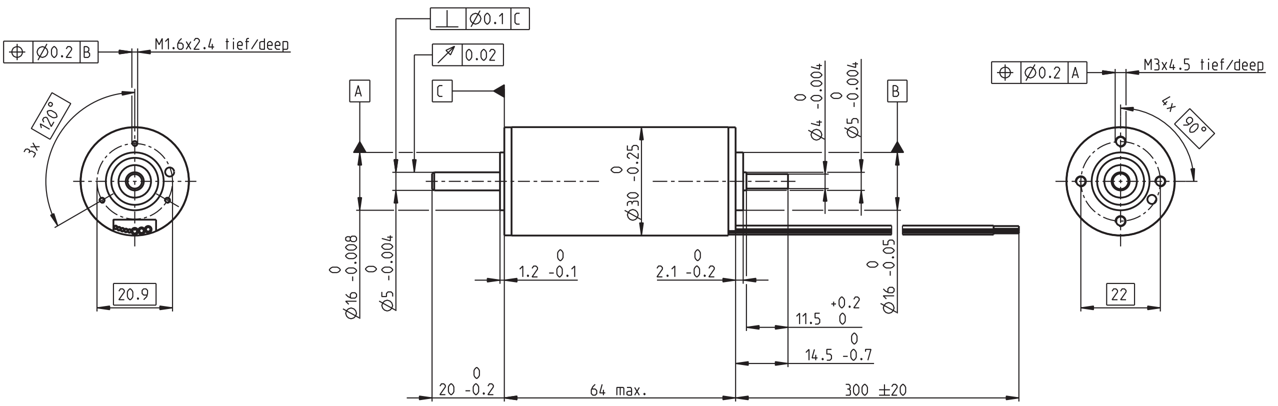

M 1:2

Stock program
Standard program
Special program (on request)

Part Numbers

Motor Data		305013	305014	305015
Values at nominal voltage				
1 Nominal voltage	V	24	36	48
2 No load speed	rpm	16700	16700	16500
3 No load current	mA	728	485	356
4 Nominal speed	rpm	16100	16200	16000
5 Nominal torque (max. continuous torque)	mNm	94.6	94.2	92.9
6 Nominal current (max. continuous current)	A	7.58	5.03	3.68
7 Stall torque	mNm	3220	3510	3430
8 Stall current	A	236	171	124
9 Max. efficiency	%	89.4	89.9	89.8
Characteristics				
10 Terminal resistance phase to phase	Ω	0.102	0.21	0.386
11 Terminal inductance phase to phase	mH	0.0163	0.0368	0.0653
12 Torque constant	mNm/A	13.6	20.5	27.6
13 Speed constant	rpm/V	700	466	346
14 Speed/torque gradient	rpm/mNm	5.21	4.78	4.83
15 Mechanical time constant	ms	1.82	1.67	1.69
16 Rotor inertia	gcm^2	33.3	33.3	33.3

Specifications

Thermal data

17 Thermal resistance housing-ambient 7.4 K/W
18 Thermal resistance winding-housing 0.21 K/W
19 Thermal time constant winding 2.11 s
20 Thermal time constant motor 1180 s
21 Ambient temperature -20…+100°C
22 Max. winding temperature +155°C

Mechanical data (preloaded ball bearings)

23 Max. speed 25000 rpm
24 Axial play at axial load < 8.0 N 0 mm
> 8.0 N 0.14 mm
25 Radial play preloaded
26 Max. axial load (dynamic) 5.5 N
27 Max. force for press fits (static) 73 N
(static, shaft supported) 1300 N
28 Max. radial load, 5 mm from flange 25 N

Other specifications

29 Number of pole pairs 2
30 Number of phases 3
31 Weight of motor 300 g

Values listed in the table are nominal.

Connection motor (Cable AWG 18)
black Motor winding 2
white Motor winding 3
red Motor winding 1
Connection sensors (Cable AWG 26)
black/grey Hall sensor 2
blue GND
green V_{Hall} 3…24 VDC
red/grey Hall sensor 1
white/grey Hall sensor 3
Wiring diagram for Hall sensors see p. 33

Operating Range

Comments

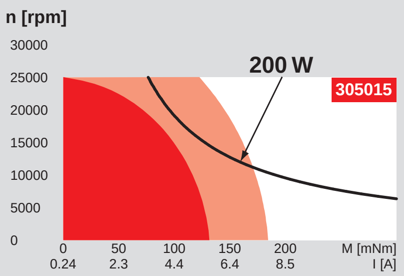

Continuous operation
Continuous operation with reduced thermal resistance R_{th2} 50%
Intermittent operation

Assigned power rating

maxon Modular System

Overview on page 20–25

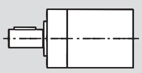

Planetary Gearhead
∅32 mm
8 Nm
Page 310

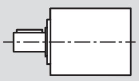

Planetary Gearhead
∅42 mm
3 - 15 Nm
Page 315

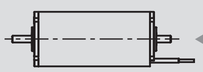

Recommended Electronics:

Notes	Page **24**
ESCON Mod. 50/5	379
ESCON Mod. 50/4 EC-S	379
ESCON 50/5	379
ESCON 70/10	380
DEC Module 50/5	382
EPOS2 50/5	387
EPOS2 70/10	387
EPOS3 70/10 EtherCAT	393
MAXPOS 50/5	396

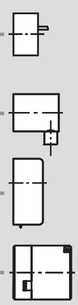

Encoder MR
128 - 1000 CPT,
3 channels
Page 355
Encoder 2RMHF
3000 - 5000 CPT,
3 channels
Page 360
Encoder HEDL 5540
500 CPT,
3 channels
Page 367
Brake AB 20
24 VDC
0.1 Nm
Page 406

EC-i 40 ∅40 mm, brushless, 70 Watt

NEW

maxon EC-i

High Torque

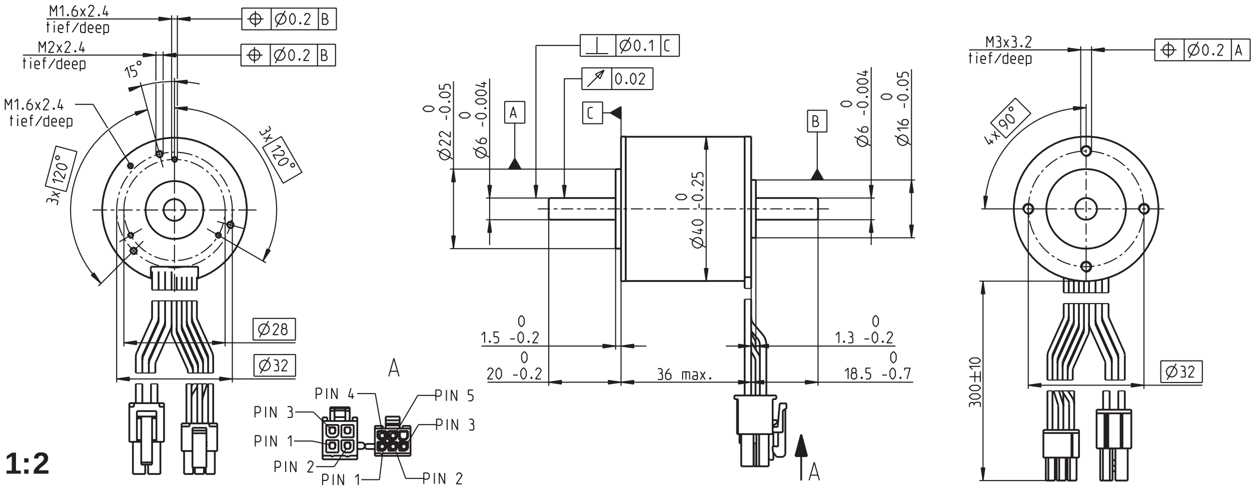

M 1:2

- Stock program
- Standard program
- Special program (on request)

Part Numbers

with Hall sensors		496654	496655	496656
Motor Data (provisional)				
Values at nominal voltage				
1 Nominal voltage	V	18	36	48
2 No load speed	rpm	7840	7390	4930
3 No load current	mA	448	205	86.4
4 Nominal speed	rpm	6900	6440	4090
5 Nominal torque (max. continuous torque)	mNm	111	137	160
6 Nominal current (max. continuous current)	A	5.13	2.87	1.64
7 Stall torque	mNm	2290	3190	2190
8 Stall current	A	106	69.3	23.8
9 Max. efficiency	%	88	90	88
Characteristics				
10 Terminal resistance phase to phase	Ω	0.17	0.519	2.02
11 Terminal inductance phase to phase	mH	0.113	0.512	2.05
12 Torque constant	mNm/A	21.7	46.1	92.1
13 Speed constant	rpm/V	441	207	104
14 Speed/torque gradient	rpm/mNm	3.47	2.34	2.27
15 Mechanical time constant	ms	0.835	0.563	0.547
16 Rotor inertia	gcm^2	23	23	23

Specifications

Thermal data

17 Thermal resistance housing-ambient	8.17 K/W
18 Thermal resistance winding-housing	2.27 K/W
19 Thermal time constant winding	21.8 s
20 Thermal time constant motor	1020 s
21 Ambient temperature	-40…+100°C
22 Max. winding temperature	+155°C

Mechanical data (preloaded ball bearings)

23 Max. speed	10000 rpm
24 Axial play at axial load < 9.0 N	0 mm
> 9.0 N	0.15 mm
25 Radial play	preloaded
26 Max. axial load (dynamic)	7 N
27 Max. force for press fits (static)	87 N
(static, shaft supported)	5000 N
28 Max. radial load, 5 mm from flange	26.1 N

Other specifications

29 Number of pole pairs	7
30 Number of phases	3
31 Weight of motor	250 g

Values listed in the table are nominal.

Connection (Cable AWG 20)

red	Motor winding 1	Pin 1
black	Motor winding 2	Pin 2
white	Motor winding 3	Pin 3
	N.C.	Pin 4
Connector	**Article number**	
Molex	39-01-2040	

Connection (Cable AWG 26)

yellow	Hall sensor 1	Pin 1
brown	Hall sensor 2	Pin 2
grey	Hall sensor 3	Pin 3
blue	GND	Pin 4
green	V_{Hall} 4.5…24 VDC	Pin 5
	N.C.	Pin 6
Connector	**Article number**	
Molex	430-25-0600	

Wiring diagram for Hall sensors see p. 35

Operating Range

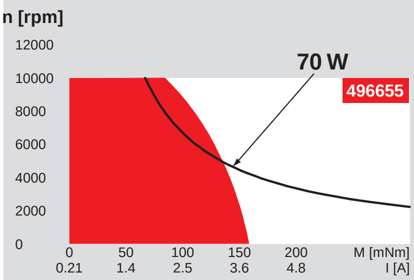

Comments

Continuous operation
In observation of above listed thermal resistance (lines 17 and 18) the maximum permissible winding temperature will be reached during continuous operation at 25°C ambient.
= Thermal limit.

Short term operation
The motor may be briefly overloaded (recurring).

Assigned power rating

maxon Modular System

Overview on page 20–25

Planetary Gearhead
∅42 mm
3 - 15 Nm
Page 315

Recommended Electronics:

Notes	Page **24**
ESCON 36/3 EC	379
ESCON Mod. 50/4 EC-S	379
ESCON Module 50/5	379
ESCON 50/5	380
ESCON 70/10	380
DEC Module 50/5	382
EPOS2 24/5	387
EPOS2 50/5	387
EPOS2 70/10	387
EPOS3 70/10 EtherCAT	393
MAXPOS 50/5	396

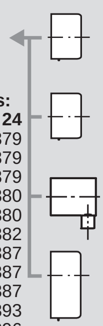

Encoder 16 EASY
128 - 1024 CPT,
3 channels
Page 345

Encoder 16 EASY Absolute
4096 steps
Page 346

Encoder 2RMHF
3000 - 5000 CTP,
3 channels
Page 360

Encoder HEDL 5540
500 CPT,
3 channels
Page 367

April 2015 edition / subject to change

ECX SPEED 22 L bürstenlos
BLDC-Motor Ø22 mm

NEW

80/111 W 24 mNm 45000 min⁻¹

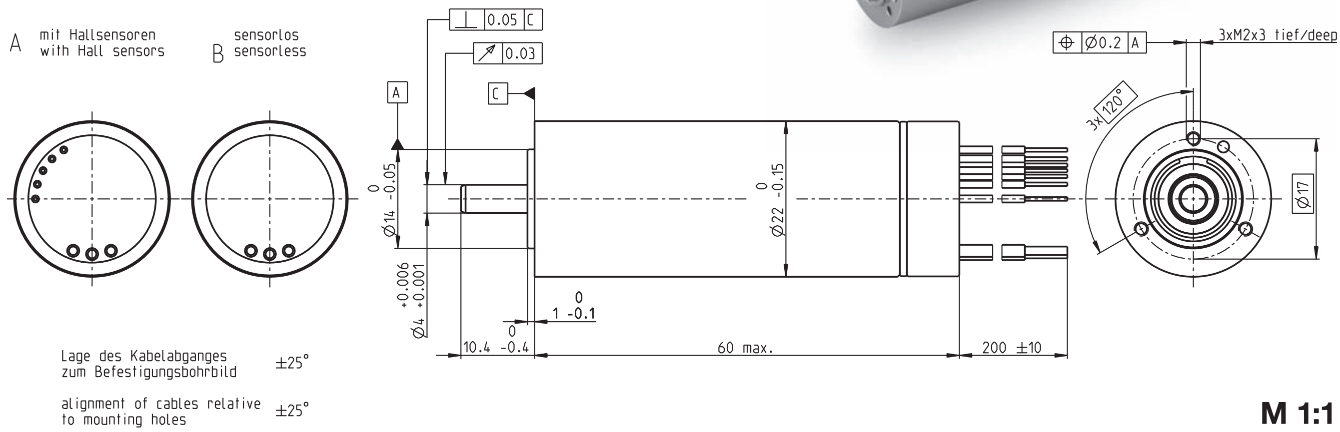

M 1:1

	Motordaten				
1_	Nennspannung	V	24	36	48
2_	Leerlaufdrehzahl	min⁻¹	38300	37100	37700
3_	Leerlaufstrom	mA	299	189	145
4_	Nenndrehzahl	min⁻¹	35800	34700	35400
5_	Nennmoment (max. Dauerdrehmoment)	mNm	22.4	23.5	24.7
6_	Nennstrom (max. Dauerbelastungsstrom)	A	4.02	2.71	2.16
7_	Anhaltemoment	mNm	381	404	458
8_	Anlaufstrom	A	64	43.8	37.8
9_	Max. Wirkungsgrad	%	87	87.5	88.2
10_	Anschlusswiderstand	Ω	0.375	0.823	1.27
11_	Anschlussinduktivität	mH	0.0234	0.0563	0.0967
12_	Drehmomentkonstante	mNm/A	5.95	9.23	12.1
13_	Drehzahlkonstante	min⁻¹/V	1610	1030	789
14_	Kennliniensteigung	min⁻¹/mNm	101	92.2	82.7
15_	Mechanische Anlaufzeitkonstante	ms	4.12	3.75	3.37
16_	Rotorträgheitsmoment	gcm²	3.89	3.89	3.89

	Thermische Daten		
17_	Therm. Widerstand Gehäuse-Luft	K/W	10
18_	Therm. Widerstand Wicklung-Gehäuse	K/W	0.871
19_	Therm. Zeitkonstante der Wicklung	s	2.74
20_	Therm. Zeitkonstante des Motors	s	507
21_	Umgebungstemperatur[1]	°C	-20…+100
22_	Max. Wicklungstemperatur	°C	155
	Mechanische Daten Kugellager		
23_	Grenzdrehzahl	min⁻¹	45000
24_	Axialspiel	mm	0…0.24
	Vorspannung	N	4
	Kraftrichtung		Zug
25_	Radialspiel		vorgespannt
26_	Max. axiale Belastung (dynamisch)	N	4
27_	Max. axiale Aufpresskraft (statisch)	N	110
	(Welle abgestützt)	N	6000
28_	Max. radiale Belastung [mm ab Flansch]	N	16 [5]
	Weitere Spezifikationen		
29_	Polpaarzahl		1
30_	Anzahl Phasen		3
31_	Motorgewicht	g	140
32_	Typischer Geräuschpegel [min⁻¹]	dBA	54 [45000]

Anschlüsse A und B, Motor (Kabel AWG 18)

rot	Motorwicklung 1
schwarz	Motorwicklung 2
weiss	Motorwicklung 3

Anschlüsse A, Sensoren (Kabel AWG 26)

orange	V_{Hall} 3…24 VDC
blau	GND
gelb	Hall-Sensor 1
braun	Hall-Sensor 2
grau	Hall-Sensor 3

Schaltbild für Hall-Sensoren siehe S. 35

Anschlüsse NTC (Kabel AWG 26)

violett	NTC
violett	NTC

Widerstand 25°C: 10 kOhm ±1%, beta (25–85°C): 3490 K

Betriebsbereiche

n [min⁻¹] Wicklung 36 V

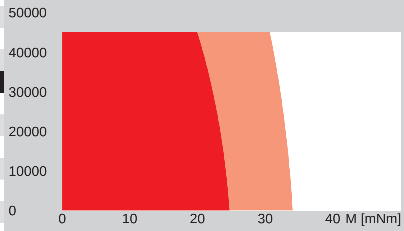

- Dauerbetriebsbereich
- Dauerbetriebsbereich bei reduziertem therm. Widerstand R_{th2} 50%
- Kurzzeitbetriebsbereich

maxon Baukastensystem

maxon gear	Stufen	maxon sensor	maxon motor control
133_GPX 22 SPEED	1–2		417_ESCON Module 50/4 EC-S
			417_ESCON Module 50/5
			418_ESCON 50/5
			418_ESCON 70/10
			420_DEC Module 50/5

Konfiguration

Flansch vorne: Gewinde im Flansch/Zentralgewinde
Flansch hinten: Kunststoffring/Zentralgewinde
Welle vorne: Länge
Elektrischer Anschluss: Kabellänge/Pin-Anschluss
Temperatursensor: NTC-Thermistor

xdrives.maxonmotor.com

Ausgabe März 2016 / Daten provisorisch / Änderungen vorbehalten

Recirculating ball spindles Ø 16, 25 mm

Ø 16 features

- Ø16 mm, rolled, hardened and polished
- Material CF 53, inductively hardened (HRC 60 ± 2); (for detailed information see DIN 17212)
- Spindle pitches: 2.5 / 4 / 5 / 10 and 20 mm
- Lengths up to max. 3052 mm available
- End machining to isel standard or according to customer specification (see "Available lengths")
- Produced to DIN 69051, Part 3, Tolerance class 7

Options

- **End machining according to customer specification**
- **Available in other lengths**

Available lengths

Without end machining
in 100 mm raster
- 352 to 3052 mm

Two-sided end machining
in 100 mm raster
- 368 mm to 3068 mm

Special length to dimensioned drawing: 211 13X XXXX

Special length to Drawing: 211 13X 0998

Ordering key

211 13X XXXX

Spindle pitch
2 = 2.5 mm
3 = 4 mm
4 = 5 mm
5 = 10 mm
6 = 20 mm

End machining
0 = not machined
5 = both-sided machining suitable for all feeds (aluminium profile length 78 mm)

Lengths
e.g. **045** = 452 mm
086 = 868 mm
305 = 3052 mm
(rounded to the final digit)

See "Available lengths" for permissible combinations.

Ordering data

Slotted nut
- Self-locking
- M 10 × 0.75 mm

Part no.: **890257 0011**

Dimensioned drawing

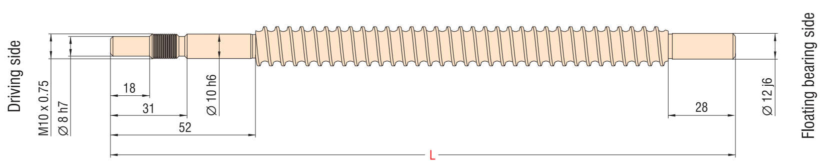

Ø 25 features

- Ø 25 mm, hardened and polished
- Material CF 53, inductively hardened (HRC 60 ± 2); (for detailed information see DIN 17212)
- Spindle pitches: 5/10 and 20 mm
- Lengths up to max. 3000 mm available
- End machining to isel standard or according to customer specification (see "Available lengths")
- Produced in accordance with DIN 69051, Part 3, Tolerance class 7

Option

- **End machining to order**

Available lengths

Without end machining
in 100 mm raster
- 500 to 3000 mm

Special length in accordance with drawing: 211 14X 0999

Two-sided end machining
in 100 mm raster
- 295 to 2995 mm

Special length in accordance with drawing: 21114X XXXX

Ordering key

211 14X XXXX

Spindle pitch
4 = 5 mm
5 = 10 mm
6 = 20 mm

End machining
0 = not machined
2 = both sides

Lengths
e.g. **050** = 500 mm
100 = 1000 mm
289 = 2895 mm
(rounded to the last digit)

See "Available lengths" for permissible combinations.

Ordering data

Slotted nut
- Self-locking
- M 17 x 1.0 mm

Part no.: **890259 0011**

dimensioned drawing

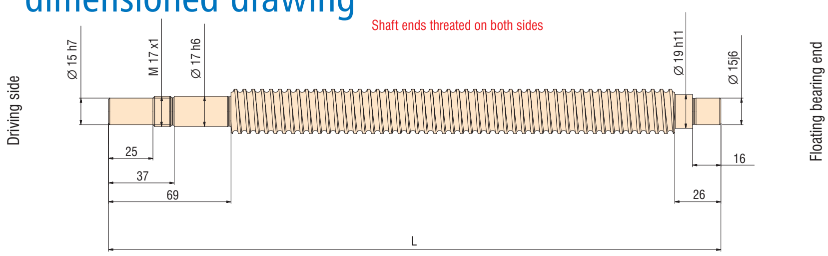

mechanics

Ball screw nut with single-path return

Rectangle nut–Ø16

Features

- Material 16MnCr5 or 20MnCr5, pressed, hardened, polished
- Versions for recirculating ball spindle Ø16 mm
- Nut pitches: 2.5 / 4 / 5 / 10 mm
- Balls are rerouted internally
- As block housing with base fixing
- Regreasing through grease nipples 90°, 0°

Load factors

Pitch	Nominal Ø	dynamic load factor	static load factor
2.5 mm	16 mm	3500 N	5500 N
4.0 mm	16 mm	4600 N	7200 N
5.0 mm	16 mm	4600 N	7200 N
10.0 mm	16 mm	4200 N	6500 N

Ordering data

only for spindles Ø16

Pitch	Part no.
2.5 mm	213 003 1003
4.0 mm	213 003 1004
5.0 mm	213 003 1005
10.0 mm	213 003 1010

with matching:

dirt scraper

- VE 2 unit Part no.: 213500 0001

Dimensioned drawings

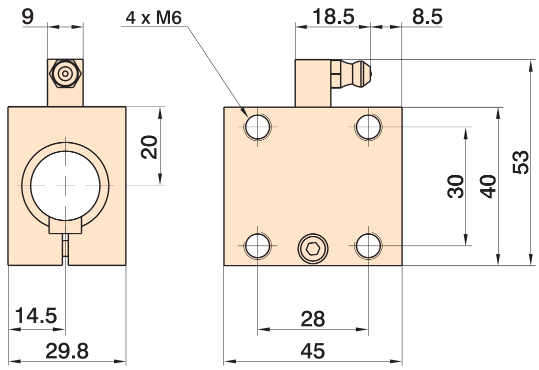

Round nut –Ø16
Ø25

Features

- Material 16MnCr5, ground
- Versions for recirculating ball spindles Ø16 and Ø25 mm
- Nut pitches: 2.5 / 4 / 5 / 10 mm
  20 mm (Ø 16 mm), 5/10 and 20 mm (Ø25 mm)
- Balls are rerouted internally
- The version with nut pitch 20 mm is supplied with scrapers

Load factors

Pitch (mm)	Nominal Ø (mm)	Dyn. load factor (N)	Static load factor (N)
2.5	16	3500	5500
4.0	16	4600	7200
5.0	16	4600	7200
10.0	16	4200	6500
5.0	25	5100	12600
10.0	25	5100	12600
20	25	3570	8800

Ordering data

only for spindles Ø25

Pitch	Part no.
5.0 mm	213 700 0005
10.0 mm	213 700 0010
20.0 mm	213 700 0020

with matching:

dirt scraper

- VE 2 unit

Part no.: 213700 9000

only for spindles Ø16

Pitch	Part no.
2.5 mm	213 503
4.0 mm	213 514
5.0 mm	213 505
10.0 mm	213 510
20.0 mm	213 520

with matching:

dirt scraper

- VE 2 unit

Part no.: 213500 0001

Dimensioned drawings

for spindle Ø 16

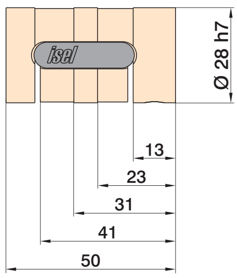

for spindle Ø 25

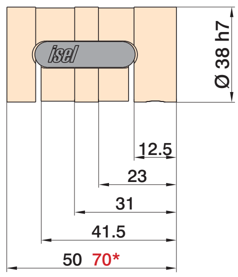

*) At pitch = 20

Flange bearing

for spindle ∅ 16 mm

Flange bearing
drive side

Flange bearing
floating bearing side

Ordering data

Flange bearing, drive side

Part no.: 216 504 0001

Flange bearing, floating bearing side

Part no.: 216 504 0002

Features

- Bearing, spindle drive side (fixed bearing side) and the spindle floating bearing side
- Flange bearing, drive side: bushing with two pressed angular contact ball bearings in an O-configuration
- Flange bearing, floating bearing side (counter-bearing): bushing with pressed needle bearing

Dimensioned drawings

Flange bearing
drive side

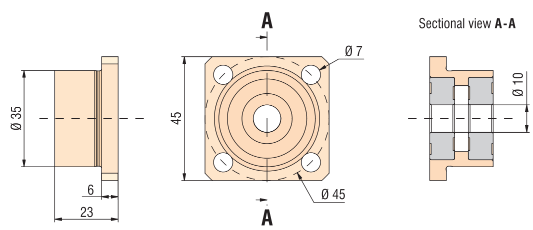

Flange bearing
floating bearing side

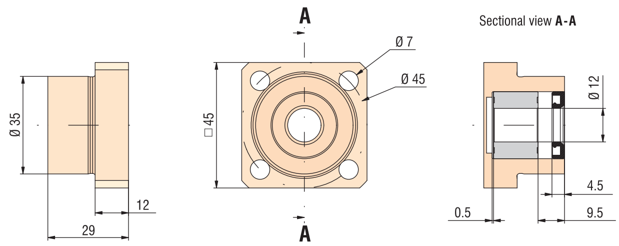

for spindle ∅ 25 mm

Flange bearing
drive side

Flange bearing
floating bearing side

Ordering data

Flange bearing, drive side

Part no.: 216 504 0006

Flange bearing, floating bearing side

Part no.: 216 504 0005

Features

- Bearing, spindle drive side (fixed bearing side) and the spindle floating bearing side
- Flange bearing, drive side: bushing with two pressed angular contact ball bearings in an O-configuration
- Flange bearing, floating bearing side (counter-bearing): bushing with pressed needle bearing

Dimensioned drawings

Flange bearing
drive side

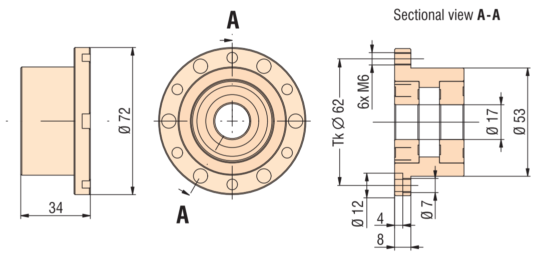

Flange bearing
floating bearing side

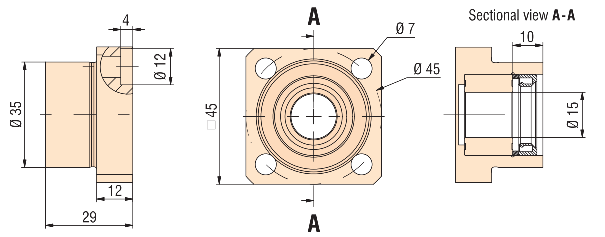

Rue Archimède, 1 bte L6.11.01, 1348 Louvain-la-Neuve **www.uclouvain.be/epl**